



University of Kerbala
College of Science
Department of Chemistry

Removal of some Metal Ions by Polysiloxane Immobilized polydonor Ligand System

A Thesis

**Submitted to the College of Science /University of Kerbala in Partial
Fulfillment of the Requirement for the Degree of Master of Science in
Chemistry**

Written By

Ayyam Tariq Abed al-Kathem

B.Sc. Chemistry (٢٠١٣) \ University of Wasit

Supervised By

Prof. Dr. Hayder Hamied Mihsen

and

Assist. Prof. Shaymaa Ibrahim Saeed

٢٠٢٤ A.D

١٤٤٥

بِسْمِ اللَّهِ الرَّحْمَنِ الرَّحِيمِ

فَتَعَالَى اللَّهُ الْمَلِكُ الْحَقُّ وَلَا تَعْجَلْ بِالْقُرْآنِ مِنْ قَبْلِ
أَنْ يُقْضَىٰ إِلَيْكَ وَحْيُهُ وَقُلْ رَبِّ زِدْنِي عِلْمًا

صدق الله العلي العظيم

سورة طه الآية ﴿١١٤﴾

Supervisors Certification

We certify that this thesis "**Removal of some Metal Ions by Polysiloxane Immobilized polydonor Ligand System**" was conducted under our supervision at the Department of Chemistry, College of Science, University of Kerbala, as a partial fulfillment of the requirements for the degree of Master of Science in Chemistry.



Signature:

Name: **Dr. Hayder Hamied Mihsen**

Title: Professor

Address: University of Kerbala,
College of Science, Department of
Chemistry

Date: / /2024



Signature:

Name: **Shaymaa Ibrahim**

Title: Assist. Prof.

Address: University of Kerbala,
College of Sciences, Department of
Chemistry

Date: / /2024

Report of the Head of the Chemistry Department

According to the recommendations presented by the Supervisors and the Postgraduate Studies Director, I forward this thesis "**Removal of some Metal Ions by Polysiloxane Immobilized polydonor Ligand System**" for examination.

Signature:



Name: **Dr. Thaer Mahdi Madloul**

Title: Assistant Professor

Head of Chemistry Department

Address: University of Kerbala, College of Science, Department of Chemistry.

Date: 3/5/2024



Kerbala University
Science College




Asst. Prof. Dr. Thaer M. M. Al-Rammahi
Head of Chemistry Department

Examination Committee Certification

We, the examining committee, certify that we have read this thesis *entitled "Removal of some Metal Ions by Polysiloxane Immobilized polydonor Ligand System"*. and examined the student "Ayyam Tariq Abed al-Kathem" in its contents and that in our opinion, it is adequate as a thesis for the degree MSc. of science in chemistry.

(Chairman)

Signature: 

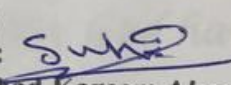
Name: Dr. Salam Hussein Alwan

Title: Assist. Professor

Address: University of Al-Qadisiyah / College of Dentistry

Date: / / 2024

(Member)

Signature: 


Name: Suhad Kareem Abass

Title: Assist. Professor

Address: University of Kerbala, College of Science, Department of Chemistry

Date: / / 2024

(Member)

Signature: 


Name: Dr. Atheer Hasan Yas

Title: Lecturer

Address: University of Kerbala, College of Science, Department of Chemistry

Date: 8/4/2024

Approved by the council of the College of Science in its session No. in / / 2024

Signature-1: 


Name: Dr. Hayder Hamied Mihsen

Title: Professor

Address: University of Kerbala, College of Science, Department of Chemistry

Date: / / 2024

Approved by the council of the College of Science in its session No. in / / 2024

Signature-2: 

Name: Shaymaa Ibrahim

Title: Assist. Prof

Address: University of Kerbala, College of Sciences, Department of Chemistry

Date: / / 2024

Approved by the council of the College of Science in its session No. in / / 2024

Signature: 

Name: Dr. Hassan Jameel Jawad Al-fatlawy

Title: Professor

Address: University of Kerbala - Dean of College of Science

Date: / / 2024

Dedication

To the one whom God has crowned with awe and reverence and taught me to give without expectation and whose name I carry with all pride, my dear father, the dearest departed to my heart and the most present absent person in my memory.

May God have mercy on you, my dear father.

*to the one who stays awake nights and days,
for me to my dear mother*

To those whom my Lord placed between him and me affection and mercy, to the highest symbols of sincerity and loyalty, a companion on the path, and to those who supported me and walked with me in my steps, my dear husband.

To those who accompanied me through thick and thin, and from them I draw strength and determination, my dear brothers and sisters.

*To my adornment in this worldly life and the apple of my eye and those whose eyes I see optimism and happiness in their laughter, my daughter and sons,
may God protect you for me.*

Acknowledgments

Praise be to Allah, Lord of the worlds, May God's blessings be upon Mohammed and his pure immediate family, and thanks to God for his countless and numberless graces and gifts.

I would like to extend my deep thanks, gratitude, and appreciation to:

My supervisor Prof.Dr. Hayder Hamied Mihsen and Assist. Prof. Shaymaa Ibrahim Saeed for her continuous support and invaluable suggestions and great contributions since the very beginning of this work.

Also, I thank all faculty members of the Department of Chemistry in the College of Science at the University of Kerbala. Finally, I thank my family and friends for their continued support throughout this journey. They were my source of encouragement along the way.

Summary

The world is moving towards using the best scientific methods to get rid of environmental pollution. Some metallic elements are natural and industrial pollutants like Cobalt, Copper, and Nickel. Also, Rice husks are one of the pollutants produced daily in all parts of the world. Therefore, rice husks were used to produce compounds to get rid of some polluting elements, thus eliminating two types of pollutants at the same time. Sodium silicate was prepared from rice husks, then reacted with γ -aminopropyltriethoxysilane to produce RH-SiO₂-PrNH₂ via the sol-gel method which was characterized by using the FTIR showed that the vibration NH₂ and NH absorbed at 3283 and 3113 cm⁻¹, respectively. Then RH-SiO₂-PrNH₂ reacted with γ -amino- α,α -dibromobenzaldehyde to produce RH-SiO₂-PrADB which was characterized by using several techniques (FTIR, XRD, FESEM-EDX, CHN, AFM, TEM, and TGA/DTA):

The FT-IR spectrum displays azomethine group (C=N) is represented by the peak at 1642 cm⁻¹. The XRD spectra were showed the amorphous nature of the prepared ligand. The elemental analysis of the RH-SiO₂-PrADB compound indicates that the percentage of carbon and nitrogen is 16.63% and 6.4%. FESEM images show an increase in the roughness of the outer surface of the sample with an increase in the rate of accumulation of nanoparticles as a result of the bonding of the RH-SiO₂-PrNH₂ with γ -amino- α,α -Dibromobenzaldehyde compound. Also, the images of AFM confirmed a clear increase in the roughness rate to reach 16.24 nm. This indicates the successful association of the RH-SiO₂-PrNH₂ with the γ -amino- α,α -Dibromobenzaldehyde compound. While TEM images were shown, the

presence of spherical clusters linked together. It was found that the average particle size is 30 nm, and this value is consistent with the results of the FESEM and XRD analysis. The TGA analysis shows that the loss percentage reached (93.4%) due to the evaporation of the adsorbed water molecules and the dissociation of the γ -amino- γ , δ -Dibromobenzaldehyde compound, thus breaking the silanol bonds and the success of the synthesis process and the production of a compound with high stability. The specific area and pore diameter of the RH-SiO₂-PrADB were using BET analysis, and it was determined to be equal to 3.11 m²/g, and 1.21 nm, respectively.

In addition, sodium silicate was treated by adding Fe₃O₄ to produce magnetic nanosilicates. Following the same previous method, Fe₃O₄@RH-SiO₂-PrADB was produced and characterized by several techniques (FTIR, XRD, FESEM-EDX, CHN, AFM, TEM, VSM and TGA/DTA):

The FT-IR spectrum showed an absorption band at 636.0 and 570.9 cm⁻¹ due to Fe-O bond in addition to bands same absorptions for compound RH-SiO₂-PrADB. the XRD spectrum composite showed a clear displacement in the broad peak at ($2\theta = 22.0^\circ - 28.8^\circ$) due to the RH-SiO₂-PrADB compound and sharp peaks at ($2\theta = 29.2^\circ, 30.4^\circ, 39.1^\circ, 42.4^\circ, 47.9^\circ, 57.0^\circ, 62.8^\circ, 67.0^\circ$) due to the cubic structure of Fe₃O₄. It was noted that the prepared composite is amorphous. The VSM showed that the prepared iron oxide (Fe₃O₄) has ferromagnetic behavior with a saturation magnetization up to 13.29 emu g⁻¹. While the results of the saturation magnetization value for the Fe₃O₄@RH-SiO₂-PrNH₂ and Fe₃O₄@RH-SiO₂-ADB compounds showed a clear decrease in magnetism up to 3.11 and 3.17 emu g⁻¹, respectively.

The results showed that the specific surface area value of the RH-SiO₂ sample is 390.12 m²/g and has a pore size distribution of 3.469 nm. While the specific surface area value of the RH-SiO₂PrNH₂ sample is 1.789 m²/g and has a pore size distribution of 10.100 nm. In contrast, the surface area value in the Fe₃O₄@RH-SiO₂PrNH₂ sample decreased to up to 1.093 m²/g and has a pore size distribution of 21.178 nm. whilst the Specific area of the RH-SiO₂PrADB was using BET analysis, to be equal to 3.818 m²/g, and has a pore size distribution of 36.216 nm. The specific surface area of Fe₃O₄@RH-SiO₂PrADB was (3.076 m²/g) and has a pore size distribution of 16.086 nm which was decreased compared with the specific surface area of RH-SiO₂PrADB. This is due to the attachment of Fe₃O₄ particles to an RH-SiO₂PrADB surface, which reduces the surface area

The preparation of hybrid solid ligands was used to uptake the metal ions from its aqueous solution by using various conditions such as:- exposure time, pH, metal ion concentration, and ligand mass.

Table of contents

<i>Summary</i>	<i>I</i>
<i>Table of contents</i>	<i>IV</i>
<i>List of Figures</i>	<i>VI</i>
<i>List of Schemes</i>	<i>IX</i>
<i>List of Tables</i>	<i>X</i>
<i>List of Abbreviations and Symbols</i>	<i>XI</i>
1. Introduction	1
1.1 Rice husk	1
1.2 Silica	3
1.3 Surface of silica	5
1.4 Polysiloxanes	7
1.5 Sol-Gel Technique	9
1.6 Modification of the surface of silica	11
1.7 Iron Oxide Nanoparticles	14
1.8 Schiff bases	15
1.9 Using silica as a solid support in metal ion extraction	16
1.10 Heavy metals pollution	20
1.11 The Aims	25
2. Experimental Part	26
2.1 Instruments:	26
2.2 Materials	27
2.3 The preparation methods	28

2.4	Removal of metal ions from aqueous solution _____	32
2.2.	Calibration curve _____	34
2.3.	Tests on the absorption of metal _____	35
2.4.	Optimization conditions:- _____	36
3.	Results and Discussion _____	38
3.1.	Introduction _____	38
3.2.	(FTIR) for Fourier Transform Infrared Spectroscopy _____	39
3.3.	N ₂ Adsorption–Desorption Analysis _____	41
3.4.	XRD Diffraction analysis _____	47
3.5.	Elemental Analysis (CHN) _____	50
3.6.	Field emission scanning electron microscopy (FESEM) _____	52
3.7.	Atomic Force Microscopy (AFM) _____	58
3.8.	Transmission electron microscopy (TEM) analysis _____	62
3.9.	Vibrating Sample Magnetometry (VSM) _____	66
3.10.	Thermo gravimetric Analysis (TGA) _____	68
4.	Metal Uptake _____	72
4.1	Introduction _____	72
4.2	Experimental of Metal Uptake _____	73
4.3	Metal Uptake by RH-SiO ₂ /PrADB _____	73
4.4	Metal Uptake by Fe ₃ O ₄ @ RH-SiO ₂ /PrADB _____	82
5.	Conclusions _____	90
6.	References _____	91

List of Figures

Figure 1-1 Rice grain and respective structures, and rice husk [2]	1
Figure 1-2 The structure of silicon dioxide (SiO ₂) is linear	3
Figure 1-3 Structure of Silicon Dioxide	4
Figure 1-4: Different types of silanol group on the surface of silica [21]	6
Figure 1-5: Q ⁿ nomenclature used to define the environment of the silicon atoms in silica [21]	6
Figure 1-6 Structure of a polysiloxane	7
Figure 1-7 Structure of the polysiloxane-immobilized triamine ligand	8
Figure 1-8: γ-aminophenylaminopropylpolysiloxane ligand systeme	17
Figure 1-9 The functionalized polysiloxane immobilized iminodiacetic acid ligand system	18
Figure 1-10: Functionalized mesoporous silica nanoparticles	21
Figure 1-11: copper(II) Schiff base complex and γ-thio-phenecarboxaldehyde	21
Figure 1-12 Ni(II) complex with functionalized silica	22
Figure 1-13 Cobalt flakes	22
Figure 1-14 Cobalt (II) complex	23
Figure 1-15 Local Copper	24
Figure 1-16 Copper complex	24
Figure 2-1 UV-Visible spectra of Ni(II), Co(II) and Cu(II) aqueous solutions	23
Figure 2-2 Calibration curve of Ni(II), Co(II) and Cu(II)	25
Figure 2-3: Research progress and results continuation	27
Figure 3-1 FTIR for (a) RH-SiO ₂ (b) RH-SiO ₂ -PrNH ₂ (c) RHSiO ₂ -PrADB (d) Fe ³⁺ O ₃ (e) Fe ³⁺ O ₃ @RH-SiO ₂ -PrNH ₂ (f) Fe ³⁺ O ₃ @RH-SiO ₂ -PrADB	40
Figure 3-2 The IUPAC Classification of Adsorption Isotherms	42
Figure 3-3: (a) Nitrogen adsorption-desorption isotherm, (b) pore size distribution for the RH-SiO ₂ (c) Nitrogen adsorption-desorption isotherm (d) pore size distribution for RH-SiO ₂ -PrNH ₂ (e) Nitrogen adsorption-desorption isotherm, (f) pore size distribution for the Fe ³⁺ O ₃ @RH-SiO ₂ -PrNH ₂ (g) Nitrogen adsorption-desorption isotherm, (h) pore size	

distribution for the RH-SiO ₂ /PrADB (I) Nitrogen adsorption-desorption isotherm, (J) pore size distribution for the Fe ₃ O ₄ @RH-SiO ₂ /PrADB _____	40
Figure 3-4 spectrum for (A) RH-SiO ₂ (B) RH-SiO ₂ /PrNH ₂ (C) RH-SiO ₂ /PrADB (D) Fe ₃ O ₄ (E) Fe ₃ O ₄ @RH-SiO ₂ /PrNH ₂ (F) Fe ₃ O ₄ @RH-SiO ₂ /PrADB _____	41
Figure 3-5 FESEM images for (A) RH-SiO ₂ (B) RH-SiO ₂ /PrNH ₂ (C) RH-SiO ₂ /PrADB (D) Fe ₃ O ₄ @RH-SiO ₂ /PrNH ₂ (E) Fe ₃ O ₄ @RH-SiO ₂ /PrADB _____	54
Figure 3-6 EDX chart for (A) RH-SiO ₂ (B) RH-SiO ₂ /PrNH ₂ (C) RH-SiO ₂ /PrADB (D) Fe ₃ O ₄ @RH-SiO ₂ /PrNH ₂ (E) Fe ₃ O ₄ @RH-SiO ₂ /PrADB _____	55
Figure 3-7 2D and 3D AFM images of (A) RH-SiO ₂ (B) RH-SiO ₂ /PrNH ₂ (C) RH-SiO ₂ /PrADB (D) Fe ₃ O ₄ @RH-SiO ₂ /PrNH ₂ (E) Fe ₃ O ₄ @RH-SiO ₂ /PrADB _____	60
Figure 3-8 TEM images for (A) RH-SiO ₂ (B) RH-SiO ₂ /PrNH ₂ (C) RH-SiO ₂ /PrADB (D) Fe ₃ O ₄ @RH-SiO ₂ /PrNH ₂ (E) Fe ₃ O ₄ @RH-SiO ₂ /PrADB _____	60
Figure 3-9 VSM spectra of (A) Fe ₃ O ₄ (B) Fe ₃ O ₄ @RH-SiO ₂ /PrNH ₂ (C) Fe ₃ O ₄ @RH-SiO ₂ /PrADB _____	61
Figure 3-10 TGA/DTA analysis of (A) RH-SiO ₂ (B) RH-SiO ₂ /PrNH ₂ (C) RH-SiO ₂ /PrADB (D) Fe ₃ O ₄ @RH-SiO ₂ /PrNH ₂ (E) Fe ₃ O ₄ @RH-SiO ₂ /PrADB _____	71
Figure 4-1 Effect of vibration time on removal of metal ions (Co(II), Ni(II) and Cu(II)) (concentration 0.01M) by the ligand RH-SiO ₂ /PrADB (dose = 0.1g) _____	76
Figure 4-2 Effects of concentration metal ions on the removal by the ligand RH-SiO ₂ /PrADB (dose= 0.1g) _____	77
Figure 4-3 Effect of the weight of the RH-SiO ₂ /PrADB on the removal of metal ions (Co(II), Ni(II) and Cu(II)) (concentration 0.01M) by the ligand RH-SiO ₂ /PrADB (dose= 0.1g) _____	78
Figure 4-4 Effect of pH on the removal of metal ions (Co(II), Ni(II), and Cu(II)) (concentration 0.01M) by the RH-SiO ₂ /PrADB (dose= 0.1g) _____	81
Figure 4-5 Effect of vibration time on removal of metal ions Co(II), Ni(II) and Cu(II) _____	83
Figure 4-6 Effect of concentration of metal ions (Co(II), Ni II and Cu(II)) on the removal by the ligand Fe ₃ O ₄ @RH-SiO ₂ /PrADB (dose= 0.1g) _____	85
Figure 4-7 Effect of the weight of the Fe ₃ O ₄ @RH-SiO ₂ /PrADB on the removal of metal ions (Co(II), Ni(II) and Cu(II)) at a concentration 0.01M _____	87

Figure 4-1 Effect of pH on the removal of metal ions (Co(II), Ni(II) at a concentration 10^{-4} M, and Cu(II) by the Fe³⁺/RH-SiO₂-PrADB (10^{-2} g) _____ 49

List of Schemes

<i>Scheme 1-1: The suggested reactions for the hydrolysis and condensation processes that occur in the sol gel method</i>	11
<i>Scheme 1-2: Modification of silica surface, (1) deposited to method (2) growing from method</i>	13
<i>Scheme 1-3: Formation and hydrolyze back of Schiff base</i>	15
<i>Scheme 2-1: The synthesis steps of RH-SiO₂PrADB</i>	20
<i>Scheme 2-2: The synthesis steps of Fe³⁺O₃@RH-SiO₂PrADB</i>	22

List of Tables

<i>Table 1-1: list of silica support materials along with examples of their applications. _____</i>	18
<i>Table 1-2 List of instruments, supplier companies and place of measurement _____</i>	26
<i>Table 1-3 Chemicals used in this work and their provider _____</i>	27
<i>Table 1-4 Surface area analysis (BET, BJH) of RH-SiO₂/PrNH₂, Fe₃O₄@RH-SiO₂/PrNH₂, RH-SiO₂/PrADB, and Fe₃O₄@RH-SiO₂/PrADB _____</i>	43
<i>Table 1-5 Crystallite size and Average crystallite size of Fe₃O₄, Fe₃O₄@RH-SiO₂/PrNH₂ and Fe₃O₄@RH-SiO₂/PrADB _____</i>	50
<i>Table 1-6: Chemical analysis of RH-SiO₂, RH-SiO₂/PrNH₂, Fe₃O₄@RH-SiO₂/PrNH₂, RH-SiO₂/PrADB, and Fe₃O₄@RH-SiO₂/PrADB using CHN _____</i>	51

List of Abbreviations

symbols	Name
%	Percentage
°C	Degree Celsius
AFM	Atomic Force Microscope
APTES	γ-(aminopropyl)triethoxysilane
BET	Brunauer-Emmett-Teller
CHNS	Elemental analysis
DMSO	Dimethylsulfoxide
Fe _γ O _z @RH-SiO _γ ADB	magnetic mesoporous silica
Fe _γ O _z @RH-SiO _γ PrNH _γ	magnetic mesoporous silica
FESEM	Field Emission Scanning Electron Microscopy
FTIR	Fourier-transform infrared spectroscopy
h	Hour
IUPAC	International Union of Pure and Applied Chemistry
L	Ligand
M	Molar
mol	Mole
RH-SiO _γ PrADB	Rice Husk Silica –γ-amino-γ,δ-Dibromobenzaldehyde
RH-SiO _γ PrNH _γ	Rice Husk Silica- γ-(Aminopropyl) Triethoxysilane
SEM	Scanning Electron Microscopy
TEM	Transmission electron microscopy
TGA	Thermo gravimetric Analysis
UV-Vis	Ultraviolet–visible spectroscopy
VSM	Vibrating Sample Magnetometry
XRD	X-ray diffraction

CHAPTER ONE

INTRODUCTION



1. Introduction

1.1 Rice husk

Rice is a kind of grass seed that originates from the species *Oryza sativa*, often known as Asian rice, or *Oryza glaberrima*, also known as African rice. Rice, which is frequently a staple food in many countries, is a widely produced food throughout the world. As a result, research has begun an extensive programme to increase rice output[1] The term "rice husk refers to the outer layer of rice. The rice grains and rice husk are normally separated during the milling process. 20% of the weight of the paddy is hull. Rice Husk layers are of four types: structural, fibrous, sponge-like, or cellular as Figure (1-1)[2]. Typically, rice husks have been thought of as a waste product that is typically burned or dumped in landfills[3]. But nowadays, rice husks are thought of as a product that can be sold[4].

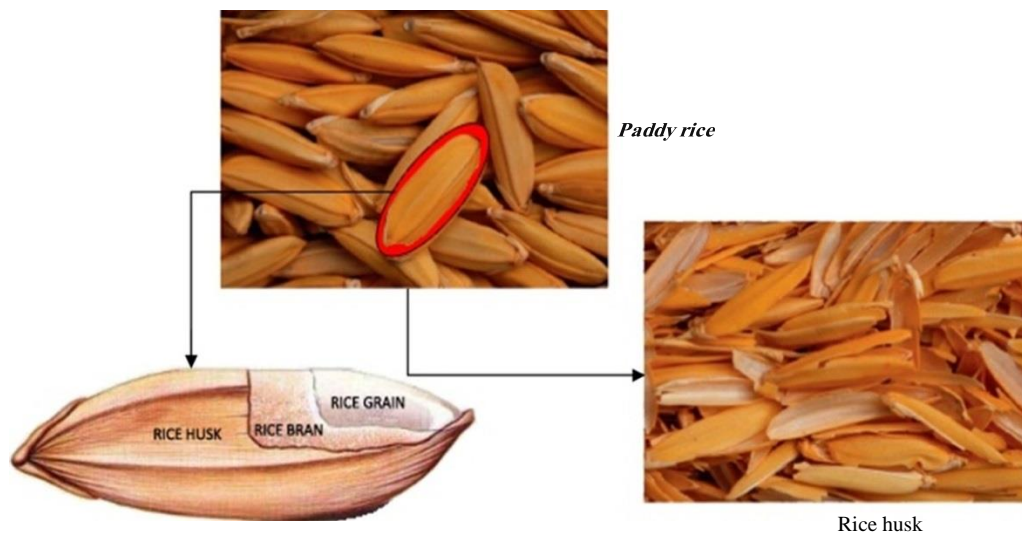


Figure 1-1 Rice grain and respective structures, and rice husk [5]

The growing quantity of rice has led to an increase in the amount of rice husks, which are frequently seen as wastes[¹]. The UNEP (United Nations Environment Programme) has suggested that nations recover valuable materials from the waste stream to improve the conversion of waste into riches[²]. Many governments and other organisations are making significant efforts to find ways to manage waste pollution caused by disposed rice husks in an effort to reduce the risk that these materials may represent to persons and regulate environmental pollution. By making such significant efforts, waste disposal expenses would be decreased, and profits from the sale of recovered materials (chemical compounds) and energy would be generated[³].

The popularity of biopolymers and bioplastics in the modern world has drawn researchers' attention to biowaste [4]. Functional materials that have found use in a variety of fields, including biotechnology and medicine, can be obtained from biowaste, which is a valuable resource. Rice husk (RH) is a type of agricultural biowaste that has a lot of silica, carbon structures, and other minor minerals that have lots of potential uses in both science and industry[5]. Rice husk has a low bulk density that ranges from 90 to 100 kg/m³. The chemical analysis of rice husk shows the following components, SiO₂ is found to be 30%, the organic material and water content is 40% and K₂O, CaO, MgO, MnO, Al₂O₃, P₂O₅, Fe₂O₃, Na₂O and TiO₂ constitute about 6%. The organic part is composed of cellulose, lignin, and hemicellulose [6].

1.2 Silica

The generic term for the chemical silica is silicon dioxide. The chemical formula for this substance, SiO_2 , is one silicon atom joined to two oxygen atoms. The crust and guts of the Earth are incredibly rich in silica, a compound of silicon and oxygen. Silica is the primary ingredient in more than 90% of known rocks and accounts up 59% of the mass of the Earth's crust. In nature, silica is present as quartz, tridymite, and cristobalite. These varieties of silicon dioxide are interchangeable at proper temperatures[12].

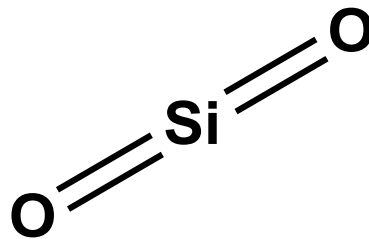


Figure 1-2 The structure of silicon dioxide (SiO_2) is linear

Silicon dioxide is classified into two types. One is amorphous silica (a-silica), also known as non-crystalline silica. And the other is crystalline silica (c-silica). Covalent bonds are used to bind it. Each silicon atom in the three-dimensional structure of silicon dioxide is covalently bound to four oxygen atoms, and each oxygen atom to two silicon atoms. Tetrahedral oxygen atom geometry surrounds silicon as shown in Figure (1-3)[13].

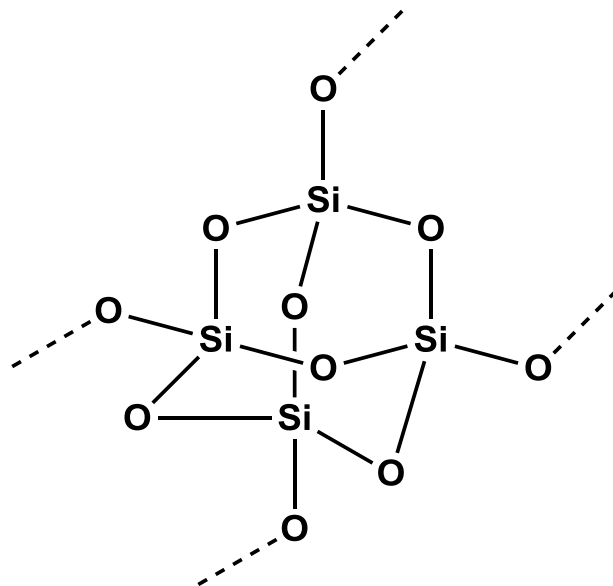


Figure 1-3 Structure of Silicon Dioxide

Silicon dioxide is used in several industries such as pharmaceuticals, food, chemicals, electronics, construction, etc [14]. In the pharmaceutical sector, silicon dioxide is a component of drug additives. It takes up moisture and keeps the medications dry[15]. Silicon dioxide is used as an anti-caking agent in spices in the food sector. Additionally, it serves as a fining agent in beers, wines, and juices. Silicon dioxide is utilised in numerous production procedures in the chemical industry. Additionally, it is employed in the production of insecticides, anti-adhesives, adhesives, corrosion inhibitors, dyes, absorbents, sealants, porcelain, and ceramics. Additionally, silicon dioxide is employed as an absorbent in column chromatography. Interestingly Optical fibres used in the electronics sector are primarily made of silicon dioxide. Additionally, silicon dioxide and hydraulic fracturing are employed in the construction sector to create concrete. Recently, To increase the antibacterial and corrosion capabilities of biomaterials, silica, a biosafe ingredient, can be combined with silver nanoparticles[16]. Due to their vast surface area, when added to thermoplastic polymers, amorphous silica

nanoparticles from sources that are natural, such as fly ash and rice husk, can act as a nucleating agent [14].

1.3 Surface of silica

The surface of silica comprises two kinds of functional groups, i.e. siloxane (Si–O–Si) and silanol (Si–OH) groups. It was discovered that the main modification pathway happens through the response of a specific molecule to the silica surface with the silanol groups [15].

Silanol groups are created by two primary procedures on the surface. First, such groups are created during silica synthesis, e.g. during condensation polymerization of $\text{Si}(\text{OH})_4$. Secondly, surface groups may form as a consequence of rehydroxylation of dehydroxylated silica when treated with water or aqueous solutions [16]. The silanol groups on silica surface can be classified into three types, Figure 1.4 [17]:

1-Isolated groups (or free silanols) where the surface silicon atom has three bonds in the bulk structure and the fourth bond is connected to a single –OH group.

2-Vicinal silanols (or bridged silanols) where two single groups of silanols connected to distinct silicon atoms are near enough to the hydrogen bond.

3-Geminal silanols consist of two hydroxyl groups that are connected to one silicon atom and that are too near to each other to form a hydrogen bond.

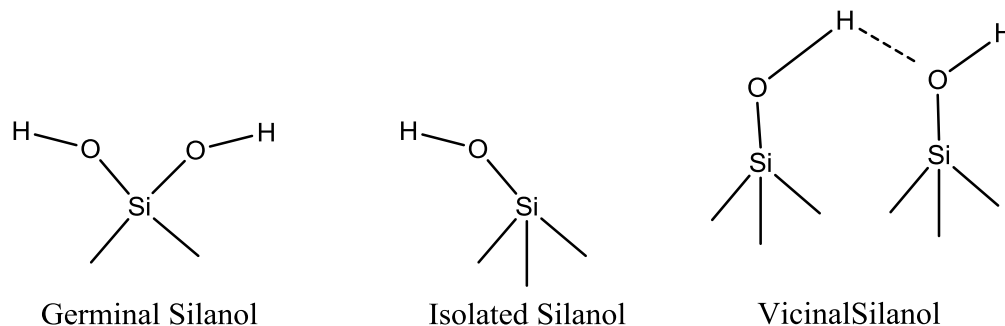


Figure 1-4: Different types of silanol group on the surface of silica [21]

On the other hand, silica shows three types of siloxane groups ($\equiv\text{Si}-\text{O}-\text{Si}\equiv$) Figure 1.5. According to NMR study of the ^{29}Si nuclei [22], these siloxane groups are represented as Q^n , where (n) indicates the number of bridging bonds ($-\text{O}-\text{Si}$) tied to the central Si atom, i.e.: Q^4 – four siloxane bonds to the silicon atom; Q^3 – three siloxane bonds to the silicon atom; and Q^2 – two siloxane bonds to the silicon atom. Generally, the number of siloxane groups can be determined from the following equation: $Q^n = \text{Si}(\text{OSi})_n(\text{OH})_{4-n}$ [23].

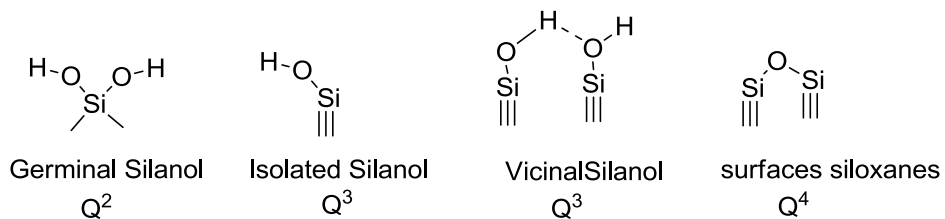


Figure 1-5 : Q^n nomenclature used to define the environment of the silicon atoms in silica [21]

1.4 Polysiloxanes

polysiloxanes The most common type of polymers known as silicones, have a Si-O core with elevated bond energy (~ 452 kJ.mol⁻¹) with organic groups, usually methyl groups, attached to the Si atoms [14]. Alkyl groups make up the side groups, whereas Si and O atoms make up the main chain (Figure 1-6). When it comes to performance characteristics, polysiloxane occupies the top of the pyramid among the various kinds of speciality polymers [15].

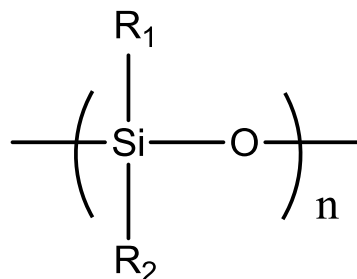


Figure 1-6 Structure of a polysiloxane

There are several commercial and domestic uses for polysiloxanes (silicons), a significant class of inorganic polymers with great temperature and oxidative stability, exceptional low temperature flexibility, and strong resistance to weathering and many chemicals [16]. Due to their inherent biological character, polysiloxanes were utilised in the medical industry. They are the fastest-growing group of polymers because to the enormous opportunities in the design, synthesis, and modification of their physical and chemical properties, and they have significant applications in cosmetology, medicine, and pharmacy [17]. Organosilicon surfactants are extremely useful in a variety of uses, including transporters that improve corticosteroid drugs [18]. Silicone materials exhibit also good biocompatibility, tolerance to sterilization, bio-durability and hemocompatibility [19]. Functionalization of

polysiloxanes by chelating ligands has been widely employed to extract and preconcentrate trace metal ions from different media[30]. In addition, because the inclusion of functional groups can alter the structure and properties of the original polysiloxanes, functionalized polysiloxanes play a significant role in organosilicon chemistry and have been used in a variety of industries[31]. Functional group can alter the structure and ownership of the original polysiloxanes. Notably, some functional groups are extremely reactive, therefore, functional polysiloxane could be expanded into multiplen organosilicon materials.

The polysiloxane-immobilized triamine ligand complexes (Figure 1.5), which have applications in numerous fields of study, are extremely important in both science and business. Their preparation involves two steps: first, the chemical modification of the silica surface. The sol-gel method is the second technique [32]

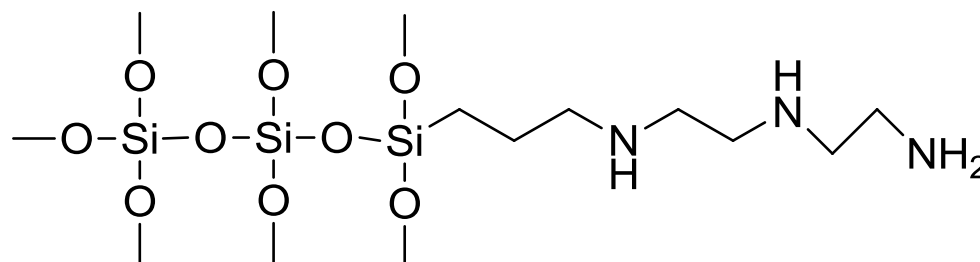


Figure 1-5 Structure of the polysiloxane-immobilized triamine ligand

Applications in areas like the extraction procedure, regrowth, and removal of metal ions from aqueous solutions and organic solvents are expanding as a result of the incorporation of binding groups into polysiloxane matrices[33].

Batch and dynamic approaches have frequently been used to extract and preconcentrate trace metal ions from different media using polysiloxanes functionalized with chelating ligands. Due to their strong potential for absorbing metal ions, functionalized polysiloxanes with suitable complexing agents are being developed with interest [34].

1.5 Sol-Gel Technique

The term "sol-gel method" refers to the process of creating inorganic polymers or ceramics from solutions by converting liquid precursors into "sols" and then into network structures known as "gels" [35]. It is thought that the sol-gel approach can be used to create materials at low temperatures that are entirely inorganic or contain both inorganic and organic components [36]. It has been widely used as a way of preparing for single component oxides as well as multiple-component oxides since Dislich developed the sol-gel approaches to make optical coatings of glassy or crystalline systems in 1971 [37].

Sol-gel silica synthesis in polymer matrixes is a common practice. Alkoxysilane precursors are primarily hydrolyzed and polycondensed during this process [38]. Precursors for a typical sol-gel process are typically metal alkoxides or inorganic metal salts that go through various hydrolysis and polycondensation processes [39].

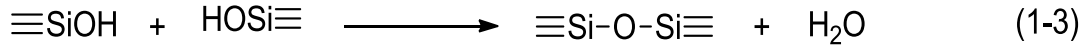
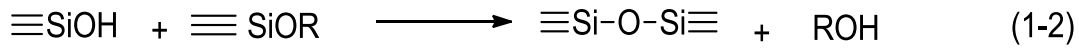
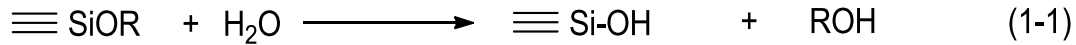
A bottom-up method called the sol-gel method entails connecting molecular building blocks like SiO_4 tetrahedra and TiO_6 octahedra with one another step by step [40].

There are four main stages to the sol-gel process in general, however extra steps are sometimes incorporated to improve the gel's mechanical properties[¹]. The framework of the gel is influenced by all synthesis processes, which also have an impact on the gel's properties and corresponding applications[²].

- I. Sol preparation: A colloidal suspension is created by dispersing solid nanoparticles made from a precursor material in a solvent.
- II. Sol to gel transition (gelation) : An interconnected chain structure is created when an acid or a basic catalyst is added, creating cross-linked and branching particles.
- III. Ageing of the gel: The gel is matured in its original solution to strengthen the gel's structure and mechanical properties.
- IV. Drying of the gel: In order to prevent gel fracture, the solvent is removed from the pores of the gel[³].

The equations for the sol-gel process given in Scheme 1-1 were proposed by Chen and Lin[⁴]. These equations clarified the steps of polymerization and hydrolysis that could take place in sol-gel processes.

Initially, the hydrolysis of the precursor results in the formation of a sol of soluble hydroxylated monomer (equation 1-1). The phase separation and polymerization operations are then used to create a hydrated oxide hydrogel (equation 1-2). The dry, porous xerogel is finally created by carefully extracting or drying the water from the wet gel (equation 1-3)[⁵].



Scheme 1-1 : The suggested reactions for the hydrolysis and condensation processes that occur in the sol gel method

Compared to traditional ceramic preparation techniques, the sol-gel process has various benefits, including:

(1) reaction temperature is low; (2) the products have high purity and homogeneity, (3) new and various compositions, (4) materials have a wide versatility in shapes; (5) reaction systems are simple; (6) the micro- and macrostructure of the host matrix may be controlled through the optimization of several parameters (e.g., water and/or alcohol content, temperature, pressure, type of catalyst, solvent); (7) the presence of the silica network provides good mechanical resistance, extraordinary thermal stability, and amorphous character; and (8) it is possible to graft organic groups into the inorganic backbone at low processing temperatures and to produce organic inorganic hybrid materials designated as ormosils (organically modified silicates), ormolytes (organically modified silicate electrolytes), or ormocers (organically modified ceramics), depending on the final application[1].

1.1 Modification of the surface of silica

The surface characteristics of silica materials, which are heavily influenced by the superficial functional groups added by various modification techniques, are crucial for their applications[2].

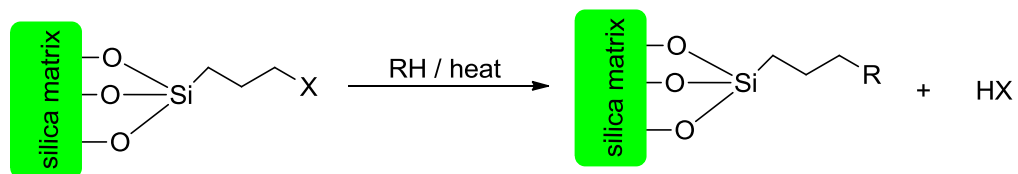
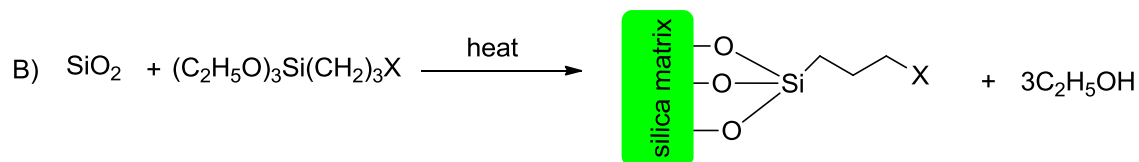
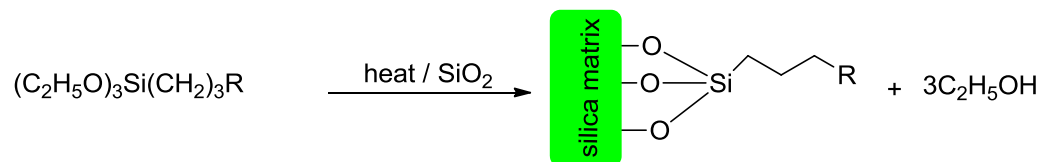
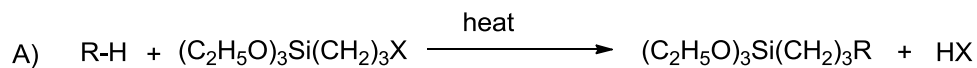
Due to its potential to enable researchers to modify the chemical composition and technology traits of the composite material, modification of the silica surface has drawn a lot of attention. For the creation of vital substances with a variety of unique properties, such as liquid crystals, nanostructured silica materials, and selective heterogeneous catalysts, it is crucial to change the surface of silica[¹].

When using alkyl silanes to modify the surface, superficial silanol groups are crucial[²]. The silanol groups on the silica surface get dehydrated as the temperature rises, whereas a steady rise in temperature causes silanol groups to become dehydrated, which results in the production of siloxane bonds[³].

According to the various methods of incorporating silica components into silica-based hybrid nanostructures, silica-based nanomaterial manufacturing can be broadly divided into two categories[⁴]:

1) The first approach entails a heterogeneous reaction, as shown in Scheme 1-1A, between the silylating agents and the ligand complex, followed by the immobilisation of the resultant ligand with the pre-formed silica.

2) The second method entails using the complex group to treat the post-polysiloxane, as shown in Scheme 1-1B.



Scheme 1-2: Modification of silica surface, (1) deposited to method (2) growing from method

Specific organic processes can lengthen the organic chain when a given alkoxy silane is bound to an inorganic support in order to encourage the surface enhancement of additional basic centers[¹⁰].

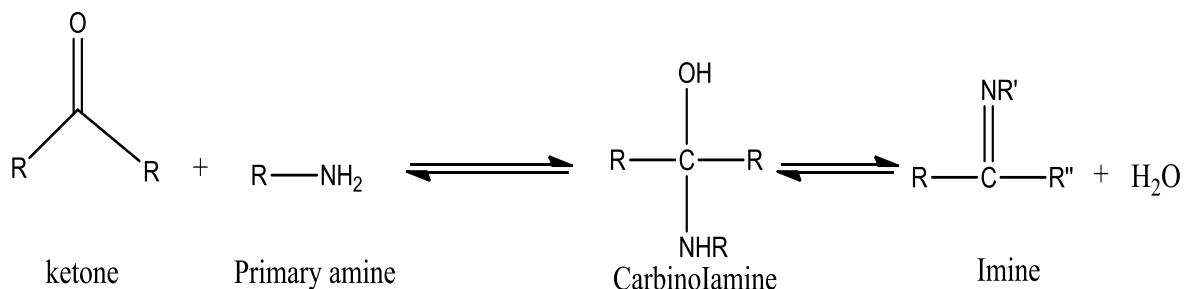
1.1 Iron Oxide Nanoparticles

Relative to the transitional elements in the same group, Iron is the most recent transitional mineral and the primary component of the earth's crust. Iron oxides are created chemically when the elements of oxygen and iron are combined to produce iron compounds. Applications involving biology and geology typically use these materials[1]. Hematite (Fe_2O_3), magnetite (Fe_3O_4), and maghemite (Fe_5O_7) are three distinct forms of iron oxide that have crystalline structures and differing magnetic and structural properties. The crystal structures of oxide form tetrahedral and octahedral can be represented by close-packed planes of iron cations and oxygen anions[2]. Oxygen ions are arranged hexagonally in the crystal structure of hematite, whereas iron ions (III) occupy the octahedral positions. The iron ions (III) are randomly distributed between the octahedral and tetrahedral regions, and the iron ions (II) occupy the octahedral positions, whereas the oxygen ions appear to be arranged in a cubic pattern in magnetite and maghemite. Consequently, the cubic inverted spinel arrangement is the ultimate form. High stability to oxidation, superparamagnetic characteristics, biocompatibility, and non-toxicity are all present in iron oxide nanoparticles[3]. Its usefulness in numerous fields, including wastewater treatment, catalysts, high-density data storage, batteries made from lithium ion, modified anti-corrosive coatings, Ferro fluids and supercapacitors, materials for electrodes, and separating of biological products, attracted researchers' attention as a result. Additionally, due to iron oxide nanoparticles' low toxicity, they are useful in the medical field for a variety of medical applications, including drug delivery, thermal therapy, tissue-specific release of therapeutic agents, magnetic sensing probes for in-vitro diagnostics (IVD), and hyperthermia-based cancer treatments[4]. Mesoporous, silica-coated magnetite nanoparticles have been known since

2004, when Wu et al. [26] reported the preparation of a novel material, comprised of magnetite nanocores and double silica shell (a dense shell closer to the core and mesoporous one next from the center). However, such particles were irregularly shaped and had a wide size distribution, from hundreds of nanometers up to few microns. A year later, Zhao et al. [27], in a two-step process, obtained almost spherically shaped particles, with narrow size distribution, containing hematite core, the inner, dense silica shell with a tunable thickness, and an outer mesoporous shell that increased the total surface area of the material up to $283 \text{ m}^2 \text{ g}^{-1}$ which enabled surface functionalization, typical of pure mesoporous silica.

1.1 Schiff bases

Aldehyde (or ketone) to Schiff base conversion is a reversible reaction that often occurs under acid (or base) catalysis or following heating. In most cases, the product is separated from the formation, the water is removed, or both are done. Aqueous acid or base has the ability to hydrolyze several Schiff bases back to their respective aldehydes, ketones, and amines. As depicted in Scheme 1.3 [28].



Scheme 1-3: Formation and hydrolyze back of Schiff base

Because of their wide range of biological activities, Schiff bases are frequently utilised as chelating ligands in coordination chemistry[10] and are crucial in the pharmaceutical industry. The majority of them exhibit biological properties such as herbicidal, antibacterial, antifungal, antidiabetic, antitumor, antiproliferative, and anticancer actions[11].

For their intriguing and significant characteristics, such as their ability to reversibly bind oxygen, catalytic activity in olefins hydrogenation and amino group transfer, photochromic properties, and complexing capacity towards specific toxic metals, a large number of Schiff bases and their complexes have been studied[12]. Schiff bases provide a flexible and adaptable set of ligands that can bind to various metal ions to produce complexes with properties that are acceptable for theoretical or practical application[13]. It has been demonstrated that an important chemical class in illuminating the transamination reaction mechanism in biological systems is the metal chelates from the Schiff bases derived from salicylaldehyde and amino acids[14].

1.9 Using silica as a solid support in metal ion extraction

Water metal contaminants have been removed using a variety of methods, including adsorption, precipitation, membrane filtration, and ion exchange. However, it has been demonstrated that adsorption is both affordable and efficient at removing heavy metals, organic pollutants, and colours from contaminated water. Activated carbon, silica, and graphene are just a few of the adsorbents that can be used to clean water[15].

It has been demonstrated that modified mesoporous silica is an efficient adsorbent for trace metal ions. The mesoporous silica's capacity for adsorption has been improved by the application of several optimization techniques[16].

The capture and removal of tiny amounts of metal from wastewater streams from different business operations is one of the most significant elements of today's study interest. As a result, there was great research potential for creating polysiloxane ligand systems (Figure 1.1), which can be used to preconcentrate and remove trace metal ions in a highly selective manner. Both hydrolytic polycondensation and silica modification were used to create these polysiloxane immobilised ligand complexes[10].

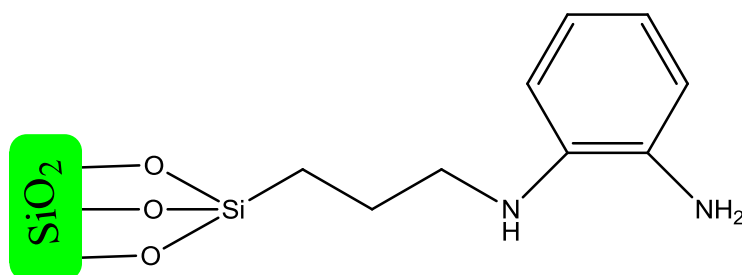


Figure 1-1 : 2-aminophenylaminopropylpolysiloxane ligand systeme

The removal of metal ions from aqueous solutions is one use for these polysiloxane immobilised ligand complexes. Compared to the more conventional organic resins and modified silica ligand architectures, these materials exhibit superior thermal and hydrolyte stability. Because they can chemisorb heavy metal ions consistently and selectively, chelating resins are frequently utilised to extract them from complex matrices[11]. It is possible to directly create these immobilised ligand complexes via the sol-gel method or by chemically altering the polysiloxanes generated in Figure 1.1[12].

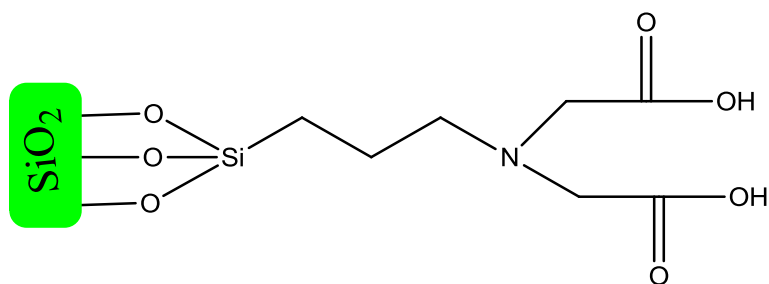
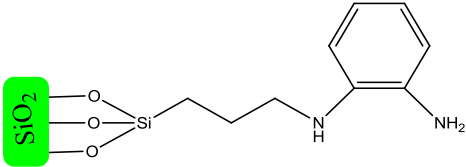
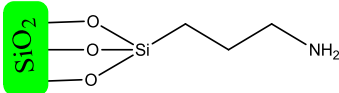
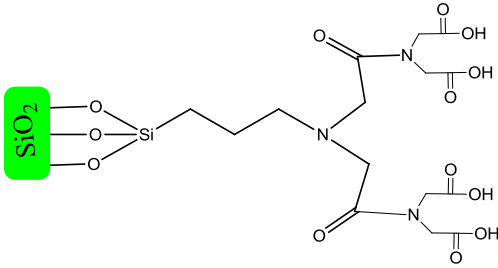
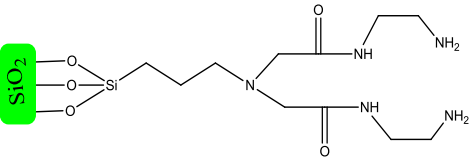
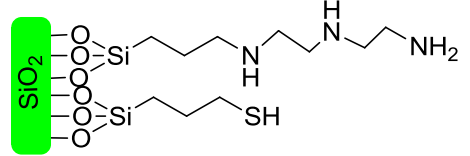
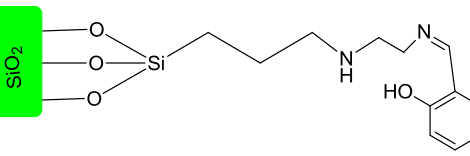
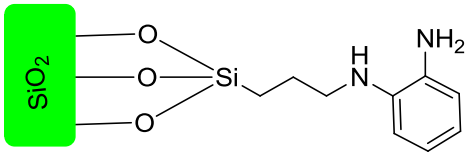


Figure 1-9 The functionalized polysiloxane immobilized iminodiacetic acid ligand system

In general, the presence of heavy metal ions in environmental samples has drawn more researchers' attention. A variety of ligands or functional groups are immobilised onto a sturdy support matrix as a solid phase extractant in order to extract and enrich trace metal ions from environmental specimens[14]. Table 1.1 displays a list of silica support materials along with examples of their applications.

Table 1-1: list of silica support materials along with examples of their applications.

Compound	Applications	Structure	Reference
γ -aminophenylaminopolysiloxae	Extraction of Co, Ni, Cu, Zn and Cd ion using γ -aminophenylaminopropylpolysiloxane		[٦٥].
γ -aminopropylpolysiloxane	Preconcentration and Separation of Copper(II) by γ -aminopropylpolysiloxane Immobilized Ligand System		[٦٨]
Di(amidomethyl)aminetetracetic Acid Polysiloxane	Extraction of divalent metal ions (Co(II), Ni(II), Cu(II), and Zn(II)) from aqueous solution		[٦٦]

<p>N-γ-aminoethylacetamide</p>	<p>Metal uptake by porous iminobis (N-γ-aminoethylacetamide)-modified polysiloxane ligand system</p>		<p>[٦٩]</p>
<p>Polysiloxane immobilized triaminethiol and thiol-acetate ligand system</p>	<p>Uptake of divalent metal ions (Cu^{2+}, Ni^{2+} and Co^{2+}) by polysiloxane immobilized triaminethiol and thiolacetate ligand system</p>		<p>[٧٠]</p>
<p>RHACSALEN ligand</p>	<p>Synthesis of Silica-Salen Derivative from Rice Husk Ash and its Use for Extraction of Divalent Metal Ions Co(II), Ni(II) and Cu(II)</p>		<p>[٧١]</p>
<p>Silica-o-Phenylenediamine</p>	<p>Uptake of Nickel(II) Ion by Silica-o-Phenylenediamine Derived from Rice Husk Ash</p>		<p>[٧٢]</p>

1.1 • Heavy metals pollution

In the environmental literature, the term "heavy metals" is frequently used to describe metals and metalloids linked to environmental pollution, toxicity, and negative effects on biota. The phrase has been defined in a variety of ways, primarily in relation to density, relative atomic mass, and atomic number.

Chemical definition: "a substance that conducts electricity, has a metallic lustre, is malleable and ductile, forms cations, and has basic oxides[¹³].

Although heavy metals are naturally occurring elements of the environment, human indiscriminate consumption has changed the geological cycles and biological equilibrium of these elements. This leads to an excessive release of heavy metals into natural resources including the soil and aquatic ecosystems, including cadmium, copper, lead, nickel, and zinc sources of heavy metals in the environment[¹⁴].

A Schiff base and its Ni(II) and Cu(II) complexes were synthesised by Leila Tahmasbia et al.[¹⁵] and supported on mesoporous silica nanoparticles. These hybrid composites were made to offer an adequate surface for effective interaction with medicines and enzymes (Figure 1-1 •).

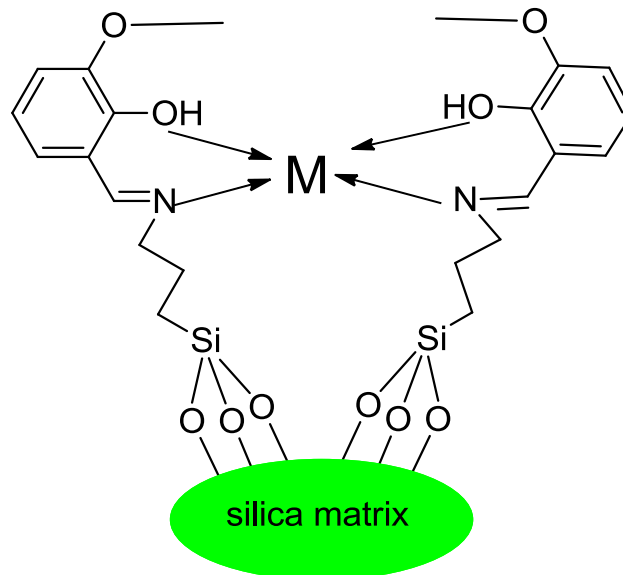


Figure 1-10 : Functionalized mesoporous silica nanoparticles

Anbarasu et al^[56], synthesised an immobilised silica material based on copper(II) Schiff base complex and γ -thio-phenecarboxaldehyde (Figure 1.11).

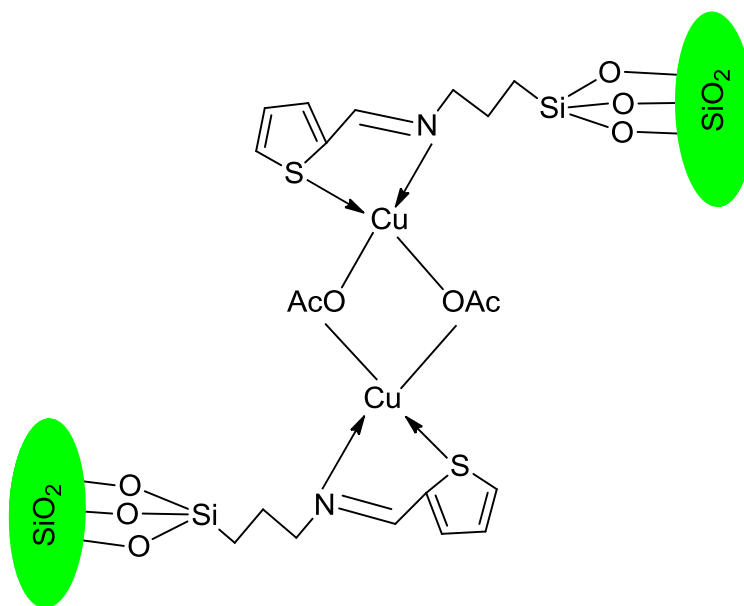


Figure 1-11 : copper(II) Schiff base complex and γ -thio-phenecarboxaldehyde

Sharma and Deepti Rawat^[55] Synthesized a covalently anchored nickel complex onto functionalized silica, depicted in Figure 1-12

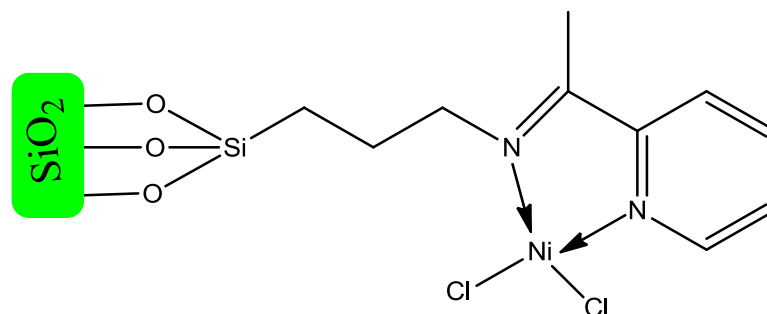


Figure 1-12 Ni(II) complex with functionalized silica

One of the most widely used cobalt compounds in laboratories is hexahydrate $\text{CoCl}_2 \cdot 6\text{H}_2\text{O}$, which is typically provided as cobalt (II) chloride^[56]. Cobalt and its many derivatives are widely used around the world and are thought to be potential environmental pollutants^[57].



Figure 1-13 Cobalt flakes

A cobalt (II) Schiff base complex supported by silica gel was created and utilised to oxidise alkyl aromatic compounds under atmospheric pressure

utilising molten oxygen as the oxidant. The synthesised catalyst demonstrated a high conversion of alkyl aromatics, was selective to benzylic ketones, and could be recycled at least five times without suffering any appreciable loss of catalytic activity[¹⁰].

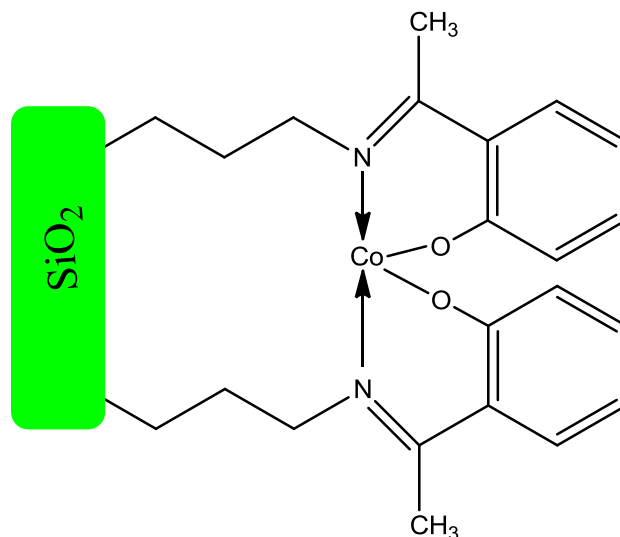


Figure 1-14 Cobalt (II) complex

The chemical atom of copper has the atomic symbol Cu which has an atomic mass of 63.5. Since the Romans first got their hands on copper metal from Cyprus, the term copper and the symbol Cu are derived from "aes cyprium" (later Cuprum) [¹¹]

As a trace dietary mineral, copper is necessary for all living things since it is an important part of the respiratory enzyme complex cytochrome c oxidase. The blood pigment hemocyanin contains copper in molluscs and crustaceans, while iron-complexed haemoglobin is used instead in fish and other vertebrates. Copper is primarily found in the liver, muscle, and bone of humans[¹²]. The amount of copper in an adult's body, per kilogramme of body weight, ranges from 1.5 to 2.1 mg [¹³].



Figure 1-15 Local Copper

Wen-Juan Zhou et al.[¹³], Figure 1-16, had created a copper (II) Schiff base complex with the N-(salicylaldimine)-(Npropyltrimethoxysilane)-diethylenetriamine.

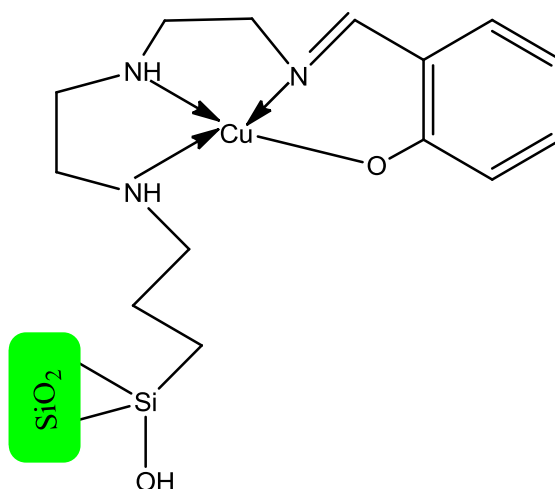


Figure 1-16 Copper complex

1.11 The Aims

1-Preparing some porous material derived from plant wastes, and their characterization using suitable physical measurements.

2- Addition of metallic nanoparticles MNPs to the prepared porous materials to obtain polymerically stable metallic nanoparticles PSMNPs and their characterization using suitable physical measurements. Such as: Fourier-transform infrared spectroscopy(FT-IR), CHNS Elemental analysis, Field Emission Scanning Electron Microscopy (FESEM), Scanning Electron Microscopy (SEM), Atomic Force Microscope(AFM), X-ray diffraction (XRD).

3- Functionalization of prepared porous material with some organic molecules to prepare solid ligands. and their characterization using suitable physical measurements. Such as: Fourier-transform infrared spectroscopy(FT-IR), CHNS Elemental analysis, Field Emission Scanning Electron Microscopy (FESEM), Transmission Electron Microscopy (TEM), Atomic Force Microscope(AFM), Energy Dispersive Spectroscopy (EDS), BET analysis, the N_2 adsorption-desorption isotherms, Thermogravimetric analysis (TGA/DTA) , X-ray diffraction (XRD).

4- Extraction of some metal ions from their aqueous solutions is suitable and optimize the physical and chemical parameters of the newly determined method, such as pH, concentration, and time of reaction etc.

CHAPTER TWO

EXPERIMENTAL PART



2. Experimental Part

2.1 Instruments:

Table 2-1 List of instruments, supplier companies and place of measurement

Instrument	Manufacturer	Place of measurement
FTIR	Shimadzu 8400S	University of Kerbala / College of science – Iraq
UV-Vis	Shimadzu double beam 1800 UV	University of Kerbala / College of science – Iraq
XRD	Shimadzu X-ray Diffractometer	Beam Gostar Taban Lab/Iran
SEM-EDX	FESEM MIRA III (TESCAN)	Beam Gostar Taban Lab/Iran
BET	BEL BELSORP MINI II	Beam Gostar Taban Lab/Iran
TGA/DTA	SDT Q600 V20.9 Build 20	Beam Gostar Taban Lab/Iran
CHNS	Eager 300 for EA1112	Beam Gostar Taban Lab/Iran
Water bath	Lab. Companion BS-11 shaking water	University of Kerbala / College of science – Iraq
Oven	Model un 110 plus	University of Kerbala / College of science – Iraq
Hot plate magnetic stirrer	LMS1003, Labtech, Techco, LTD	University of Kerbala / College of science – Iraq
TEM	Philips CM12	Beam Gostar Taban Lab/Iran
AFM	CSPM-AA3000	Beam Gostar Taban Lab/Iran
VSM	Xiamen Dexing Magnet Tech. Co., Ltd	Beam Gostar Taban Lab/Iran

2.2 Materials

All chemicals were used directly without further purification. Rice husks were collected from a local factory for rice production in Najaf Governorate-Abbasiya city. Table 2-2 shows the chemicals used in this work.

Table 2-2 Chemicals used in this work and their provider

Chemical	Formula	Purity (%)	Provider
Acetone	C_3H_6O	98	ROML British
Dimethylsulfoxide	$(CH_3)_2SO$	99	GCC, England
Ethanol	C_2H_5OH	99	Sigma-Aldrich, Germany
Toluene	C_7H_8	99	Merk, KGaA, Germany
γ-(aminopropyl)-triethoxysilane	$H_2N(CH_2)_3Si(OC_2H_5)_3$	99	Sigma-Aldrich, Germany
Nitric acid	HNO_3	70	CDH, India
γ-amino-γ,δ-Dibromobenzaldehyde	$C_7H_5Br_2NO$	99	CDH, India
Sodium hydroxide	$NaOH$	96	BDH, England
Ferric(III) Chloride hexahydrate	$FeCl_3 \cdot 6H_2O$	98	HIMEDIA
Urea	$CO(NH_2)_2$	98	HIMEDIA
Citric acid	$C_6H_8O_7$	98	HIMEDIA
Copper(II)chloride dehydrate	$CuCl_2 \cdot 2H_2O$	96	BDH, England
Nickel(II)chloride hexahydrate	$NiCl_2 \cdot 6H_2O$	96	BDH, England
Cobalt(II)chloride hexahydrate	$CoCl_2 \cdot 6H_2O$	97	BDH, England

2.3 The preparation methods

2.3.1. Preparation of sodium silicate solution and solid silica (RH-SiO₂) from rice husks

The rice husk (RH) was washed with distilled water for the first time to remove adhering materials. It was leached for about 24 h at room temperature. A 30.0 g sample of dried RH was weighed and transferred into a glass container. 500 mL of 1.0 M HNO₃ was added into the container and stirred for 24 h in order to remove unwanted metal. The acid treated RH-NO₃ was filtered and washed with distilled water until it reached a constant pH (7 - 7.5) and dried in oven at 110 °C overnight, The weight of the product is 26.6 g. The cleaned RH-NO₃ was stirred in 200 mL of 1.0 M NaOH for 24 h. The mixture was suction filtered to obtain a dark brown filtrate (sodium silicate) which was kept in a covered plastic container, as for the weight of the remaining cellulose on the filter paper, it is 22 grams.(i.e. the ratio of silica in used husk is 17%).

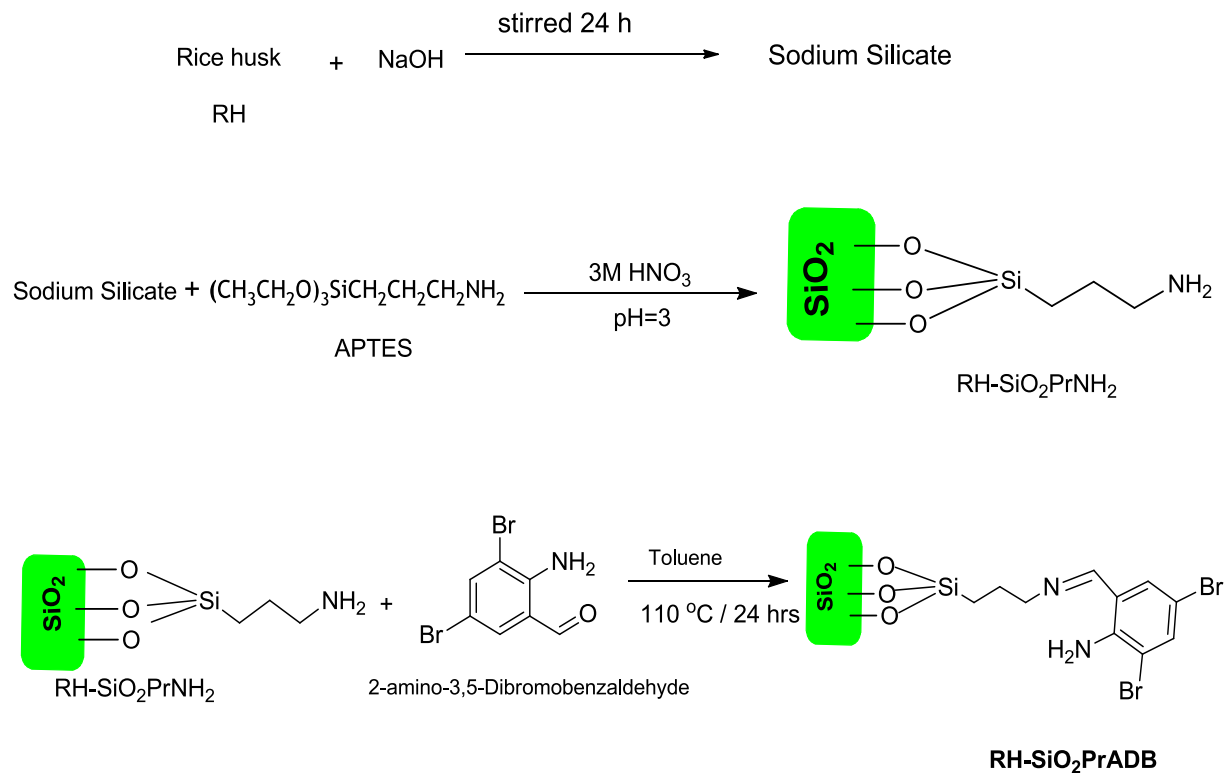
The prepared sodium silicate was titrated slowly with 3.0 M HNO₃ until it reached pH 9.5. The yellowish gel obtained was aged in a covered container for 3 days. The gel was recovered by centrifuge at 4000 r/minute and followed by washing with copious amount of distilled water. It was dried in an oven at 110 °C for 24 h. It was allowed to cool in a desiccator. Finally, the product (solid silica) was ground into fine powder labeled as RH-SiO₂. The weight of the product is 9 g.

2.1.2. Preparation of Rice Husk Silica- γ -(Aminopropyl) Triethoxysilane, RH-SiO $_2$ -PrNH $_2$

The prepared sodium silicate was added 6 mL of γ -(aminopropyl)triethoxysilane (APTES) and titrated with 3.0 M nitric acid until the value of pH reached to 3. The formed gel was separated by centrifuge at 4000 r/min for 10 min and washed with distilled water for five times and finally in acetone, then dried up to 24 h at 110°C in oven. The powder obtained was labeled as RH-SiO $_2$ -PrNH $_2$. The weight of the product was 8.5 g.

2.1.3. Preparation of Rice Husk Silica - γ -amino- β , δ -Dibromobenzaldehyde, RH-SiO $_2$ -PrADB

One gram of RH-SiO $_2$ -PrNH $_2$ was added to γ -amino- β , δ -dibromobenzaldehyde about 0.5 g and the mixture was refluxed in 30 mL of toluene at 110°C for 24 h. The yellow solid product was filtered and washed with an amount of ethanol, acetone and DMSO. Then dried at 110°C for 24 h. Finally, 1.1 g of powder obtained was labeled as RH-SiO $_2$ -PrADB.



Scheme 2-1: The synthesis steps of RH-SiO₂PrADB

2.1.4. Synthesis of magnetic Fe₃O₄ nanoparticles

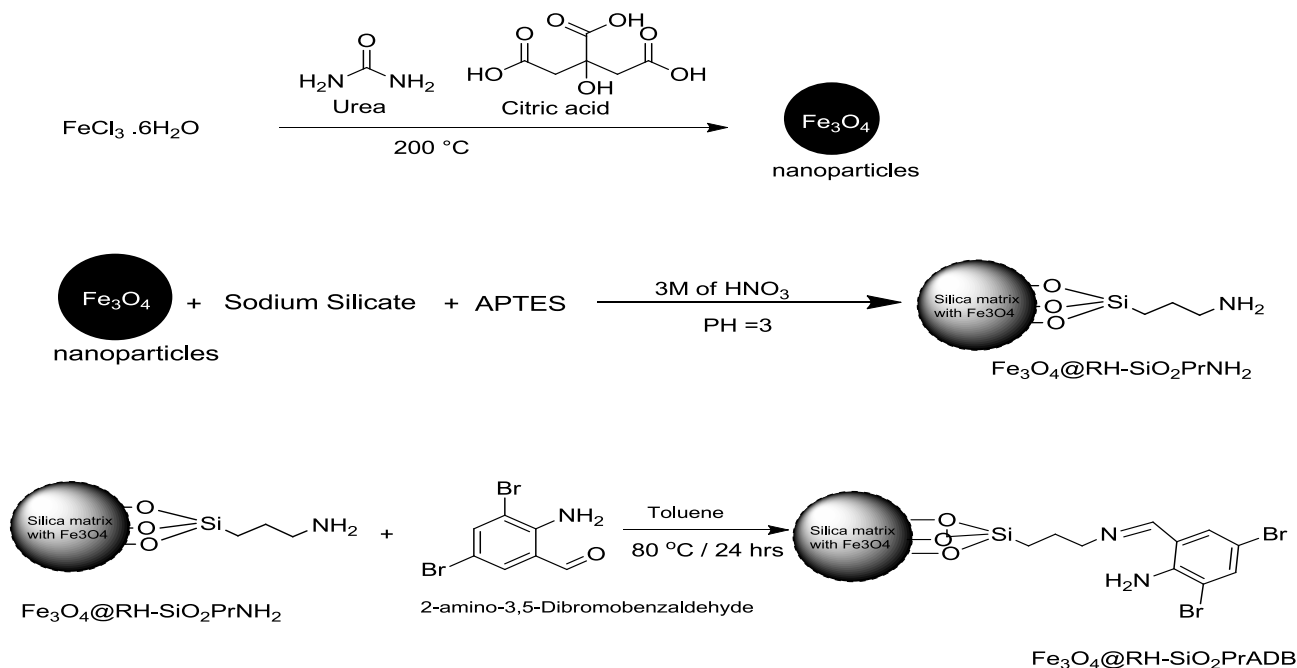
Fe₃O₄ nanoparticles method were synthesized through a solvothermal method. 6 g (0.022 mole) FeCl₃·6H₂O, 10 g (0.16 mole) Urea and 1.6 g (0.0083 mole) Citric acid were loaded into a 100 ml Teflon-lined stainless steel autoclave, which was then fill 60 mL absolute ethylene glycol (EG) heated to 200 °C and maintained there for about 18 h. After cooling to room temperature naturally. The black products were filtered off, washed with distilled water and ethanol for several times and dried in vacuum at 60 °C for 12 h.[14]

2.1.5. Synthesis of magnetic mesoporous silica; Fe₃O₄ @ RH-SiO₂-PrNH₂

One gram of Fe₃O₄ was added into sodium silicate for 30 minutes in Ultrasound. The mixture was treated with 1 ml APTES and titrated with 3.0 M nitric acid until the value of pH reached to 3, stirred for 24 h. The formed product was separated by centrifuge at 4000 r/min for 10 min and washed with distilled water for five times and finally in ethanol, then dried up to 24 h at 110°C in oven obtained black powder (0.5 g).

2.1.6. Synthesis of magnetic mesoporous silica Fe₃O₄ @ RH-SiO₂-PrADB

Three grams of Fe₃O₄@RH-SiO₂-PrNH₂ was added to 2-amino-3,5-dibromobenzaldehyde (1.0 g) and the mixture was refluxed in 30 mL of toluene at 110°C for 24 h. The dark brown solid product was filtered and washed with an amount of ethanol, acetone and DMSO. Then dried at 110°C for 24 h. Finally, 3.6 g of powder obtained.



Scheme 2-2: The synthesis steps of Fe₃O₄@RH-SiO₂PrADB

2.4 Removal of metal ions from aqueous solution

2.4.1. UV-Visible measurements for aqueous solutions of Ni(II), Co(II) and Cu(II)

UV-Visible spectroscopy of aqueous alternatives diluted Ni(II), Co(II) and Cu(II) was registered to explore λ max of each solution. The spectra acquired are shown in Figure 2.1. The spectra acquired shows that λ max of Ni(II), Co(II) and Cu(II) alternatives are 394, 511 and 809 nm respectively. These wavelengths were used in these solutions ' calibration research.

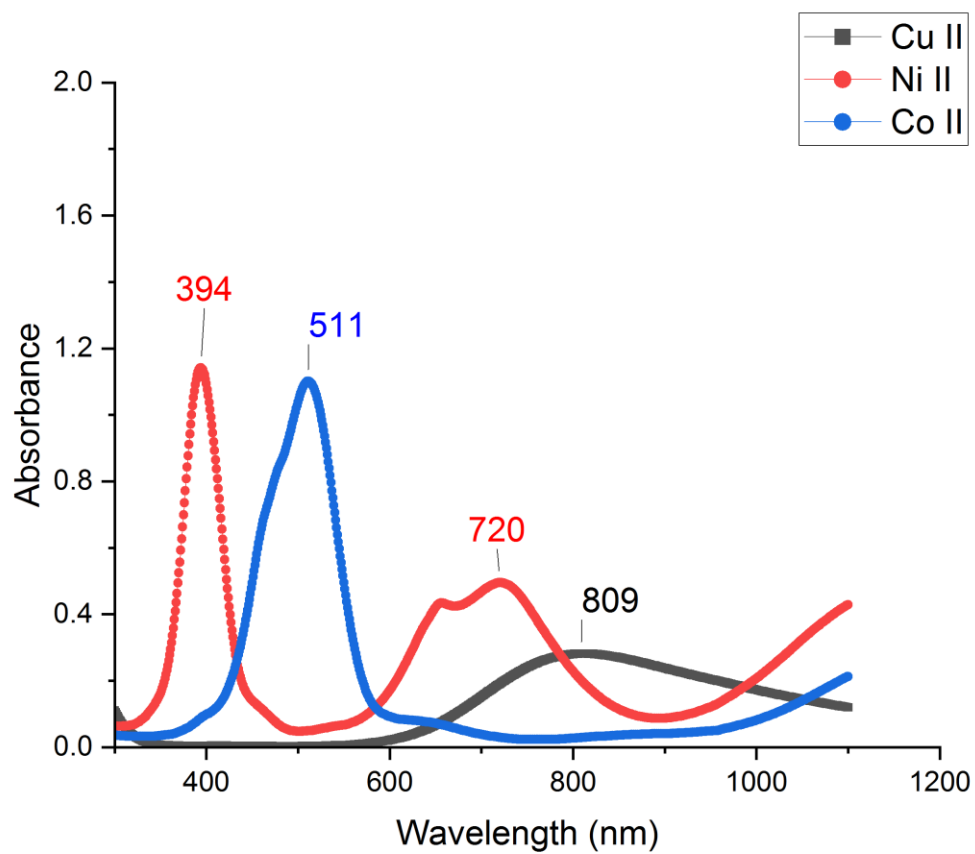
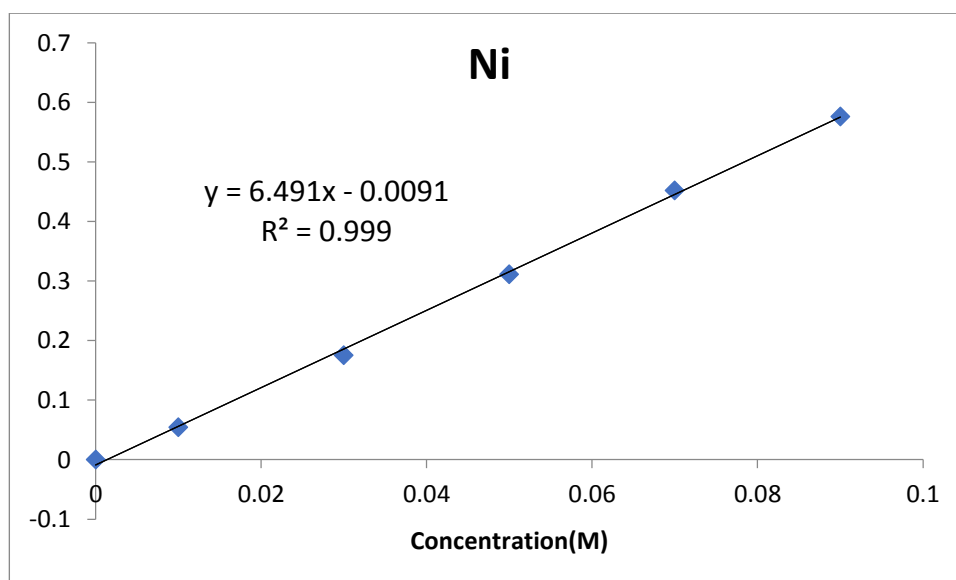
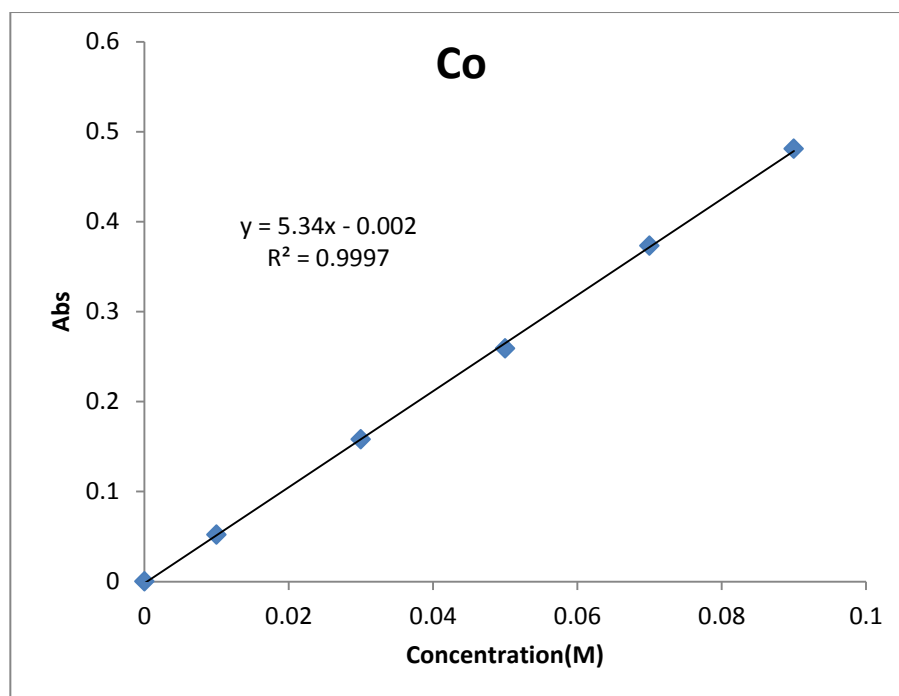


Figure 2-1 UV-Visible spectra of Ni(II), Co(II) and Cu(II) aqueous solutions

2.2. Calibration curve

Figure 2.2 shows the calibration curve of Ni(II), Co(II) and Cu(II) that performed by calculating the absorption of known metal concentration.



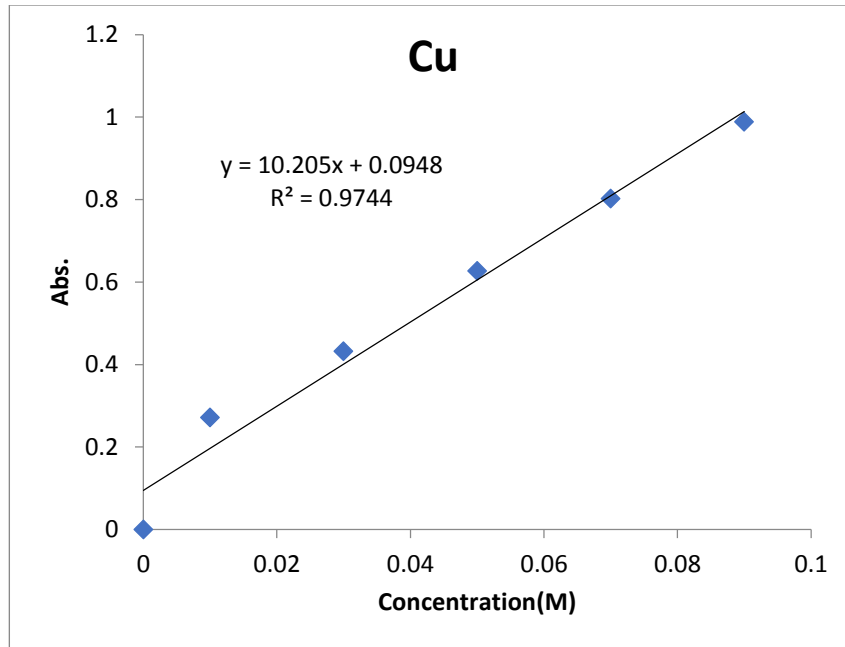


Figure 2-2 Calibration curve of Ni(II), Co(II) and Cu(II)

2.3. Tests on the absorption of metal

Two types of ligands (RH-SiO₂-PrADB & Fe₃O₄@RH-SiO₂-PrADB) were used to remove a number of ions represented by cobalt, nickel and copper. The method was done using a volumetric vial containing 10 mL of one of the ions such as cobalt with 0.02 g of one of the ligands such as of (RH-SiO₂-PrADB), and it was shaken for ten minutes. After that, 10 mL of the mixture was withdrawn and filtered. Through the needle of the syringe to remove the solid particles, then the residual concentration of the metal ion was measured by the solution absorption measurement every hour for ten hours. This method was used for nickel, and copper ions with one ligand at a time. The following equation was used to calculate the removal efficiency (E%) of copper, nickel and cobalt from aqueous solutions [10] :

$$\% E = \frac{C_o - C_e}{C_o} \times 100$$

Where C_o and C_e are the initial concentration at zero and the adsorbed concentrations after contact time, respectively, The effects of trembling time, pH effect, ion concentration, and weight for (RH-SiO₂PrADB & Fe₃O₄@RH-SiO₂PrADB) were studied as optimization conditions.

2.4. Optimization conditions:-

2.4.1. Experience Time

The impact of reaction time on the absorption of metal ions by (RH-SiO₂PrADB, Fe₃O₄@RH-SiO₂PrADB) were explored. The response was performed with 0.2 g ligands and shaken for 1 h with an aqueous solution of divalent metal ions. The absorption was calculated every 1 h.

2.4.2. Concentration of metal ion

The effect of metal ion concentration was studied using different concentrations (0.1 M, 0.2 M, 0.3 M, and 0.4 M) for each metal in with ligands (RH-SiO₂PrADB, Fe₃O₄@RH-SiO₂PrADB)

2.4.3. Weight of the ligand

The effect of the weight of the ligand was investigated using three different weights (0.1, 0.2, 0.3, 0.4 g) of ligands (RH-SiO₂PrADB, Fe₃O₄@RH-SiO₂PrADB)

2.4.4. Effect of pH

The effect of the pH function on the adsorption of ions by the prepared compounds was used pH (2, 3, 4).

Diagram: This diagram briefly explains the method of preparing the compounds $RH-SiO_2-PrNH_2$, $Fe_3O_4@RH-SiO_2-PrNH_2$, $RH-SiO_2-PrABD$ and $Fe_3O_4@RH-SiO_2-PrABD$

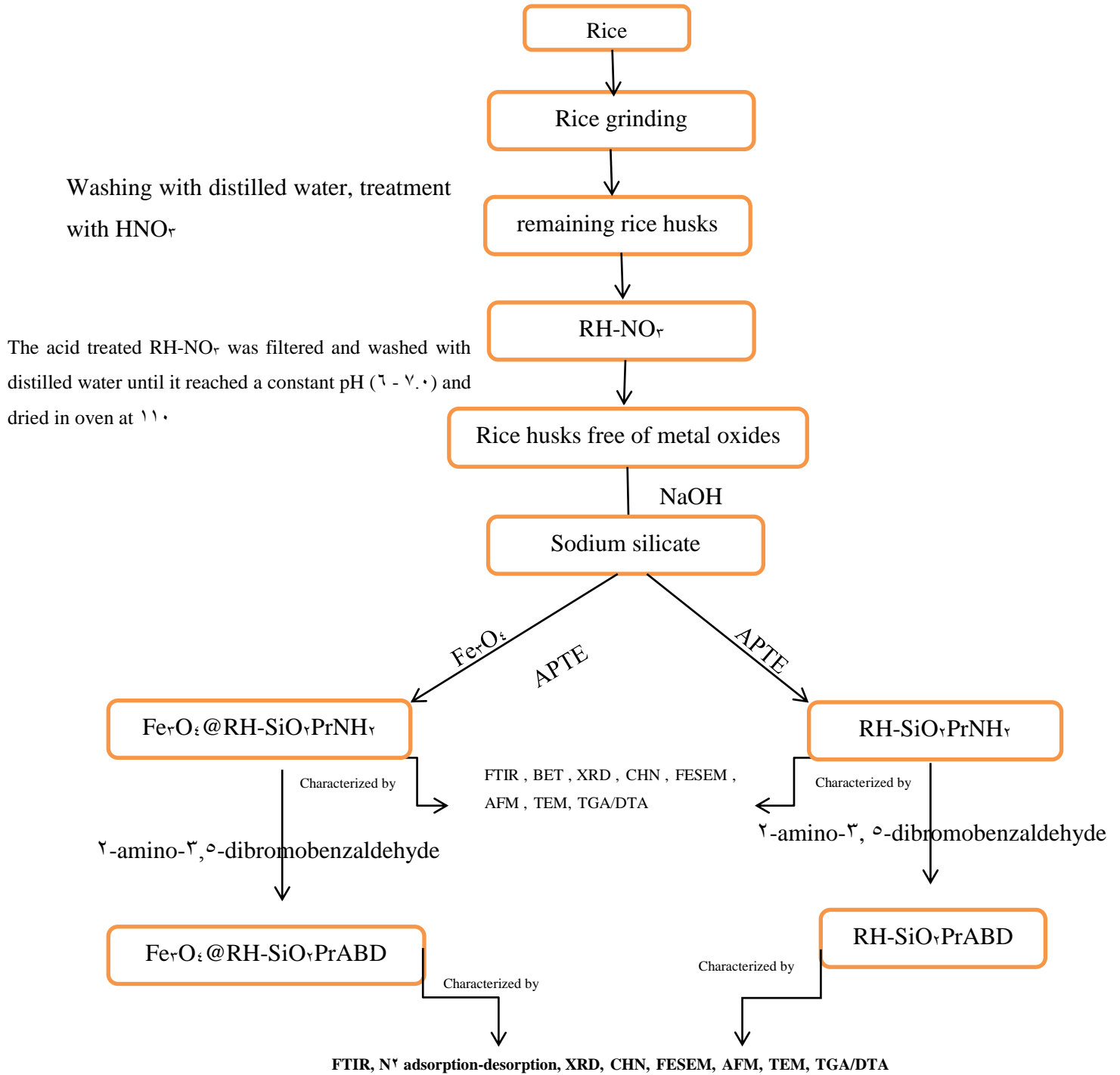


Figure 2-3 : Research progress and results continuation

CHAPTER THREE

RESULTS AND

DISCUSSION



3. Results and Discussion

3.1. Introduction

The researchers is moving towards using the best scientific methods to eliminate environmental pollution. Some metallic elements are natural and industrial pollutants like Cobalt, Copper, and Nickel. Rice husks can produce silica-based porous materials with a large surface area developed to eliminate these elements.

The method for preparing two types of porous materials includes washing rice husks with distilled water and then treating them with nitric acid. RH-NO_r was filtered and shaken in distilled water until it reached a stable pH (7 - 9). The product was dried at 110 °C in an oven overnight. After that reacted with sodium hydroxide to produce sodium silicate, which was finally ground to get a fine powder called RH-SiO_r. Sodium silicate was added to γ-(aminopropyl) triethoxysilane and calibrated with nitric acid (3 M) until the pH value reached 3, then the gel formed was separated by centrifuge after that washed away with distilled water and finally in γ-propanone. Then dried in an oven to produce a powder of RH-SiO_rPrNH_r.

Toluene was refluxed with the mixture of γ-amino-γ,δ-dibromobenzaldehyde and RH-SiO_rPrNH_r. The ethanol, acetone, and DMSO were used to filter and wash the yellow solid result. then 24 hours of drying at 110 °C. Finally, the resulting powder was identified as RH-SiO_rPrADB.

Fe_rO₃ was add into sodium silicate for 30 minutes in Ultrasound. The mixture was treated with APTES and titrated with 3.0 M nitric acid until the value of pH reached to 3, stirred for 4 h. The formed was separated by

centrifuge and washed with distilled water for five times and finally in ethanol, then dried up to 24 h at 110 °C in oven obtained Fe₃O₄@RH-SiO₂/PrNH₂ which was added to 2-amino-3,5-dibromobenzaldehyde and the mixture was refluxed in of toluene at 110 °C for 24 h . The dark brown solid product was filtered and washed with an amount of ethanol, acetone and DMSO. Then dried at 110 °C for 24 h.

3.2. Fourier Transform Infrared Spectroscopy (FTIR)

Infrared spectroscopy (IR spectroscopy or vibrational spectroscopy) is the measurement of the interaction of infrared radiation with matter by absorption, emission, or reflection. It is used to study and identify chemical substances or functional groups in solid, liquid, or gaseous forms.. The technique of infrared spectroscopy is conducted with an instrument called an infrared spectrometer (or spectrophotometer) which produces an infrared spectrum. An IR spectrum can be visualized in a graph of infrared light absorbance (or transmittance) on the vertical axis vs. frequency, wavenumber or wavelength on the horizontal axis. A common laboratory instrument that uses this technique is a Fourier transform infrared (FTIR) spectrometer. In order for a vibrational mode in a sample to be "IR active", it must be associated with changes in the molecular dipole moment. A permanent dipole is not necessary, as the rule requires only a change in dipole moment. Simple diatomic molecules have only one bond and only one vibrational band. If the molecule is symmetrical, e.g. N₂, the band is not observed in the IR spectrum, but only in the Raman spectrum. Asymmetrical diatomic molecules, e.g. carbon monoxide (CO), absorb in the IR spectrum. More complex molecules have many bonds, and their vibrational spectra are correspondingly more

complex, i.e. big molecules have many peaks in their IR spectra.[¹⁷]. Figure (3-1) shows FTIR for the compounds group was preparation.

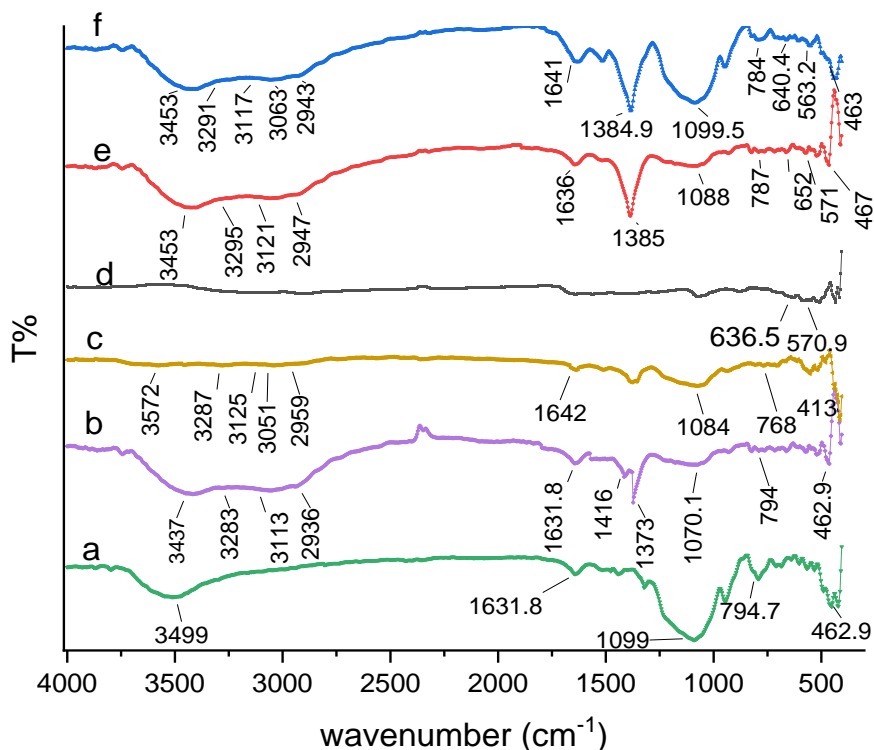


Figure 3-1 FTIR for (a) RH-SiO₂, (b) RH-SiO₂/PrNH₂, (c) Rhsio₂/PrADB (d) Fe₃O₄, (e) Fe₃O₄@RH-SiO₂/PrNH₂, (f) Fe₃O₄@RH-SiO₂/PrADB

Figure 3-1 A displays the FTIR of the rice husk (RH-SiO₂) which contains a group of distinct bands at 3499 cm⁻¹ and a medium sharp band at 1631 cm⁻¹, due to surface hydroxyls on the silica surface and coordination water [¹⁷].while the band at 1099 , 794.7 and 462 cm⁻¹ which hand over to siloxane to the expansion shaking of Si-O-Si bond[¹⁸]. Whilst Figure 3-1 B the FT-IR spectrum for RH-SiO₂/PrNH₂ showed that the vibration NH₂ and NH absorbed at 3283 and 3113 cm⁻¹, respectively. The C-H group in propyl moiety of RH-SiO₂/PrNH₂ absorbed at 2936 cm⁻¹. The C-H bending and CH₂

vibrations were assigned the bands at 1416 cm^{-1} and 1373 cm^{-1} , respectively [93]. Figure 3-1 C also displays the FT-IR spectrum for RH-SiO₂/PrADB gave bands as follows;. The C-H Aromatic peak is at 3051 cm^{-1} . The CH₂ moiety is responsible for the peak at 2909 cm^{-1} [89]. The azomethine group (C=N) is represented by the peak at 1642 cm^{-1} [90]. Figure 3-1d indicates that The FTIR spectrum of iron oxide (Fe₃O₄) showed an absorption band at 736.0 and 570.9 cm^{-1} due to Fe-O bond [91]. As shown in Figure 3-1e the FT-IR spectrum for Fe₃O₄@RH-SiO₂/PrNH₂ showed that the absorption bands same absorption for Fe₃O₄ and RH-SiO₂/PrNH₂ [92]. Whilst Figure 3-1f shows the FTIR spectrum of Fe₃O₄@RH-SiO₂/PrADB showed that the absorption bands same absorptions for compounds Fe₃O₄ and RH-SiO₂/PrADB [90].

3.3. Surface area analysis

Adsorption of gases onto porous particles is one of the key methods for defining the shapes of ceramic substances. The most important morphological parameters can be determined or inferred from analyses of the connection between the amount of material adsorbed and the pressure distribution of a physiologically adsorbing gas. These calculations and estimates are based on the pore representation assumptions and the equations connecting the pressure distribution to the gaseous physisorbed state [93]. As a result, the Brunauer-Emmett-Teller (BET) gas adsorption approach has emerged as the most popular standard method for calculating the surface area of finely split and porous materials.. Using the Barrett- Joyner-Halenda (BJH) method, the materials pore diameter and pore size distribution were determined using the adsorption isotherms [94].

The IUPAC in Figure(3-2) has given an empirical classification of hysteresis loops in which the shape of the hysteresis loops (types H¹–H⁴). The technique of a microporous adsorbent is often described by type I isotherm, which approaches a limit value. With weak and strong adsorbate and adsorbent interactions, respectively, Types II and III characterise the adsorption of macroporous adsorbents. Types IV and V consist of capillary condensation in addition to mono- and multi-layer adsorption. Adsorption isotherms may contain one or more steps, as demonstrated by Type VI, which wasn't included in the Gibbs classification.[90]. Table (3-1) and Figure (3-3) show information about the results obtained regarding the value of the specific surface area, pore diameter, and hysteresis loops for the prepared compounds.

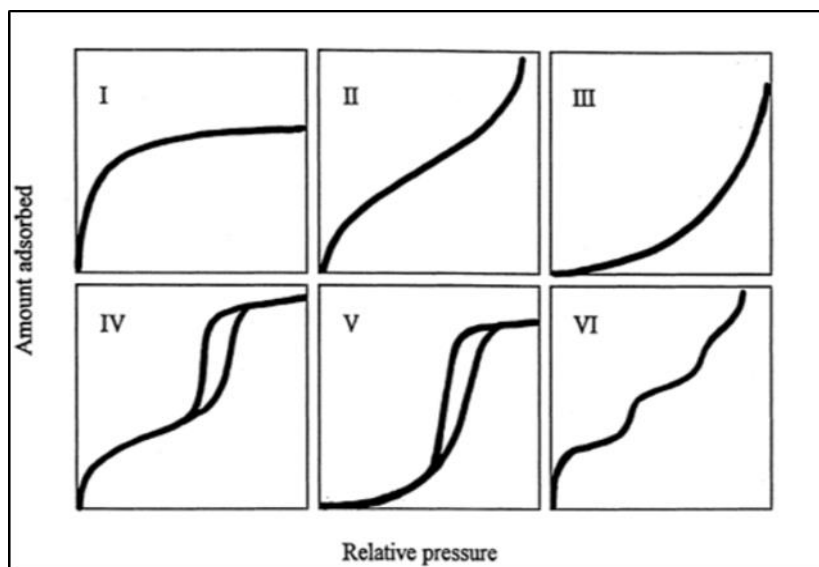
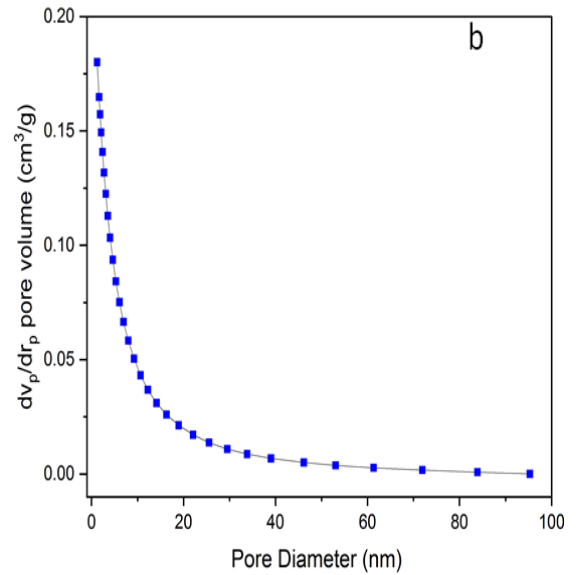
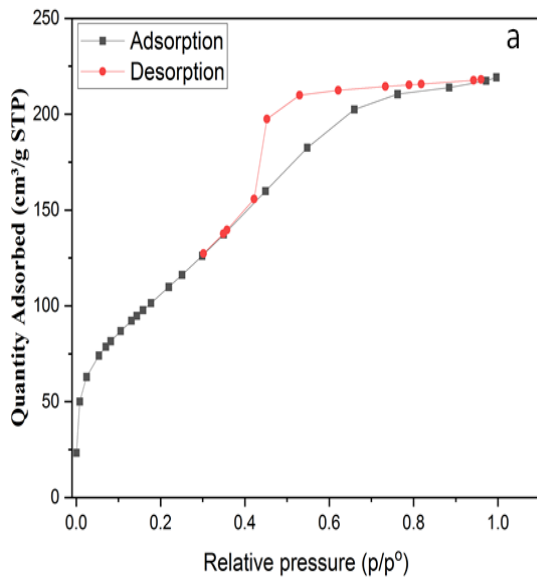
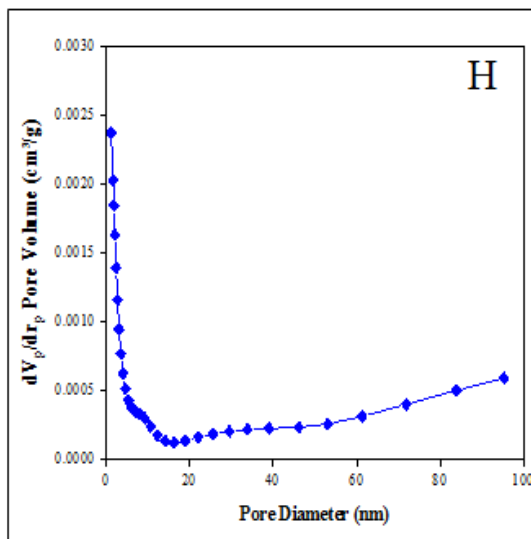
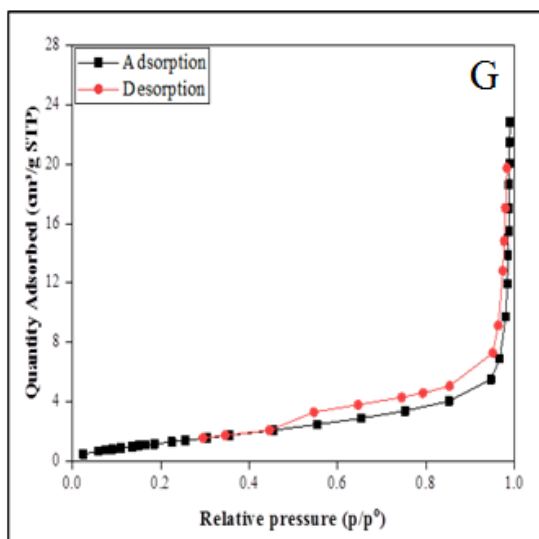
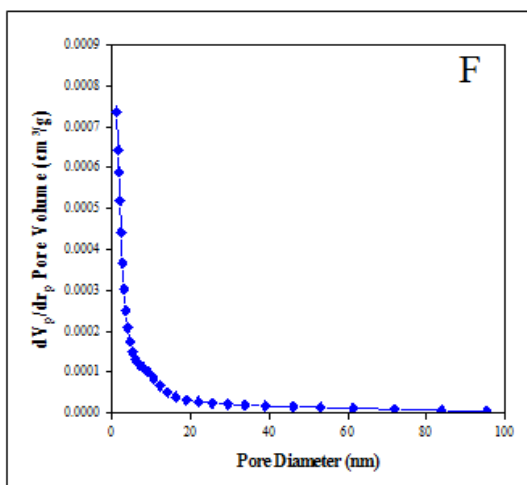
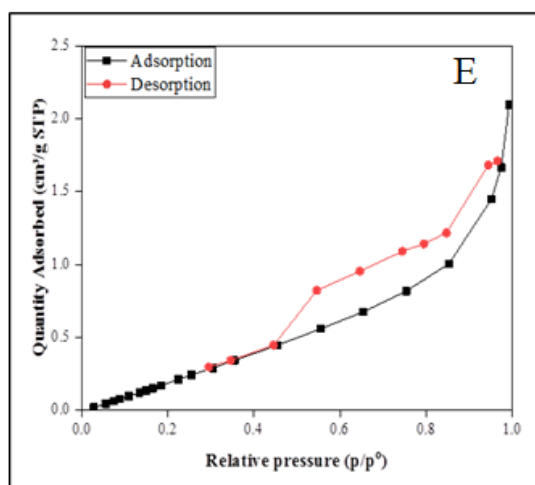
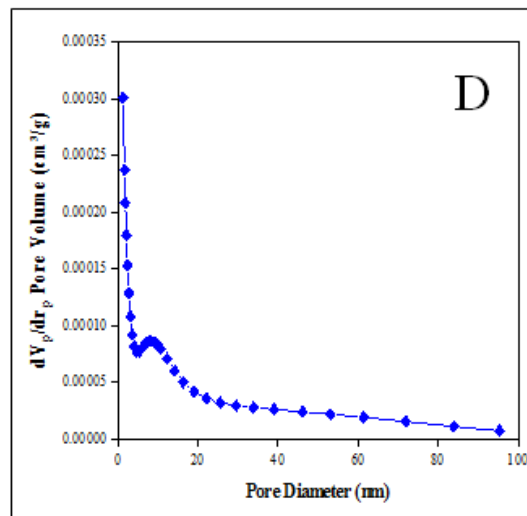
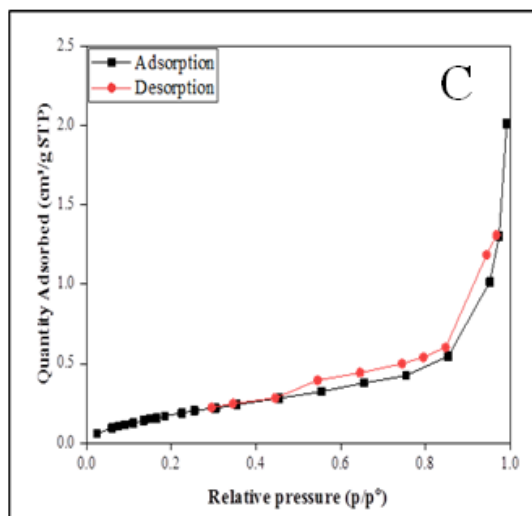


Figure 3-2 The IUPAC Classification of Adsorption Isotherms[90]

Table 3-1 Surface area analysis (BET, BJH) of RH-SiO₂/PrNH₂, Fe₃O₄@RH-SiO₂/PrNH₂, RH-SiO₂/PrADB, and Fe₃O₄@RH-SiO₂/PrADB

Sample	Specific surface area (m ² /g)	Average pore volume	Mean pore diameter (nm)
RH-SiO ₂	390.12	0.307	3.4698
RH-SiO ₂ /PrNH ₂	0.789	0.030	10.000
Fe ₃ O ₄ @RH-SiO ₂ /PrNH ₂	0.093	0.030	21.078
RH-SiO ₂ /PrADB	3.818	0.301	36.216
Fe ₃ O ₄ @RH-SiO ₂ /PrADB	3.076	0.161	16.086





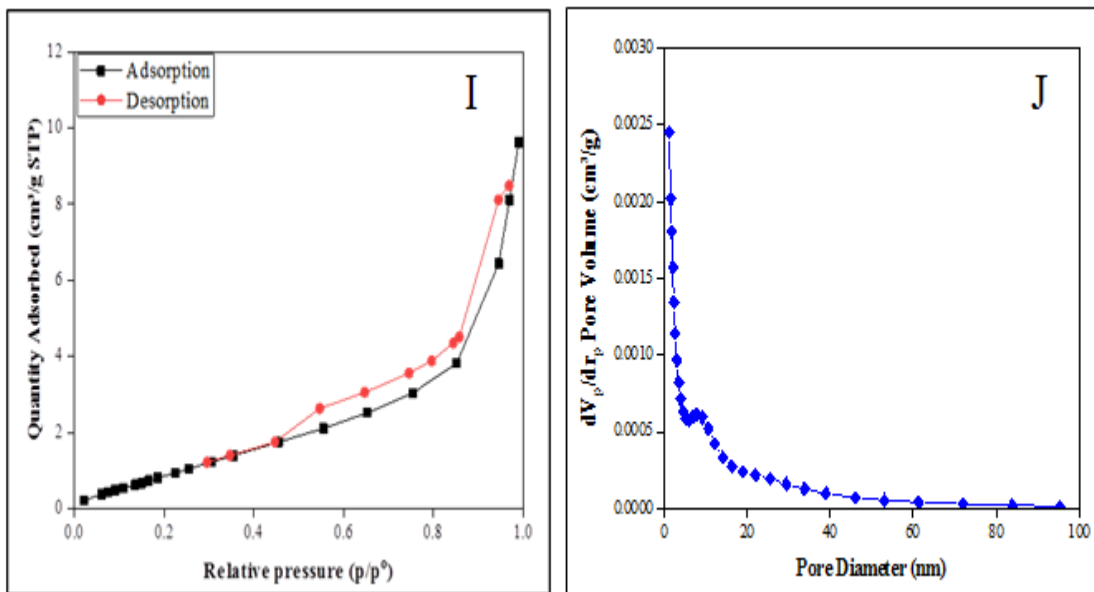


Figure 3-3: (a) Nitrogen adsorption-desorption isotherm, (b) pore size distribution for the RH-SiO₂ (C) Nitrogen adsorption-desorption isotherm (D) pore size distribution for RH-SiO₂/PrNH₂ (E) Nitrogen adsorption-desorption isotherm, (F) pore size distribution for the Fe₃O₄@RH-SiO₂/PrNH₂ (G) Nitrogen adsorption-desorption isotherm, (H) pore size distribution for the RH-SiO₂/PrADB (I) Nitrogen adsorption-desorption isotherm, (J) pore size distribution for the Fe₃O₄@RH-SiO₂/prADB

The results showed that the mean pore diameter of the RH-SiO₂ sample is 3.4698 nm and has a pore size distribution which occur between (2 and 20 nm) which fall in the mesoporous range, as shown in Figure(3-2a and b) and Table (3-1). The results showed that the adsorption and desorption isotherms follow type (IV) and show H₂ hysteresis loops based on the IUPAC classification. Hysteresis H₂ is often associated with a pore shape resembling a round-bottom flask[96]. While the mean pore diameter value of the RH-SiO₂/PrNH₂ sample is 10.000 nm and has a pore size distribution which occur between (2 and 10 nm) which fall in the mesoporous range, as shown in

Figure(3-2 C and D) and Table (3-1). The adsorption-desorption isotherm follows the (IV) type and hysteresis loops H₃, this indicates strong attractive interactions between the molecules. In contrast, the mean pore diameter value in the Fe₃O₄@RH-SiO₂/PrNH₂ sample decreased to up to 21.07 nm, and has a pore size distribution which occur between (2 and 10 nm) which falls in the mesoporous range as shown in Figure(3-2 E and F) and Table (3-1). This refers to the immobilization of Fe₃O₄ nanoparticles on the RH-SiO₂/PrNH₂ surface. Adsorption-desorption isotherm belongs to type (IV) and the hysteresis loop is of type (H₃). This indicates the presence of narrow interconnected pores with a complex network. whilst mean pore diameter of the RH-SiO₂/PrADB were using BET analysis, to be equal to 36.21 nm, and has a pore size distribution which occur between (2 and 10 nm) which falls in the mesoporous range as shown in Figure(3-2 G and H) and Table (3-1). These isotherms exhibited a typical type IV curve and the hysteresis loop is of type (H₃). It was noted that the reaction of RH-SiO₂/PrNH₂ with the 2-amino-3,5-Dibromobenzaldehyde compound increased the value of the surface area as a result of the presence of a carbon network that works to increase the effective sites, and this makes the surface highly effective towards adsorbed nitrogen gas. This type of isotherm shows that the particles are plate-like[50]. The mean pore diameter of Fe₃O₄@RH-SiO₂/PrADB was 16.08 nm and has a pore size distribution which occur between (2 and 10 nm) which falls in the mesoporous range, as shown in Figure(3-2 I and J) and Table (3-1) which was decreased compared with the specific surface area of RH-SiO₂/PrADB. This is due to the attachment of Fe₃O₄ particles to an RH-SiO₂/prADB surface, which reduces the surface area. The adsorption-desorption isotherm follows the (III) type and hysteresis loops H₃.

3.4. X-ray Diffraction analysis XRD

The innovation of X-rays paved the way for important developments in all branches of science as well as the invention of new technological applications. The investigation of X-ray diffraction (XRD) by crystals has given a new direction to the study of crystalline materials. These processes have now undergone predictive refinement into highly effective tools in the fields of engineering and materials science. Experimental X-ray processes have three basic categories that are used in materials science and engineering. X-ray spectroscopy is often used in quantitative and qualitative chemical study, particularly with electron microscopes. In X-ray radiography, the force flowing from a material is recorded using films or detectors, which, thanks to a local change in absorption, allow one to examine the internal structure of the item. One of the most important developments in this field over the past few decades is X-ray tomography. XRD techniques, which allow a comprehensive analysis of the structure of crystal phases, are based on the ability of the crystals to have X-ray diffraction. Several micro-sample components and the overall structure additionally contributed to the obtained diffraction patterns. The peak position can be used to study lattice properties, space groups, chemical composition, or qualitative phase analyses. The peak intensity can be used for crystal structure determination (atomic position, temperature factor, occupancy), quantitative phase analyses, and other information. Finally, the peak pattern reveals the sample magnification aids (microstrains and crystal size) That is, XRD analysis reveals whether the materials are crystalline or non-crystalline^[97]. The crystalline type, phase, and crystal size of solid nanomaterials can be ascertained quickly and accurately by XRD analysis^[98]. Figure (3-4) shows the XRD spectrum of compounds that were prepared.

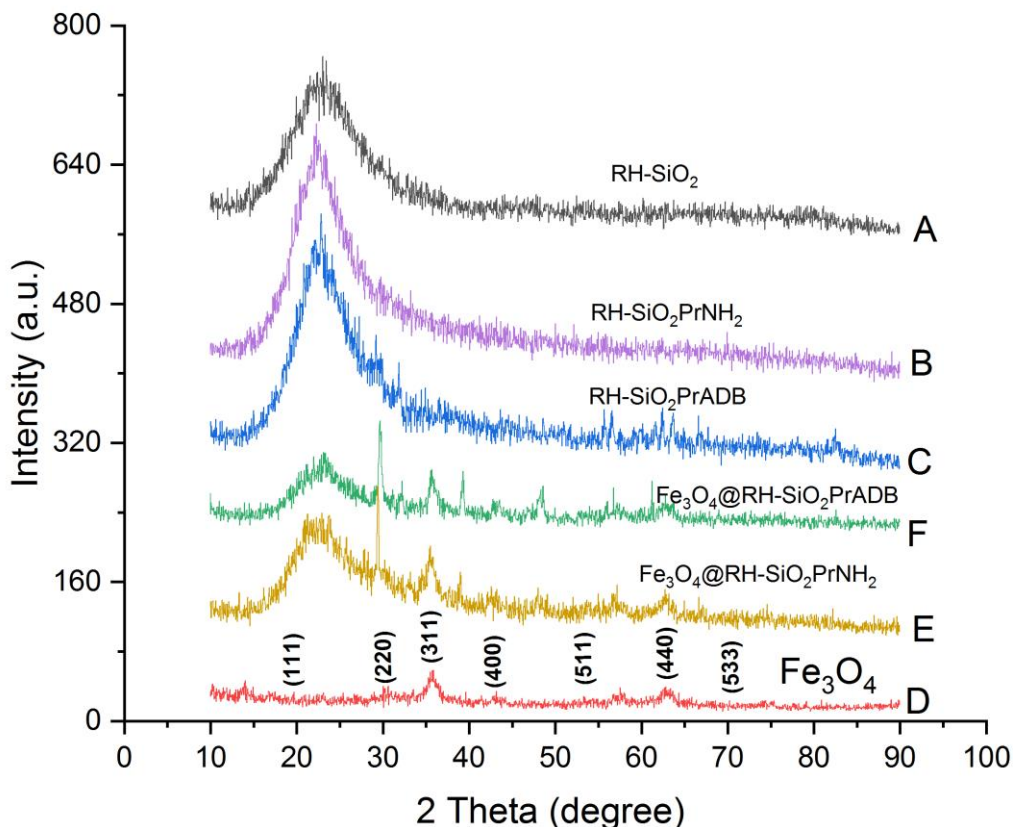


Figure 3-4: XRD spectrum for (A) RH-SiO₂, (B) RH-SiO₂PrNH₂, (C) RH-SiO₂PrADB (D) Fe₃O₄, (E) Fe₃O₄@RH-SiO₂PrNH₂, (F) Fe₃O₄@RH-SiO₂PrADB

The XRD spectrum of RH-SiO₂ in Figure 3-4A the existence of a wide diffraction peak at ($2\theta = 22.2^\circ$) and the absence of sharp peaks in the other regions of the spectrum indicates the amorphous nature of the prepared RH-SiO₂ sample. While RH-SiO₂PrNH₂ can show in Figure 3-4B. As the spectrum showed the existence of a wide diffraction peak at ($2\theta = 22^\circ$) and the absence of sharp peaks in the other regions of the spectrum indicates the amorphous nature of the prepared RH-SiO₂PrNH₂ sample [99]. Figure 3-4C shows the RH-SiO₂PrADB sample. As it was noticed that sharp peaks disappeared in the spectrum with the existence of one broad peak at ($2\theta = 22.0^\circ$). The spectrum

data confirmed that the material is of an amorphous nature and high purity because no additional peaks appeared in the spectrum [100].

XRD patterns of Fe₃O₄ NPs are shown in Figure 3-4D. The diffraction peaks of $2\theta = 30.33^\circ, 35.61^\circ, 43.03^\circ, 53.17^\circ, 57.72^\circ, \text{ and } 62.66^\circ$ were visible in the XRD patterns of Fe₃O₄ NPs. This illustrates Fe₃O₄'s cubic spinel structure (JCPDS Card No. 19-0629). The exceptional purity of the Fe₃O₄ NPs is indicated by the absence of other peaks in the spectrum [100]. The crystalline size of all compounds was calculated according to the Scherrer equation as shown in Table (3-2).

$$D = \frac{K * \lambda}{\beta * \cos(\theta)}$$

Where (D) Crystallite size, (K) A dimensionless shape factor with a value without unity. The shape factor has a typical value of about 0.9, but varies with the actual shape of the crystallite, (λ) is the X-ray wavelength, (β) is the line broadening at half the maximum intensity (FWHM) and (θ) is the Bragg angle, While showed the **Figure 3-4E** XRD spectrum of the Fe₃O₄@RH-SiO₂/PrNH₂ composite showed diffraction peaks at ($2\theta = 29.6^\circ, 32.3^\circ, 35.7^\circ, 39.2^\circ, 43.1^\circ, 48.5^\circ, 56.8^\circ, 61.3^\circ, 62.7^\circ$) assigned to the cubic crystalline structure of Fe₃O₄, and the broad peak ($2\theta = 17.8^\circ - 28.6^\circ$) due to the presence of carbon in the RH-SiO₂/PrNH₂ structure, as in the Figure 3-17. This indicates the success of the Fe₃O₄ bonding with the RH-SiO₂/PrNH₂, which has an amorphous nature (102). On the other hand, the XRD spectrum of the Fe₃O₄@RH-SiO₂/PrABD in **Figure 3-4F** composite showed a clear displacement in the broad peak at ($2\theta = 18.6^\circ - 28.8^\circ$) due to RH-SiO₂/PrABD compound and sharp peaks at ($2\theta = 29.2^\circ, 35.4^\circ, 39.1^\circ, 42.4^\circ, 47.9^\circ, 57.4^\circ,$

62.8°, 67.0°) due to the cubic structure of Fe₃O₄. As it was noted that the prepared composite is of an amorphous nature.

Table 3-2 Crystallite size and Average crystallite size of Fe₃O₄, Fe₃O₄@RH-SiO₂PrNH₂ and Fe₃O₄@ RH-SiO₂PrABD

Compounds	Pos. [°Th.]	FWHM [°Th.]	Rel. Int. [%]	crystallite size D (nm)	D(nm) Average)
Fe ₃ O ₄	14.8677	0.2773	01.20	28.896	18.713
	30.7926	0.02	100	16.004	
	04.274	0.4402	30.84	20.002	
	62.7209	0.984	43.41	9.400	
Fe ₃ O ₄ @RH-SiO ₂ PrNH ₂	30.1023	0.0761	74.01	14.281	34.066
	30.70	0.7160	100	13.040	
	61.2990	0.1217	83.01	70.878	
Fe ₃ O ₄ @ RH-SiO ₂ PrABD	29.70	0.0641	40.37	14.071	41.141
	30.4967	0.4842	100	17.227	
	39.0249	0.2833	01.02	29.701	
	62.6966	0.0903	46.01	103.010	

3.5. Elemental Analysis (CHN)

Determine the carbon (C), hydrogen (H), and nitrogen (N) contents of organic and inorganic samples using CHN elemental analysis. Can identify even minute amounts of elements and the technique is dependent on the sample being completely burned. Solid, liquid, volatile, and viscous materials can all be subjected to CHN measurements. The sample size can be quite small. Based on the conventional Pregl-Dumas method, this analysis is

conducted at a high temperature (about 1000°C) in an oxygen-rich environment[1, 2].

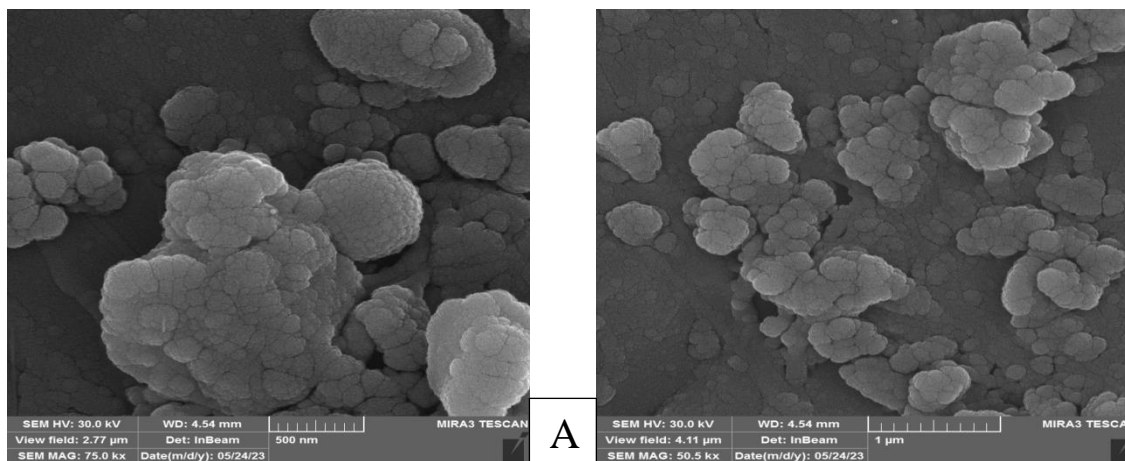
Table (3-3) shows the results obtained for the ratio of carbon and Nitrogen as it was for the compound RH-SiO₂ showing that the percentage of carbon and nitrogen reaches 8.6% and 0.0%. The RH-SiO₂PrNH₂ showed that the percentage of carbon and nitrogen reaches 14.44% and 8.46%, respectively. On the other hand, their percentage in the Fe₂O₃@RH-SiO₂PrNH₂ compound decreased slightly, which indicates the success of the ligand binding with Fe₂O₃. Also, the elemental analysis of the RH-SiO₂PrADB compound indicates that the percentage of carbon and nitrogen is 16.63% and 6.4%, as the high percentage of carbon is due to the association of the RH-SiO₂PrNH₂ with 2-amino-3,5-Dibromobenzaldehyde. As it was observed that the association of the RH-SiO₂PrADB with Fe₂O₃ increases the percentage of carbon to about 18.77%. The silica extraction process was carried out by base digestion and not by burning, and therefore there was a percentage of organic materials in the sodium silicate solution and thus appeared in the CHN analysis[1, 3].

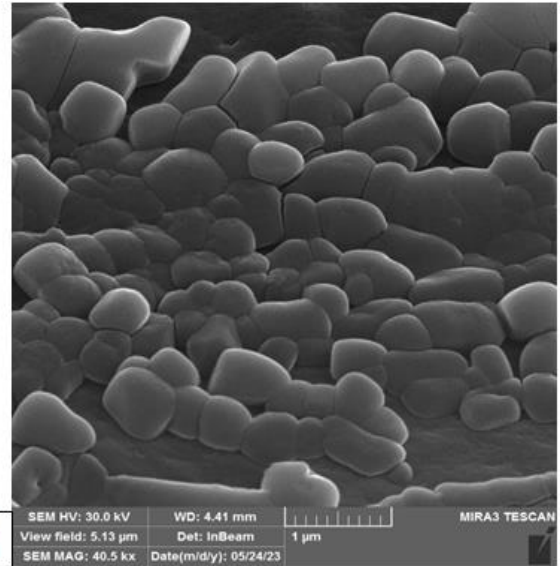
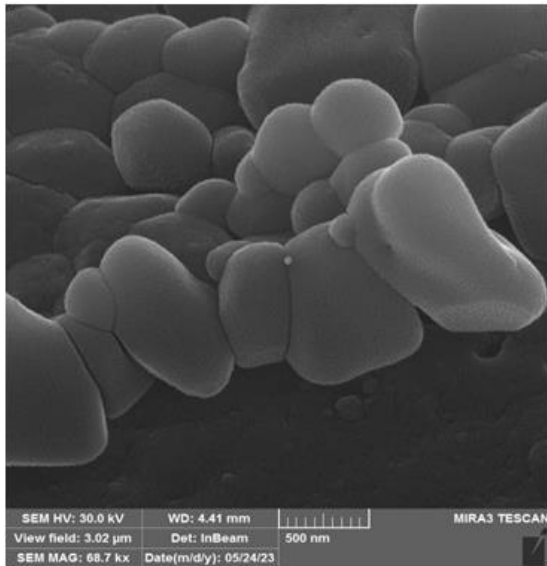
Table 3-3 : Chemical analysis of RH-SiO₂, RH-SiO₂PrNH₂, Fe₂O₃@RH-SiO₂PrNH₂, RH-SiO₂PrADB, and Fe₂O₃@RH-SiO₂PrADB using CHN

Sample	C (%)	H (%)	N (%)
RH-SiO ₂	8.6	2.64	0.0
RH-SiO ₂ PrNH ₂	14.44	2.60	8.46
Fe ₂ O ₃ @RH-SiO ₂ PrNH ₂	14.43	3.13	8.2
RH-SiO ₂ prADB	16.63	3.16	6.4
Fe ₂ O ₃ @RH-SiO ₂ PrADB	18.77	0.90	7.0

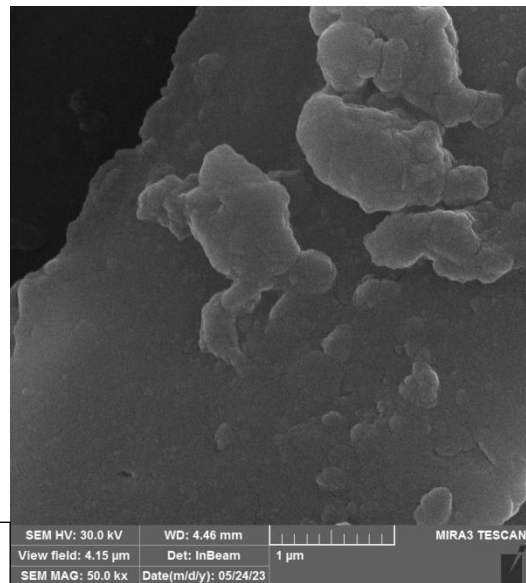
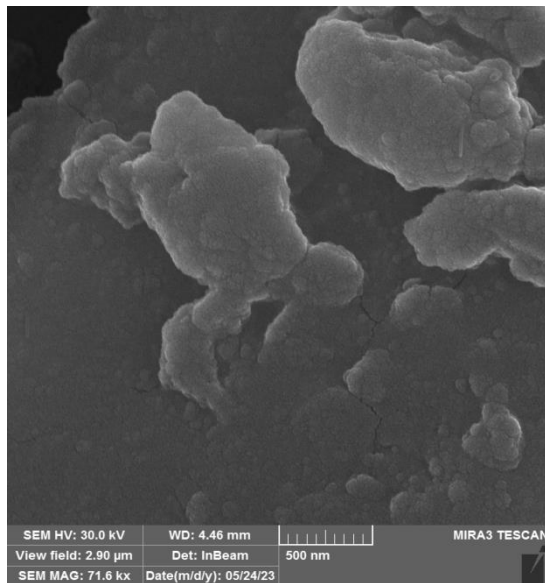
3.6. Field emission scanning electron microscopy (FESEM)

FESEM is an important technique that reveals the morphology, size, and crystalline nature of the prepared compounds. Secondary electrons are released from the sample surface when it is exposed to a strong electron beam (also known as an electron probe). Surface morphology can be seen by performing a double-dimensional scan of the electron sample over the surface and acquiring an image from the secondary electrons found [14]. Figure (3-5) shows the FESEM images for the group of compounds that were prepared. while Figure (3-6) displays the EDX analysis for the group of compounds that were prepared.





B



C

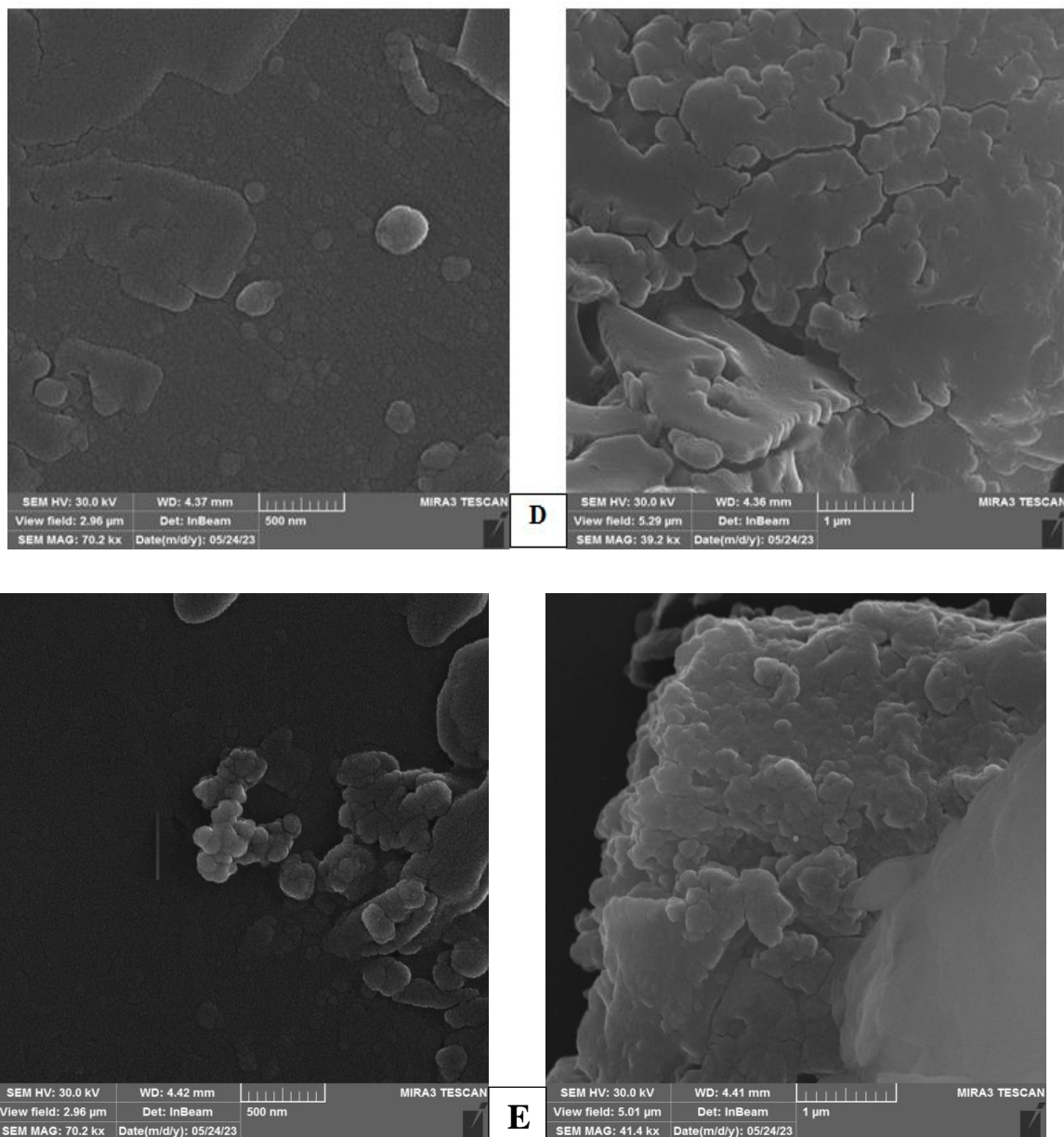


Figure 3-5 FESEM images for (A) RH-SiO₂, (B) RH-SiO₂/PrNH₂, (C) RH-SiO₂/PrADB, (D) Fe₃O₄@ RH-SiO₂/PrNH₂, (E) Fe₃O₄@ RH-SiO₂/PrADB

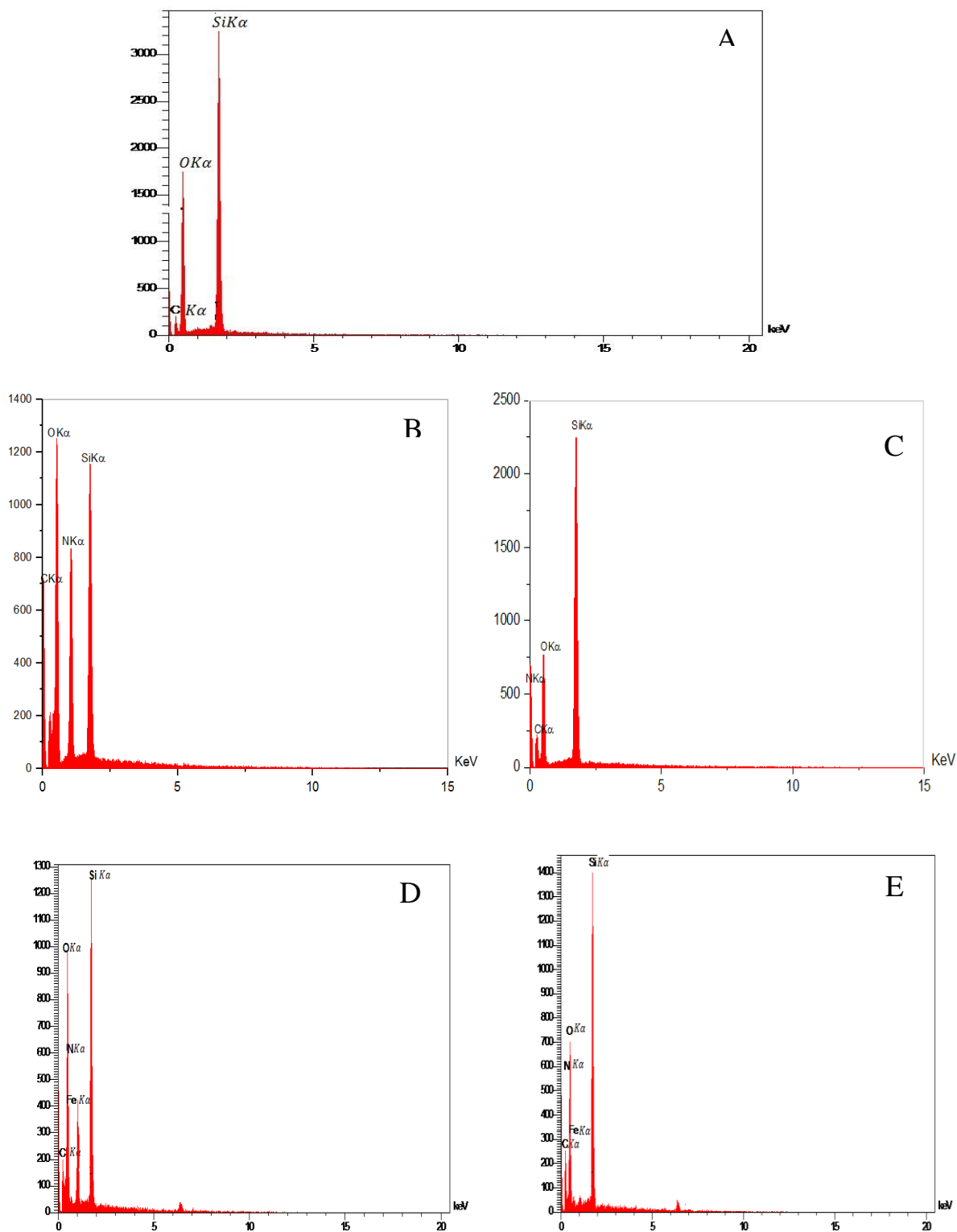


Figure 3-3 EDX chart for (A) RH-SiO₂ (B) RH-SiO₂PrNH₃ (C) RH-SiO₂PrADB (D) Fe₃O₄@ RH-SiO₂PrNH₃ (E) Fe₃O₄@ RH-SiO₂PrADB

Table 3-4 : shows the EDX analysis the weight percentages of compound

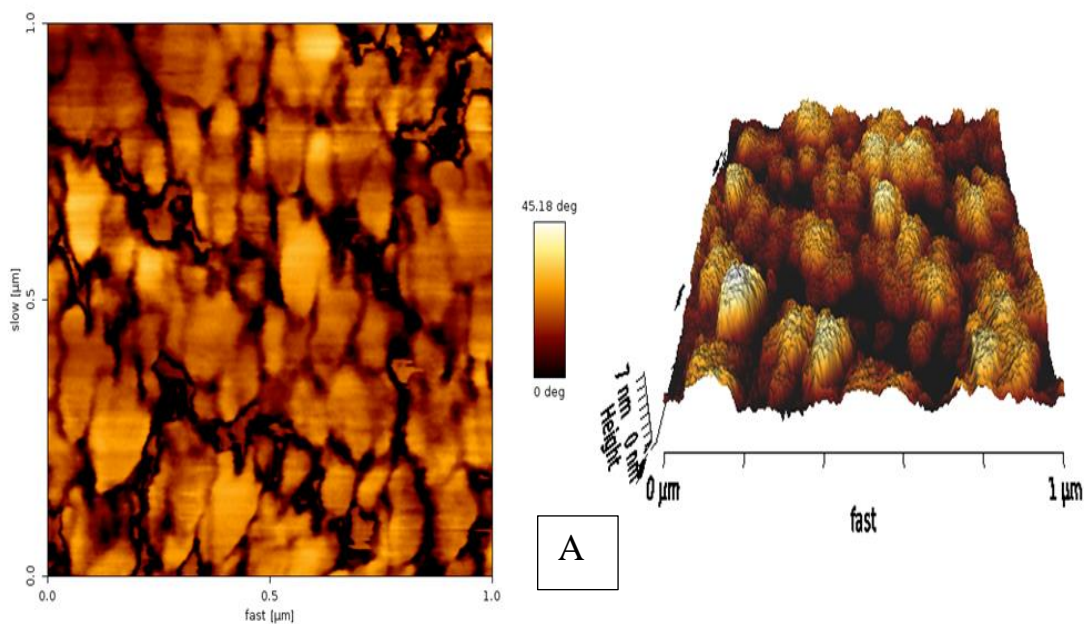
Compounds	carbon	nitrogen	oxygen	silicon	Iron
RH-SiO ₂	21.67%		57.38%	20.95%	
RH-SiO ₂ PrNH ₂	13.88%	20.42%	57.13%	8.57%	
RH-SiO ₂ PrADB	24.63%	12.01 %	44.36%	18.84%	
Fe ₃ O ₄ @RH-SiO ₂ PrNH ₂	14.34%	18.21%	54.14%	11.32%	1.99%
Fe ₃ O ₄ @RH-SiO ₂ PrADB	23.10%	13.72%	46.83%	13.79%	2.33%

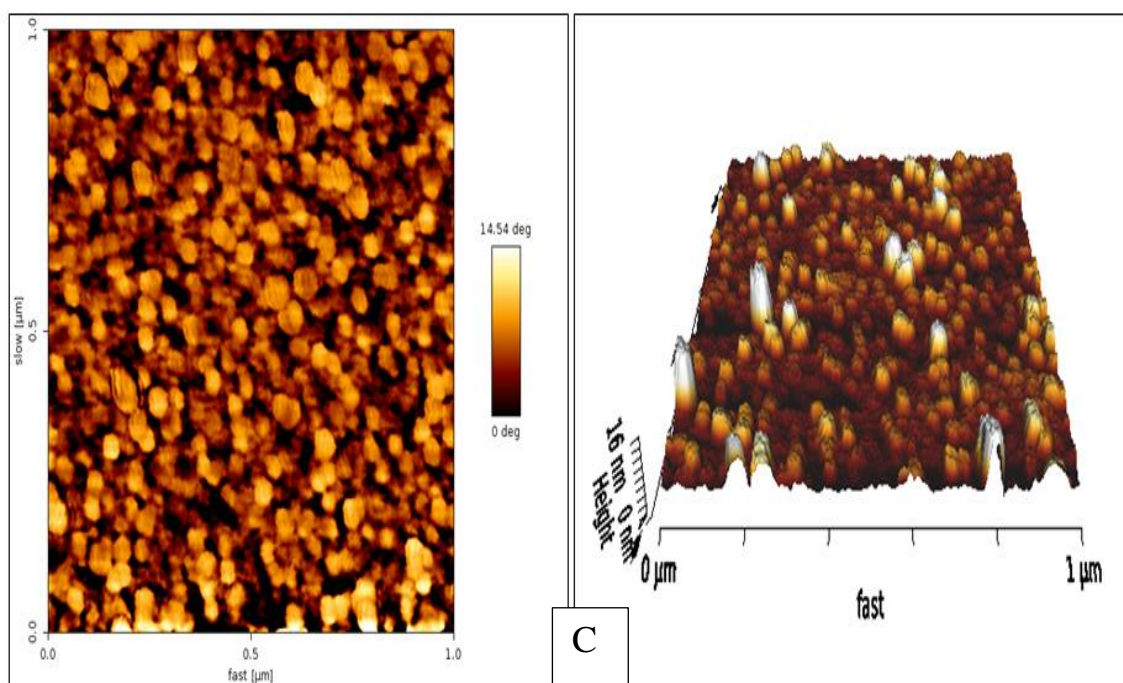
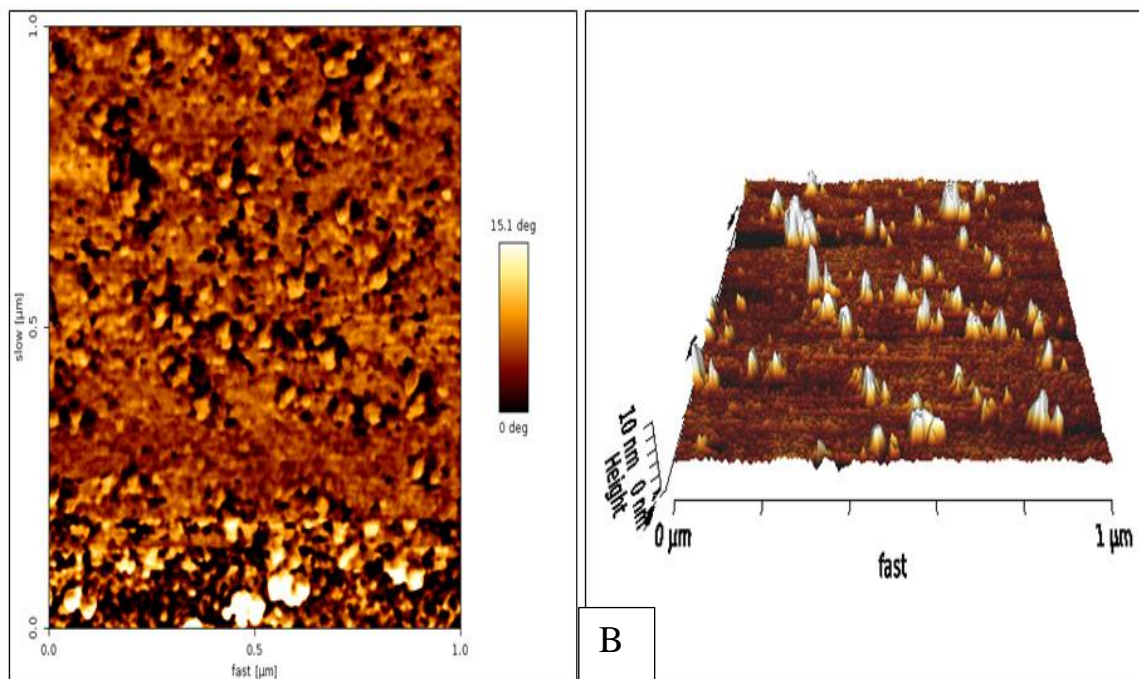
Figure (3-0A) shows the FESEM images of the RH-SiO₂. The images shows that the rice husk is composed mostly of amorphous silica. While the EDX analysis also showed as shown in **Figure (3-1a)** shows the weight percentages of RH-SiO₂ as follows: carbon (21.67%), oxygen (57.38%), and silicon (20.95%)(96). **Figure 3-0B** shows the FESEM images of the RH-SiO₂PrNH₂ compound, as it was observed that there are semi-spherical clusters with a smooth outer surface and irregularly distributed[10]. While **Figure(3-1B)** shows the EDX spectrum of RH-SiO₂PrNH₂. It explains the presence of the most important basic elements in the different intensities. According to the EDX analysis of RH-SiO₂PrNH₂, the weight percentage of an elements indicates the presence of carbon (13.88%), nitrogen (20.42%), oxygen (57.13%), and silicon (8.57%). This result is somewhat consistent with

the results of the elemental analysis of carbon and nitrogen in Table (3-5). FESEM images of the RH-SiO₂/PrADB are shown in **Figure 3-5C**. The images showed an increase in the roughness of the outer surface of the sample with an increase in the rate of accumulation of nanoparticles as a result of the bonding of the RH-SiO₂/PrNH₂ with γ -amino- α , ω -Dibromobenzaldehyde compound [11]. This is highly consistent with previous studies [11]. While the EDX analysis also showed as shown in **Figure (3-5C)** the weight percentages of sample elements as follows: carbon (24.63%), nitrogen (12.01%), oxygen (44.36%) and silicon (18.84%). The percentages shown confirm the success of the association of RH-SiO₂/PrNH₂ with the γ -amino- α , ω -Dibromobenzaldehyde compound. FESEM images of the Fe₃O₄@RH-SiO₂/PrNH₂ are shown in **Figure 3-5D**. The FESEM analysis showed the presence of spherical shapes of different sizes and heterogeneities distributed on a rough and bumpy surface, and this confirms the successful attachment of iron oxide to the silica surface. In addition to increasing the surface area and pore diameter, this gives it a high efficiency in removing many pollutants [11]. While **Figure (3-5D)** showed the EDX analysis the weight percentages of sample elements as follows: carbon (14.34%), nitrogen (18.21%), oxygen (44.14%), silicon (11.32%), and iron (1.99%). Finally, **Figure 3-5E** shows the FESEM images of the Fe₃O₄@RH-SiO₂/PrADB compound. As the images showed the presence of spherical clusters distributed on one side over a wrinkled surface with a dark black color, and this is similar to the above compound images and also confirms the increase in the rate of accumulation of particles due to the association of iron oxide with silica [11]. The EDX spectrum of Fe₃O₄@RH-SiO₂/prADB sample is shown in **Figure (3-5E)**, which clearly illustrates the presence of carbon (23.10%), nitrogen (13.72%), oxygen (46.83%), silicon (13.79%), and iron (2.33%) [11].

3.7. Atomic Force Microscopy (AFM)

Almost any surface, including polymers, ceramics, composites, glass, and biological samples, can be imaged using the efficient AFM technique. AFM is used to quantify and localise a variety of forces, including mechanical properties, magnetic properties, and adhesion forces. With this kind of microscope, the electron force between a cantilever tip and the atoms on a specimen's surface is measured. High spatial resolution and extremely light surface forces are two of an AFM's primary benefits over other comparable techniques. Imaging non-conducting materials using AFM is achievable, which is necessary for research on the polymer/silica interface[1, 2]. Figure (3-7) shows the AFM technique used to photograph the surface for the group of compounds that were prepared.





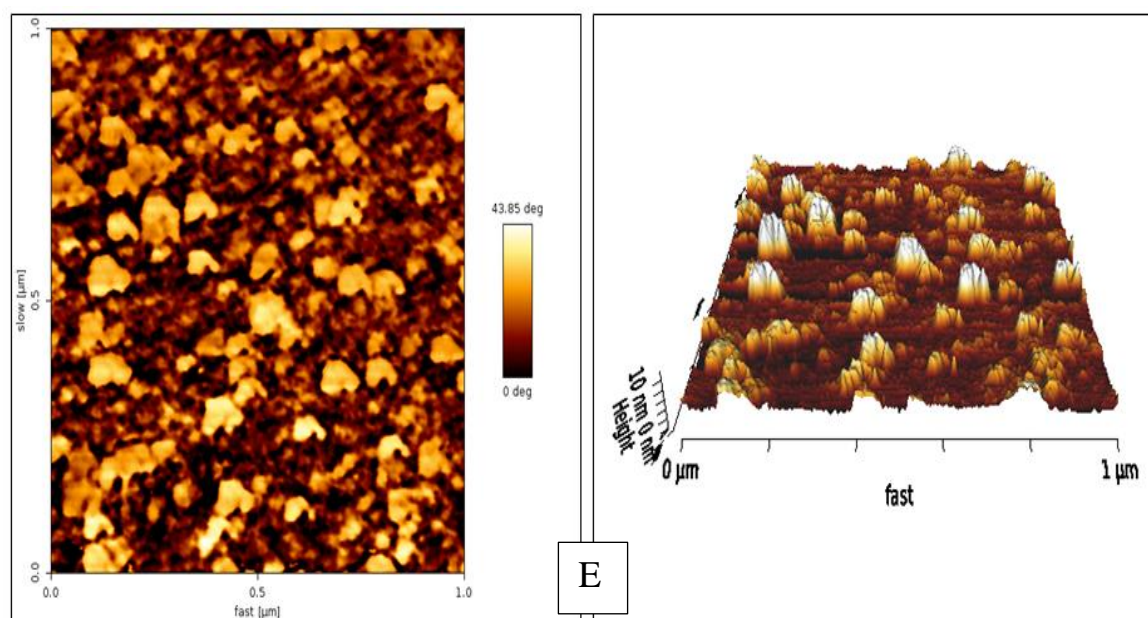
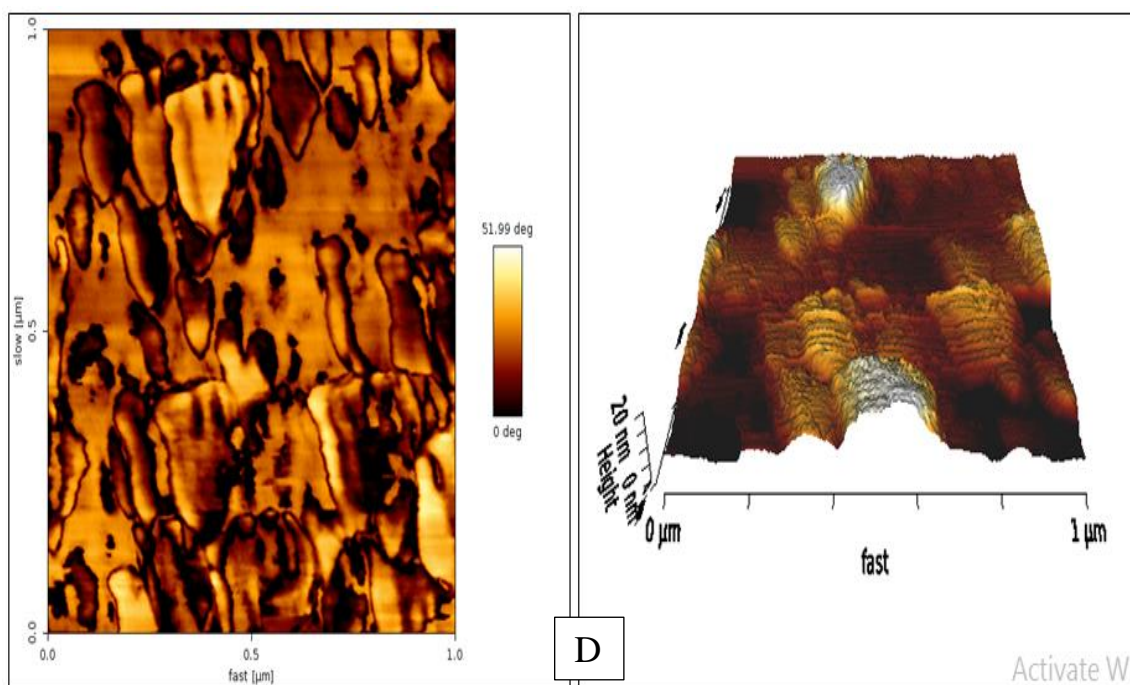


Figure 3-10 2D and 3D AFM images of (A) RH-SiO₂ (B) RH-SiO₂/PrNH₂ (C) RH-SiO₂/PrADB (D) Fe₃O₄@RH-SiO₂/PrNH₂ (E) Fe₃O₄@RH-SiO₂/PrADB

Table 3-5 : shows the AFM analysis

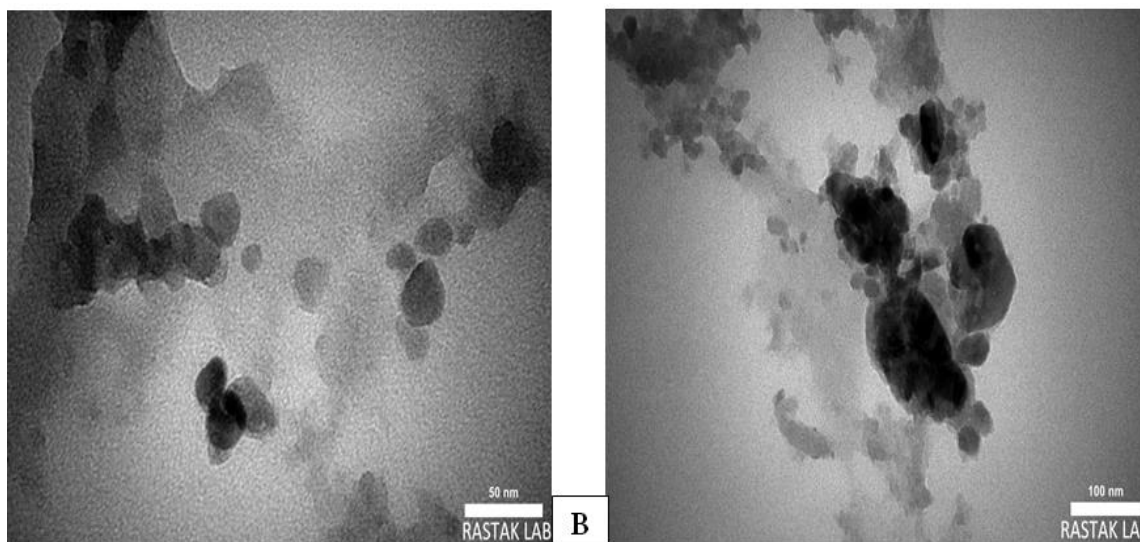
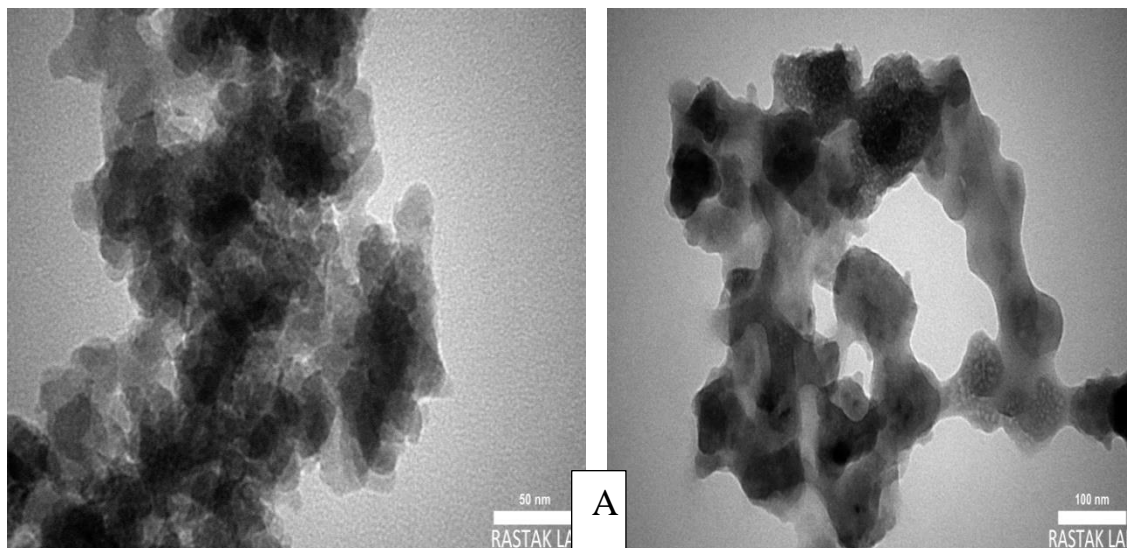
Compounds	Average roughness Ra	RMS roughness Rq	peak-to-valley roughness Rt
RH-SiO ₂	993.9 pm	1.222 nm	7.306 nm
RH-SiO ₂ PrNH ₂	440.2 pm	807.1 pm	10.17 nm
RH-SiO ₂ PrADB	1.114 nm	1.663 nm	16.24 nm
Fe ₃ O ₄ @RH-SiO ₂ PrNH ₂	2.363 nm	3.209 nm	20.36 nm
Fe ₃ O ₄ @RH-SiO ₂ PrADB	908.9 pm	1.382 nm	11.80 nm

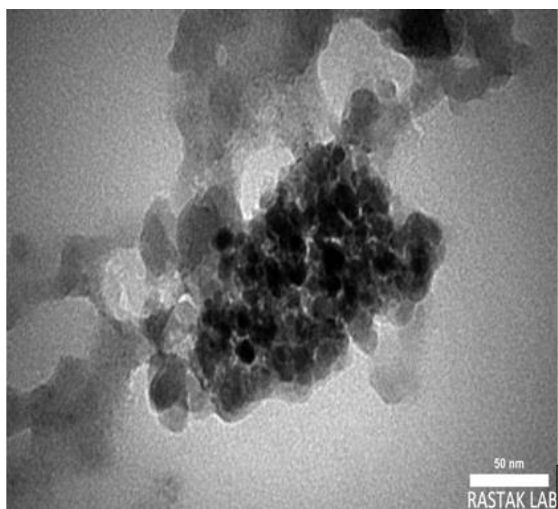
The results of RH-SiO₂ are shown in Figure (3-7A), where the images showed the presence of blocks of different shapes with a peak-to-valley roughness (Rt) value of 7.30 nm and RMS roughness (Rq) value of 1.22 nm. This is due to the agglomeration of nanoparticles. While photographing the surface of the RH-SiO₂PrNH₂, as shown in **Fig.(3-7B)**. The images showed the presence of blocks of different shapes with a peak-to-valley roughness (Rt) value of 10.17 nm and RMS roughness (Rq) value of 1.807 nm. This is due to the increase in the rate of agglomeration of nanoparticles [109]. On the other hand, the images of the RH-SiO₂PrADB compound confirmed a clear increase in a peak-to-valley roughness (Rt) value of 16.24 nm and as shown RMS roughness (Rq) value of 1.663 nm as shown in **Figure(3-7C)**. This indicates the successful association of the RH-SiO₂PrNH₂ with the 2-amino-3,5-Dibromobenzaldehyde compound. **Figure3-7D** shows the images of the Fe₃O₄@RH-SiO₂PrNH₂ compound, as it was

found that the addition of Fe_3O_4 to the ligand changes the morphology of the prepared surface and significantly increases a peak-to-valley roughness (Rt) value of 20.36 nm and RMS roughness (Rq) value of 3.209 nm. The Fe_3O_4 acts as a barrier between the layers of ligand, which increases the thickness of the layer and makes the surface bumpy and wrinkled. Finally, the Fe_3O_4 @RH-SiO₂/PrADB compound showed a decrease in surface roughness, as shown in (Figure 3-1E). It was observed that the bonding between Fe_3O_4 increased with the ligand, which leads to a decrease in the surface roughness and the disappearance of the nanoparticle clusters. It is found that the peak-to-valley roughness (Rt) value of 11.80 nm and an RMS roughness (Rq) value of 1.382 nm. [110].

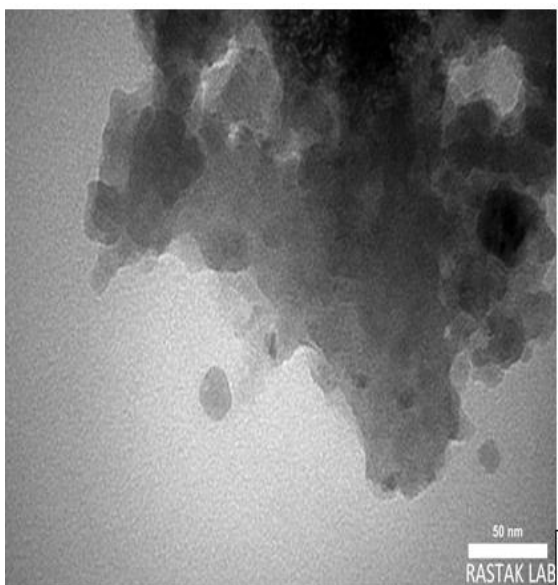
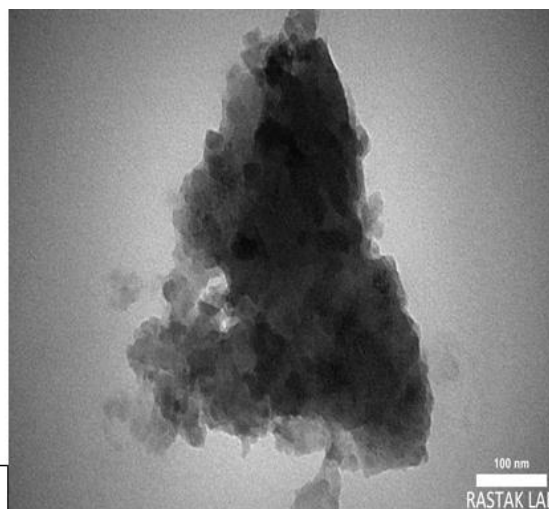
3.8. Transmission electron microscopy (TEM) analysis

Transmission electron microscopy (TEM) is the most useful technique for determining the morphology of NPs. A powerful electron beam is used in this sort of microscopy to travel through a sample, and the interaction between the electrons and the sample causes a picture to be created. After that, the image is magnified and focussed onto an imaging medium, such as a charge-coupled device, a screen made of fluorescent material, or a sheet of film for photography. When viewing TEM images at lower magnifications, contrast is produced by the material differential absorption of electrons as a result of variations in the material structure or thickness [111], the prepared compounds were analyzed using TEM technology shown in Figure (3-8)

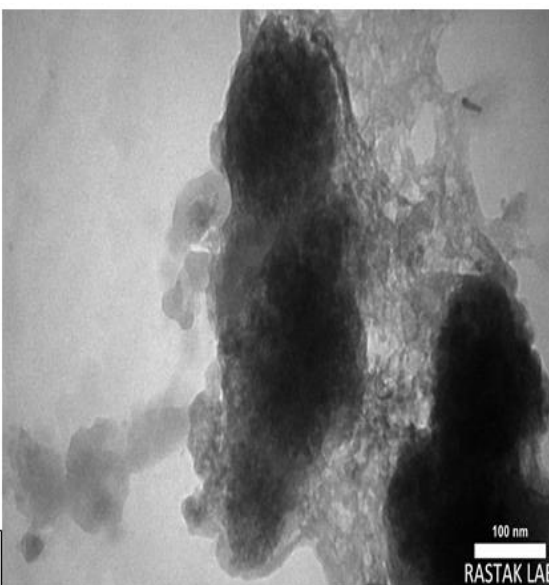




C



D



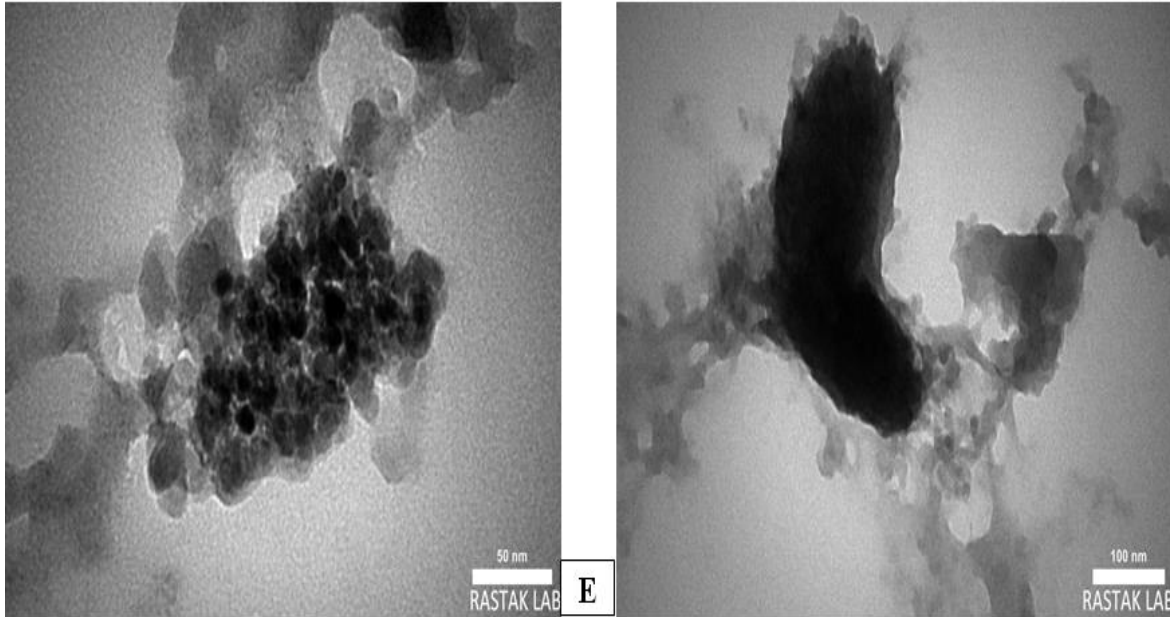


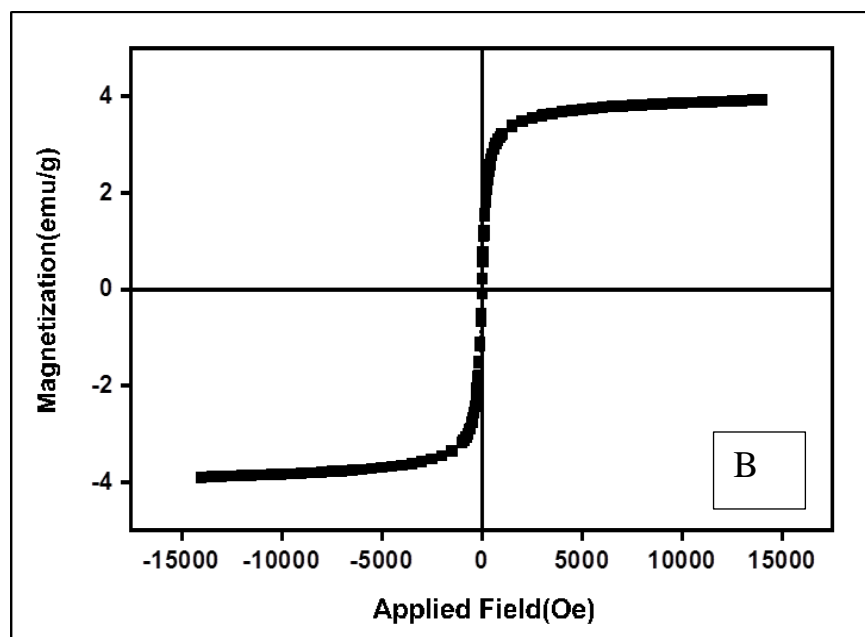
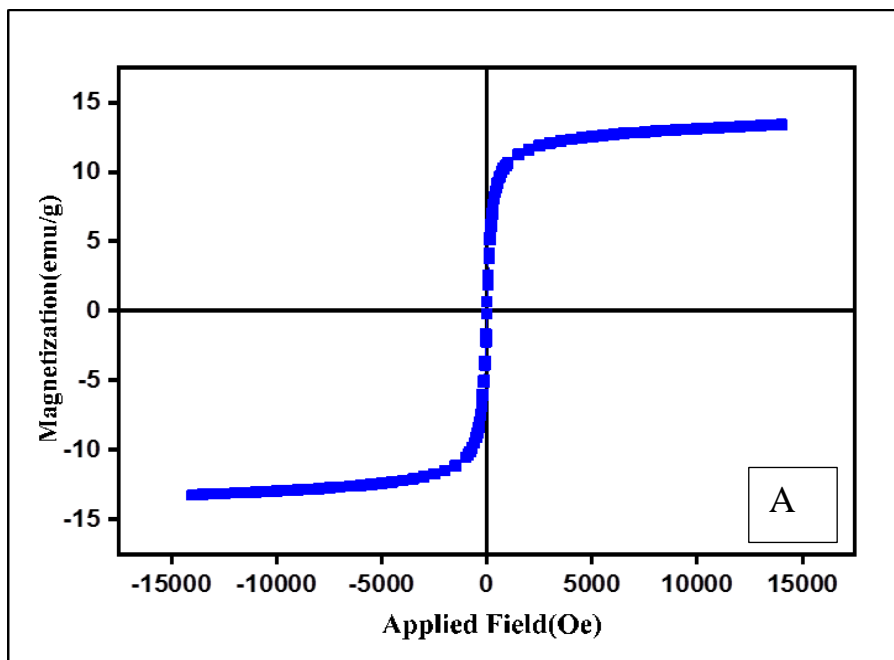
Figure 3-1 TEM images for (A) RH-SiO₂ (B) RH-SiO₂/PrNH₂ (C) RH-SiO₂/PrADB (D) Fe₃O₄@RH-SiO₂/PrNH₂ (E) Fe₃O₄@RH-SiO₂/PrADB

Through the images shown in Figure(3-1A) of the RH-SiO₂, it was found that there were irregularly agglomerated aggregates, which indicates that the shape of the particles is amorphous[112] **Figure (3-1B)** shows the RH-SiO₂/PrNH₂ sample, as it was observed that a transparent cloud appeared, with irregular and lumpy oval clusters in the middle, and this indicates that the silica coatings obtained from the rice husks are of an amorphous nature [113]. While The RH-SiO₂/PrADB was shown in **Figure (3-1C)**, the presence of spherical clusters linked together. It was found that the average particle size is 30 nm, and this value is consistent with the results of the FESEM and XRD analysis. The Fe₃O₄@RH-SiO₂/PrNH₂ compound is shown in **Figure(3-1D)** the Fe₃O₄ showed heterogeneous spherical shapes distributed on transparent Nano layers representing the RH-SiO₂/PrNH₂ compound. This confirms the success of iron oxide grafting on the surface of the RH-SiO₂/PrNH₂. In

addition, the rate of agglomeration of particles decreased as a result of the penetration of Fe_3O_4 particles between the nanoscale layers. Finally, the $\text{Fe}_3\text{O}_4@\text{RH-SiO}_2/\text{PrADB}$ compound is shown in the **Figure(3-1E)**. The images confirmed the success of Fe_3O_4 bonding on the $\text{RH-SiO}_2/\text{PrADB}$ surface, through the presence of black clusters spread on a wavy transparent surface. It was found that the average particle size was about 20 nm.

3.9. Vibrating Sample Magnetometry (VSM)

VSM is a flexible method for determining a sample magnetic moment when it is vibrated perpendicular to a uniform magnetizing field. This approach can identify changes as tiny as 10^{-9} to 10^{-1} emu. Using Faraday law of magnetic induction as a foundation, the VSM approach can be used to determine a sample magnetic moment information where included the magnetic hysteresis curves of the Fe_3O_4 , $\text{Fe}_3\text{O}_4@\text{RH-SiO}_2/\text{PrNH}_2$, and $\text{Fe}_3\text{O}_4@\text{RH-SiO}_2/\text{ADB}$ nanocomposites are shown in **Figures (3-9 A ,B, and C)**



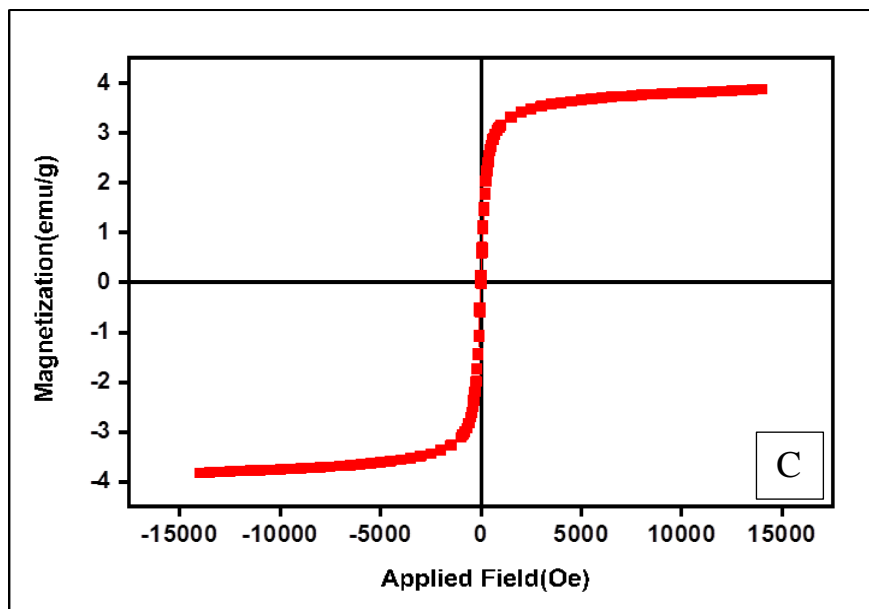


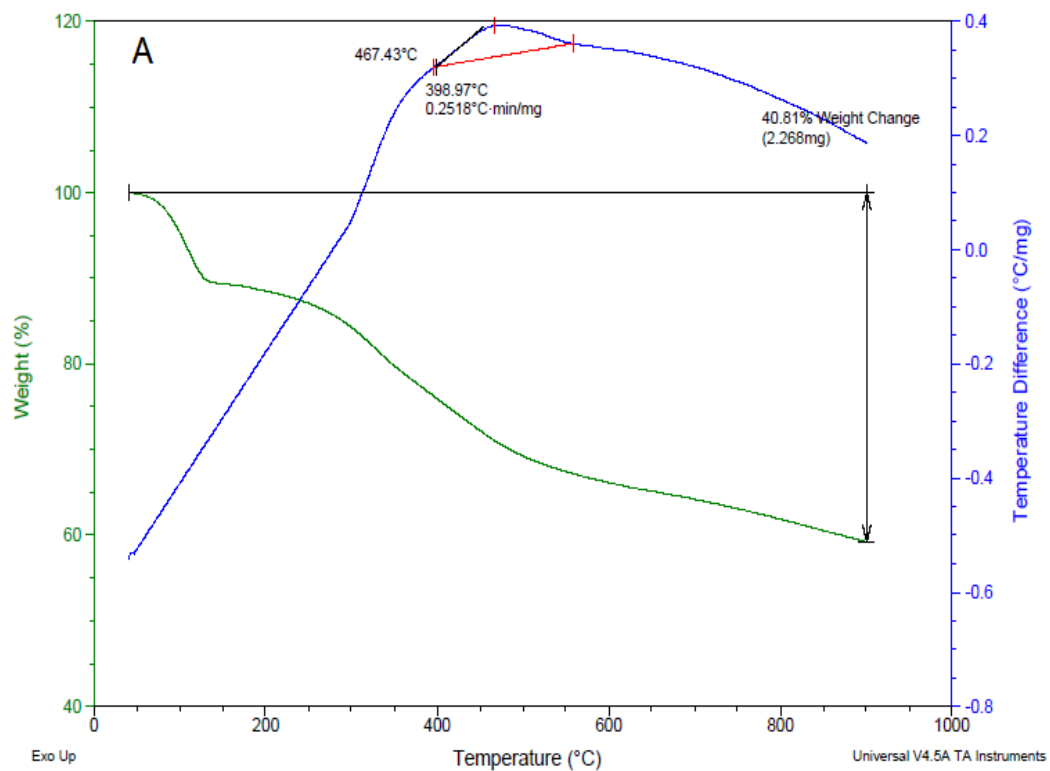
Figure 3-9 VSM spectra of (A) Fe_3O_4 (B) $\text{Fe}_3\text{O}_4@RH\text{-SiO}_2\text{PrNH}_2$ (C) $\text{Fe}_3\text{O}_4@RH\text{-SiO}_2\text{PrADB}$

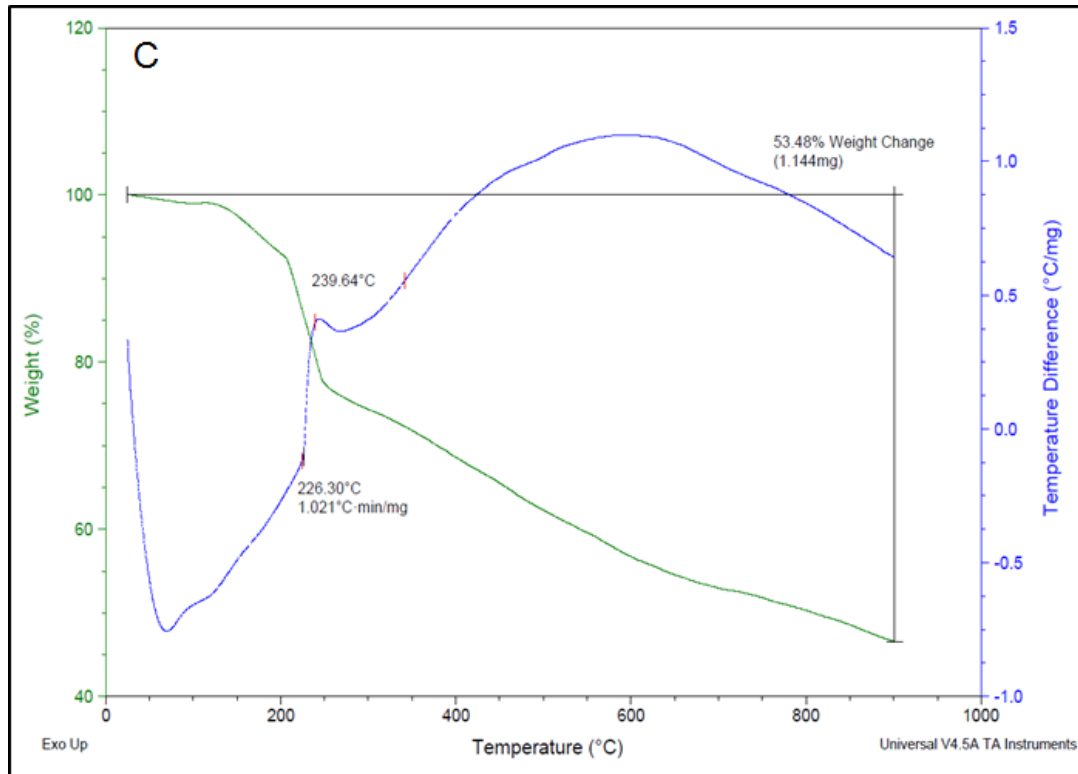
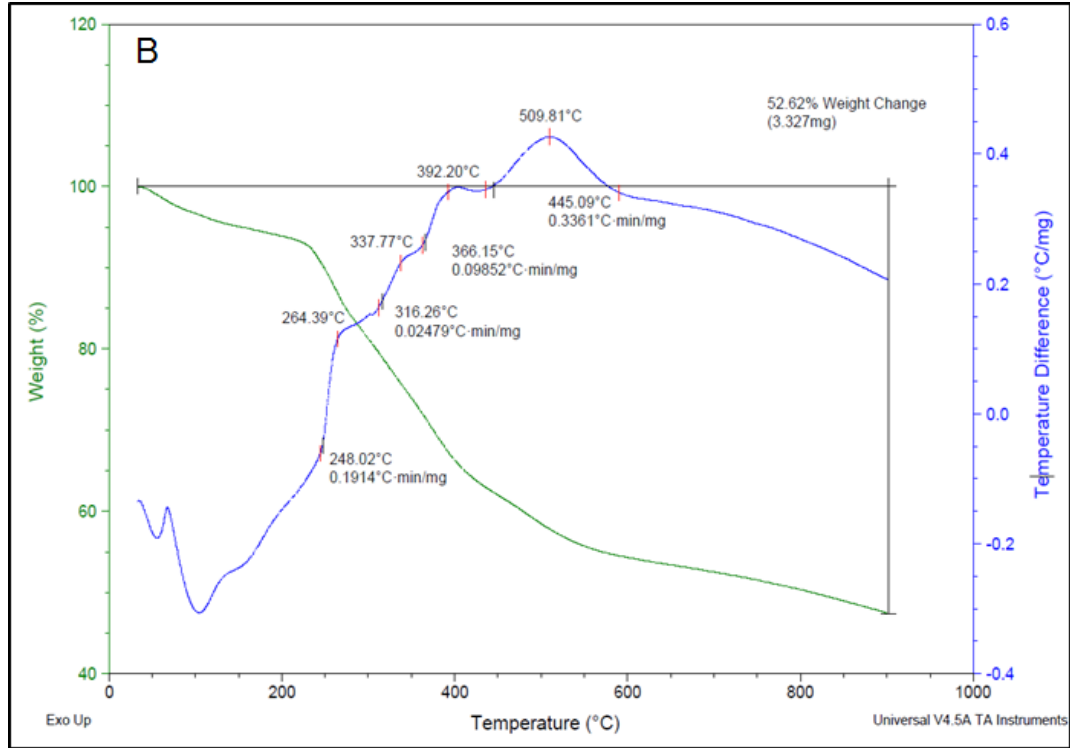
The hysteresis loop showed that the prepared iron oxide (Fe_3O_4) has ferromagnetic behavior with a saturation magnetization up to 3.89 emu g^{-1} [114]. While the results of the saturation magnetization value for the $\text{Fe}_3\text{O}_4@RH\text{-SiO}_2\text{PrNH}_2$ and $\text{Fe}_3\text{O}_4@RH\text{-SiO}_2\text{ADB}$ compounds showed a clear decrease in magnetism up to 3.88 and 3.87 emu g^{-1} , respectively. This is due to the addition of non-magnetic materials to the iron oxide that reduces the magnet moment of the compound. The addition of these materials with iron oxide leads to a complete coverage of the iron, and thus the attraction with the applied magnetic field decreases.

3.1.1. Thermo gravimetric Analysis (TGA)

The main purpose of a TGA is to assess the thermal stability of various substances up to temperatures of about $1000 \text{ }^\circ\text{C}$. To detect variations in weight as an effect of rising temperature, TGA features a weight balance that

is incredibly sensitive. The instrument has a temperature limit of 1000°C and a sensitivity of 0.1 g. To make sure thermal equilibrium was reached inside the sample, a heating rate of $1^{\circ}\text{C}/\text{min}$ was used. To guarantee that the sample is not adversely affected by contaminants, the TGA is housed inside an inert gas glove box. The thermogravimetric analysis has been shown to be useful in the analytical technique of evaluating the kinetic parameters of different materials, which in turn provides valuable quantitative information on the stability of the material, as the thermogravimetric decomposition of the samples prepared in the temperature range of 10 - 900°C is shown in Figure (3-10).





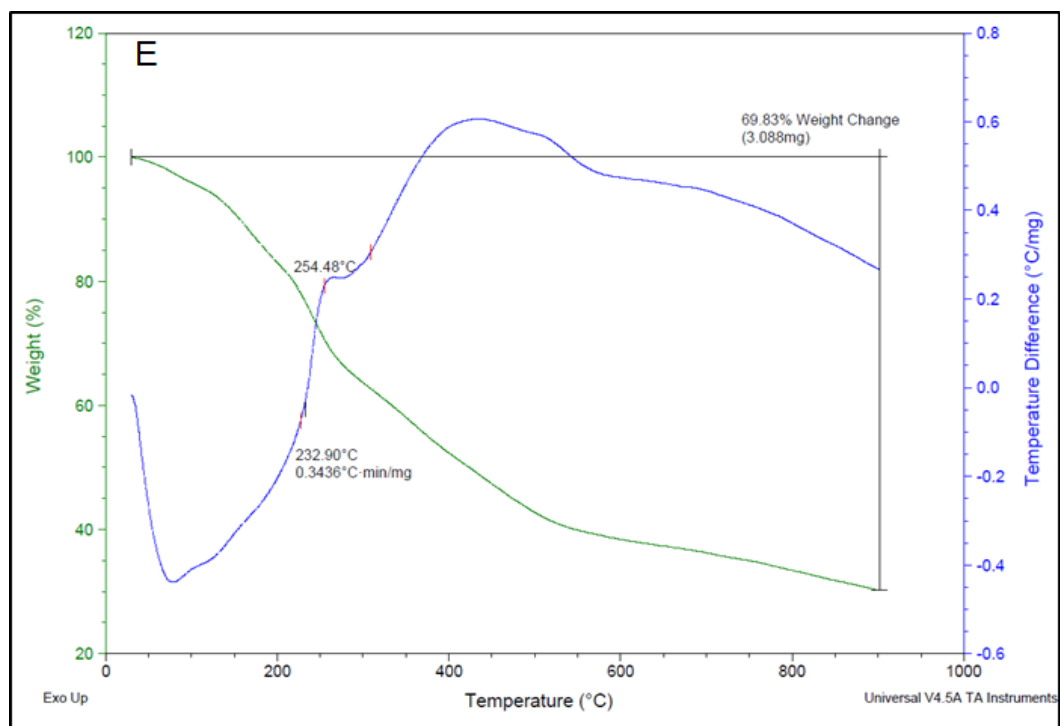
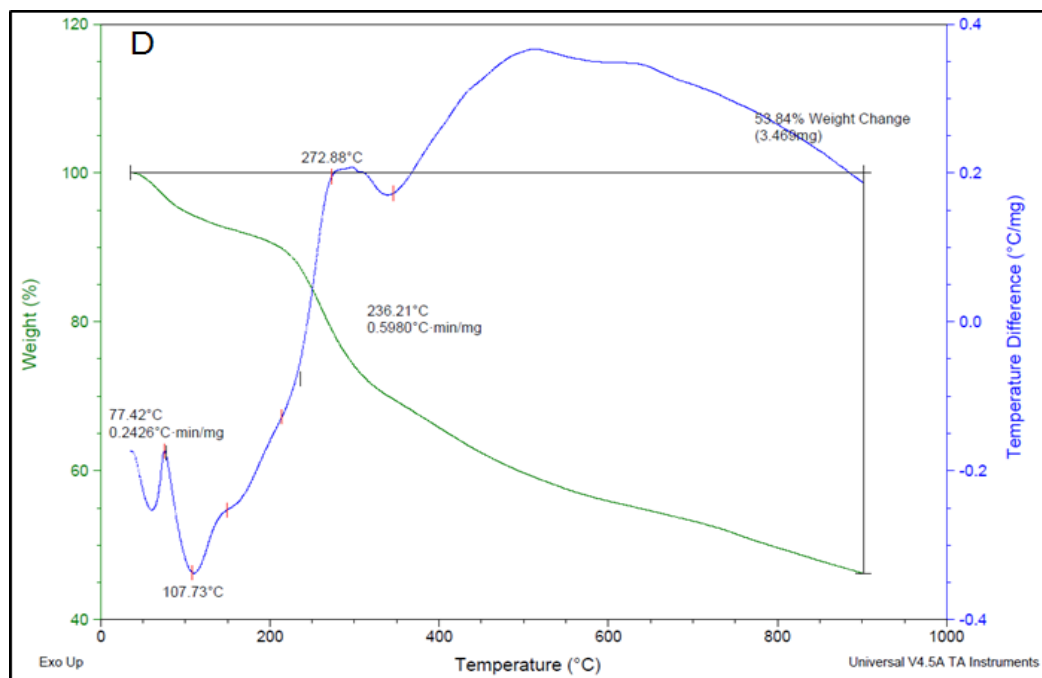


Figure 3-10 TGA/DTA analysis of (A) RH-SiO₂ (B) RH-SiO₂/PrNH₂ (C) RH-SiO₂/PrADB (D) Fe₃O₄@RH-SiO₂/PrNH₂ (E) Fe₃O₄@RH-SiO₂/PrADB

Figure (3-1·A) shows of the RH-SiO₂ sample, as it was noted that the total loss percentage of 41.81% was attributed to the loss of 10% of water molecules at 100°C, The second weight loss was 17% which was assigned to the decomposition of the salen moiety that happened between 200 and 300°C, and also 14% due to the condensation of silanol groups and the breaking of all bonds at 300°C. The TGA spectrum showed that the compound has good thermal stability due to the fact that the percentage of loss by weight of the material is low at high temperatures[110]. **Figure(3-1·B)** shows a decomposition of the RH-SiO₂PrNH₂ sample, as it was noted that the total loss percentage of 52.62% at temperatures between 10 and 900 °C has included the loss of 12% of water molecules, 26% of weight loss belong to the aminopropyl group, and finally about 14% attributed to the breakdown of the silanol bonds[103]. The TGA spectrum showed that the compound has good thermal stability due to the fact that the percentage of loss by weight of the material is low at high temperatures [116] In contrast, the RH-SiO₂PrADB compound is shown in **Figure (3-1·C)**. The results indicated that the loss percentage reached (53.48%) included the evaporation of 12% of water molecules, the dissociation of 27% which was assigned to the decomposition of the 2-amino-3,5-Dibromobenzaldehyde compound, And 14% weight loss due to the breaking of silanol bonds and the success of the synthesis process and the production of a compound with high stability [117]. The Fe₃O₄@RH-SiO₂prNH₂ sample is shown in **Figure (3-1·D)**. displays the results of the TGA analysis of the Fe₃O₄@RH-SiO₂PrNH₂ sample. The weight change was (53.48%) at temperatures between 10 and 900 °C, and this was attributed to; about 11 % of mass loss of the physically absorbed water molecules, 32 % of mass loss belong to the aminopropyl group, and finally about 10% attributed to the breakdown of the silanol bonds[103][118]. While the thermogravimetric

analysis of Fe₃O₄@RH-SiO₂PrADB material was illustrated in **Figure (3-10E)**, revealing three distinct stages of decomposition. The initial loss, about 14% of the sample mass, occurred at a temperature of 50 °C and was attributed to the physical adsorption of water[119]. The second mass loss, comprising approximately 34% of the total sample mass, was observed within the temperature range of 200–600 °C and can be attributed to the loss of organic compounds onto the silica matrix, specifically aminopropyl group and 2-amino-3,5-dibromobenzaldehyde, and finally about 21% attributed to the breakdown of the silanol bonds and transform to silicon oxide[36]. The outcomes show that the synthesis procedure was successful and that a high-stability material was produced.

CHAPTER FOUR

METAL UPTAKE



4. Metal Uptake

4.1 Introduction

Numerous potentially harmful compounds have been introduced to the environment as a result of accelerated development and human activity activity [120]. Toxic heavy metal pollution of the environment resulting from numerous industrial activity is a global phenomenon[121]. Because heavy metal contamination has a direct impact on public health[122], it is crucial to address this issue. Wastewater from contemporary chemical industries are the main sources of heavy metals.

The capture and removing of tiny amounts of metal from wastewater streams coming from diverse industrial processes is one of the most important aspects of the study under consideration today. Therefore, there was a lot of room for study into creating polysiloxane ligand systems that could preconcentrate and extract trace metal ions in a very selective manner[123].

In the scientific community, a number of common methods to remove tiny amounts of metal from wastewater were listed, such oxidation, membrane filtration, adsorption, ion exchange, and others. The most popular adsorbents, such as silica gel, activated carbon, and aluminium oxide, are employed frequently as an effective physical separation method to remove or reduce the concentration of contaminants (organic and inorganic) in contaminated waters[124].

4.2 Experimental of Metal Uptake

Two types of ligands (RH-SiO₂PrADB & Fe₃O₄@RH-SiO₂PrADB) were used to remove a number of ions represented by cobalt, nickel and copper. The method was done using a volumetric vial containing 10 ml of one of the ions such as cobalt with 0.02 g of one of the ligands such as of (RH-SiO₂PrADB), and it was shaken for ten minutes. After that, 10 ml of the mixture was withdrawn and filtered. Through the needle of the syringe to remove the solid particles, then the residual concentration of the metal ion was measured by the solution absorption measurement every hour for ten hours. This method was used for nickel, and copper ions with one ligand at a time. The following equation was used to calculate the removal efficiency (E%) of copper, nickel and cobalt from aqueous solutions [10]:

$$E \% = \frac{C_o - C_e}{C_o} \times 100$$

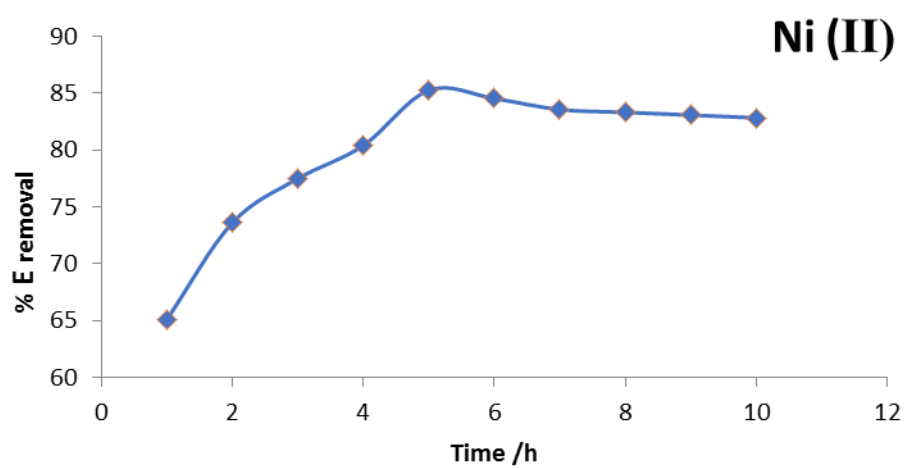
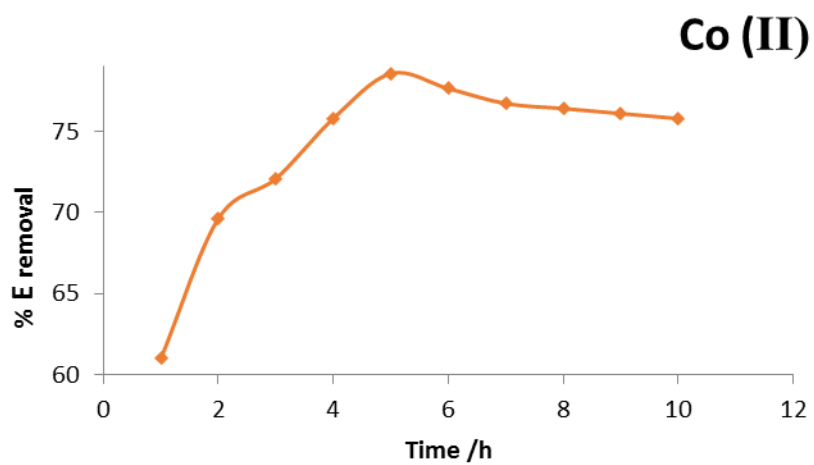
Where C_o and C_e are the initial concentration at zero and the adsorbed concentrations after contact time, respectively, The effects of trembling time, pH effect, ion concentration, and solid ligand mass (RH-SiO₂PrADB & Fe₃O₄@RH-SiO₂PrADB) were studied as optimization conditions.

4.3 Metal Uptake by RH-SiO₂PrADB

4.3.1. Effect of vibration time on Removal of metal ions from aqueous solution

The impact of reaction time on the removal of metal ions by (RH-SiO₂PrADB) was explored. The response was performed with 0.02 g ligands and shaken for 10 h with an aqueous solution of divalent metal ions at a

concentration of 1.0×10^{-4} M. Calculation of the ion concentration removed by ligand every 1 h. The amount of time spent stirring is a crucial component of process the removal of metal ion since it demonstrates how quickly metal ions bind entirely to the surface. The impact of contact time on the adsorption process is depicted in Figure (4-1). An excellent heavy metal removal (of cobalt, nickel, and copper) requires a minimum contact duration of 1 h, as can be seen from the fact that metals removal increases with increasing time in the first five hours and then becomes negligible beyond that, where it was the following results have been obtained at five o'clock (Co(II) 98%, Ni(II) 82%, and Cu(II) 86%). This suggests that heavy metal removal reaches its maximum within five hours, at which point the concentration of metals in the solution stabilizes. This may be attributed to the initial availability of many unoccupied sites for adsorption, which finally slowed down as a result of the solute molecule's attraction to the bulk phase and the exhaustion of the remaining surface sites[99]. The optimal stirring time for the following studies has been determined to be 5 hours based on the results.



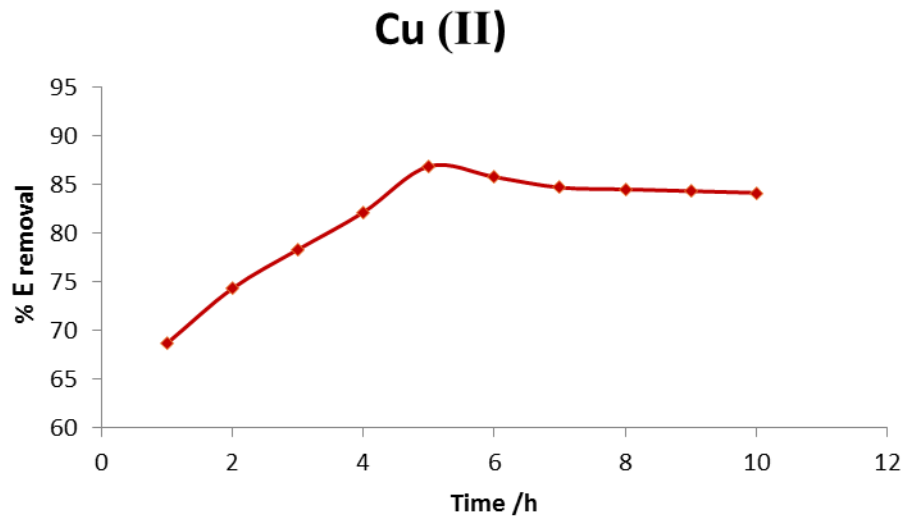
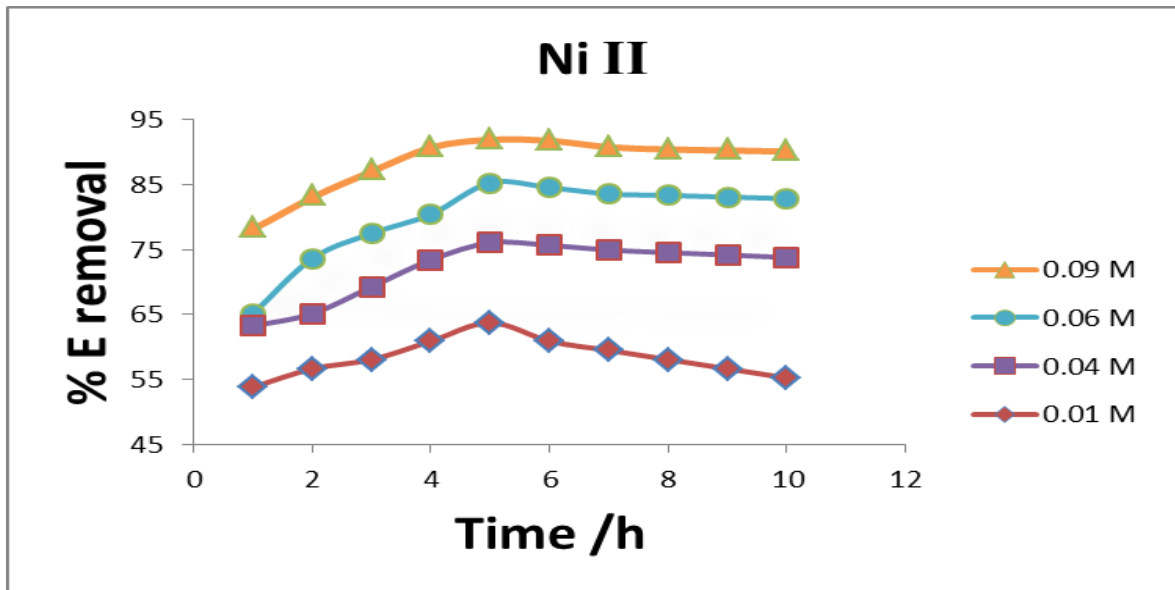
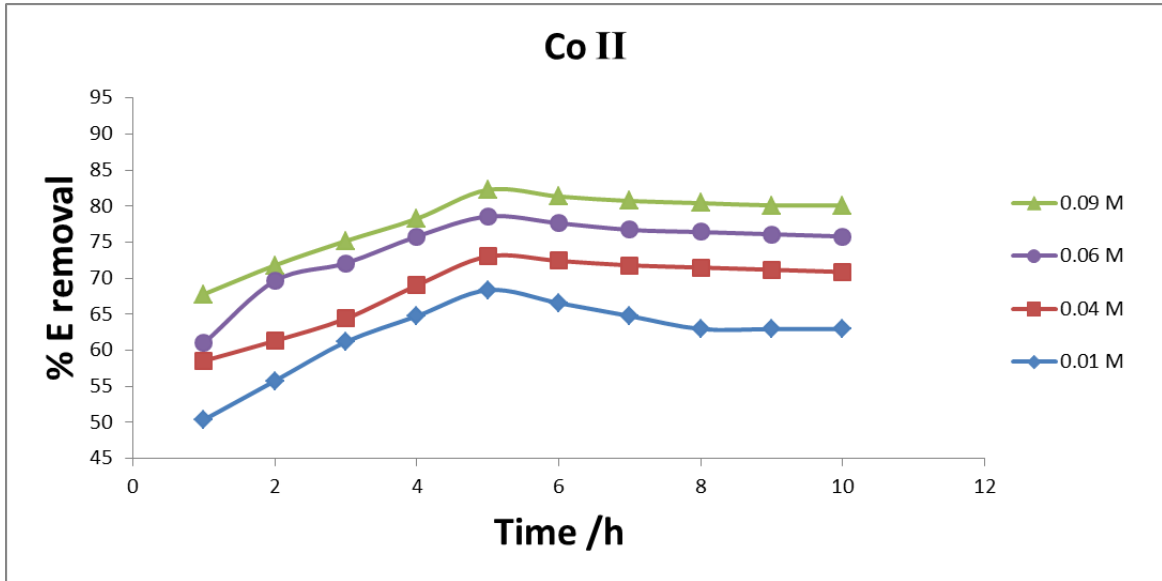


Figure 4-1 Effect of vibration time on removal of metal ions(Co(II), Ni(II) and Cu(II) (concentration 0.01M) by the ligand RH-SiO₂PrADB (dose = 0.02 g)

4.4.6. Effects of concentration metal ions on the removal by the ligand RH-SiO₂PrADB

The impact of metal ion concentration was studied at different concentrations (0.01 , 0.02 , 0.04 , and 0.08 M) for each metal ion. Which was removed by the ligand RH-SiO₂PrADB (0.02 g). The results shown in Figure (4-2) show that the removal rate of ions increases with the increase in the concentration used, where the removal rate is (Co 68% , Ni 63% , and Cu 58%) when using 0.01 M , while it rises to (Co 82% , Ni 77% , and Cu 65%) when using 0.08 M . This can also be explained by the fact that as the ion concentration increases, more adsorption sites are being covered. The reason for this is due to the availability of a greater number of ions in the solution with an increase in the concentration used, which gives a greater opportunity to occupy most of the ligand site. It should be noted that the removal rate decreases after five hours [12].



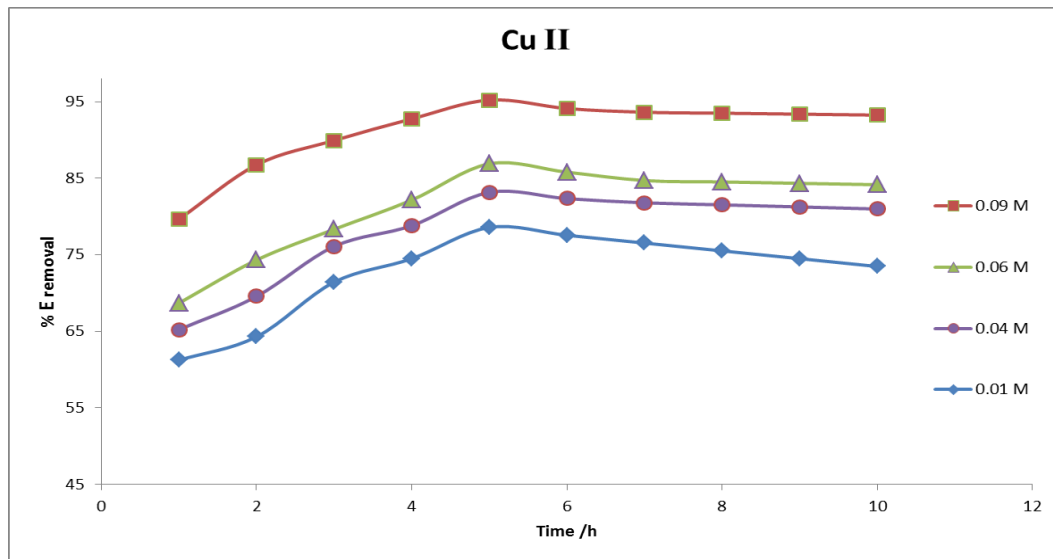
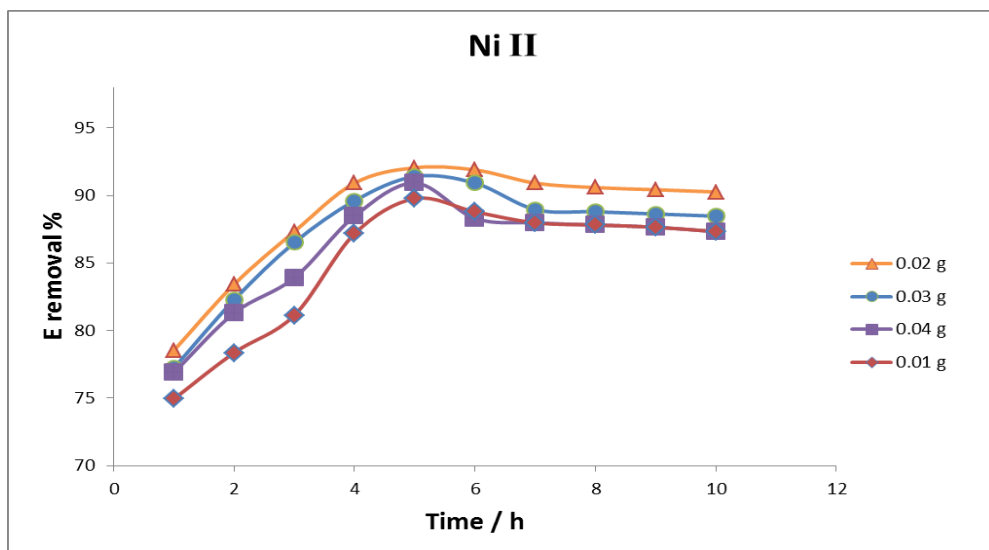
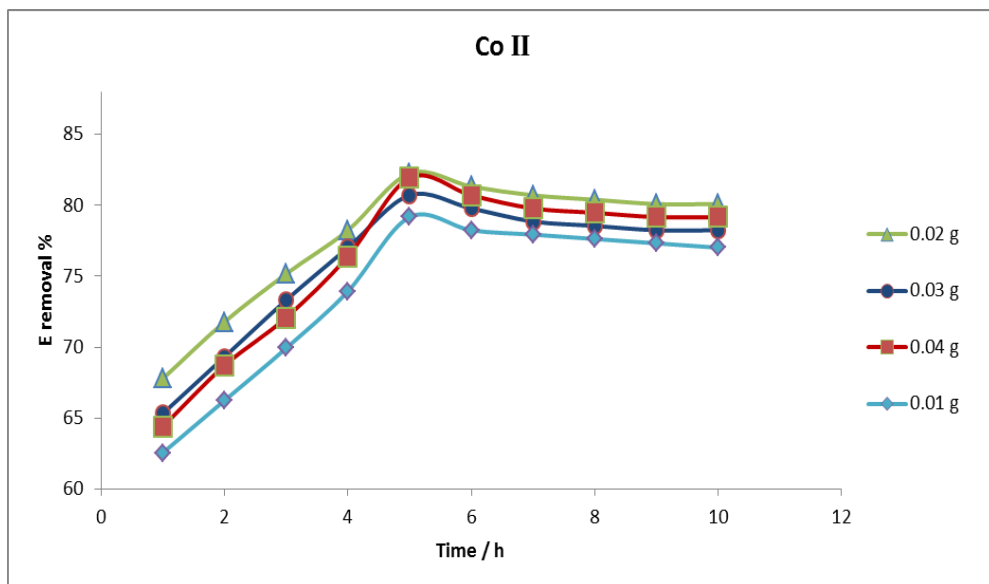


Figure 4-2 Effects of concentration metal ions on the removal by the ligand RH-SiO₂PrADB (dose= 0.02 g)

4.4.4. Effect of the weight of the RH-SiO₂PrADB

Different weights of the ligand were used, which are (0.01, 0.02, 0.03, 0.04 g) in solution of metal ions at a concentration of 0.01 M. It was observed through the results as shown in Figure (4-3) that the removal rate of ions is as high as possible when using 0.02 g of the weight of the ligand, where the rates of removal of ions were (cobalt 82%, nickel 92%, and copper 90%), then the percentage decreased slightly when the weight of the ligand increased. This decrease in the removal value is explained by the agglomeration of the ligand at The use of weights higher than 0.02 g in the same volume used in the study, which causes agglomeration, closure of some active sites on the surface of the ligand, and this leads to a decrease in the surface area of the adsorbent surface[120].



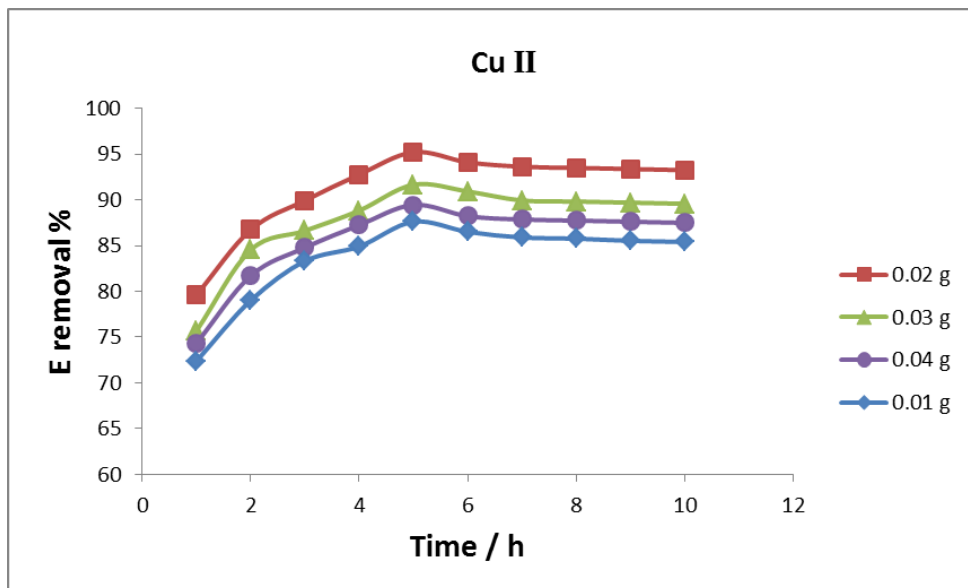
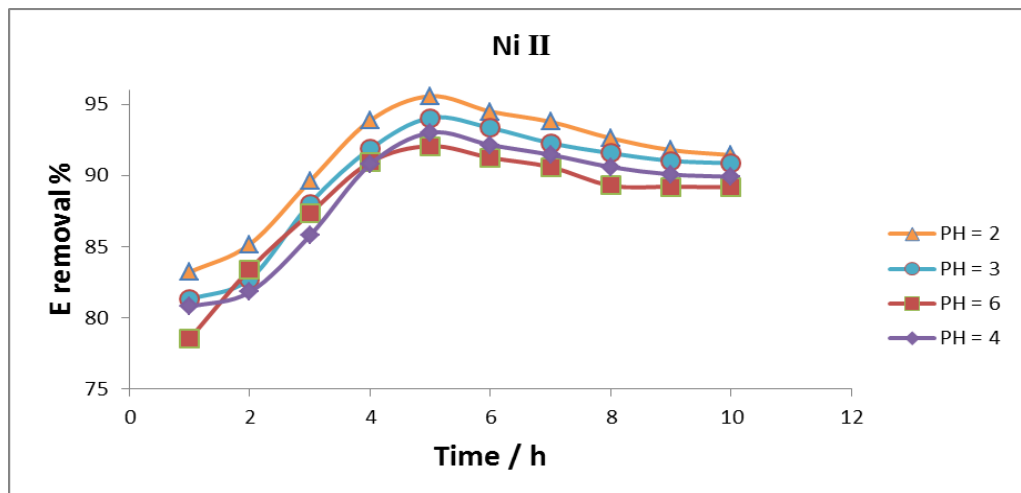
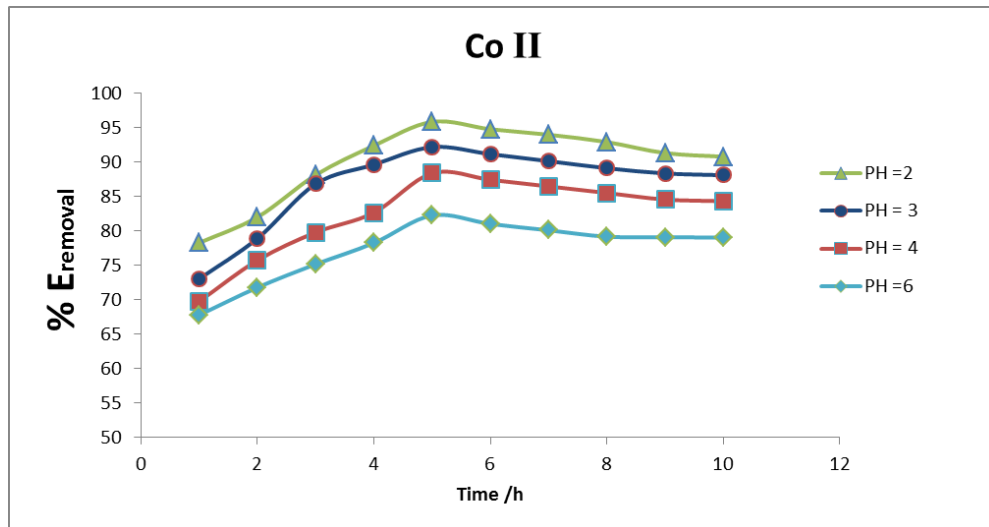


Figure 4-3 Effect of the weight of the RH-SiO₂PrADB on the removal of metal ions (Co(II), Ni(II) and Cu(II) (concentration 0.01 M) by the ligand RH-SiO₂PrADB (dose= 0.02 g)

4.4.8. Effect of pH on E removal of metal ions by the ligand RH-SiO₂PrADB

The effect of pH on the removal of metal ions was studied at a concentration of 0.01 M of ion with use 0.02 g of the ligand RH-SiO₂PrADB. The results shown in Figure (4-4) showed that the removal percentage of cobalt and nickel was as high as possible at pH= 2 (Co 90.8% and Ni 90.0%), while copper ions had the highest removal percentage at The pH= 0 (Cu 90.2%). The reason for this is due to the fact that cobalt and nickel ions in aqueous solutions are surrounded by water molecules in the form of hexagons, In highly acidic environments, the hydrogen ion will react with water molecules to form the hydronium ion, thus making the metal ions more free in solution and therefore the removal rate is higher. As for the copper molecules, they take either a tetrahedral shape or an angular shape with the water molecules. Therefore, the copper particles in the high acid medium pH² tend to interact with the negative ions in the solution, so they return again to CuCl₂,

but in the weak acid medium their effect is almost non-existent, so the removal rate is high[30].



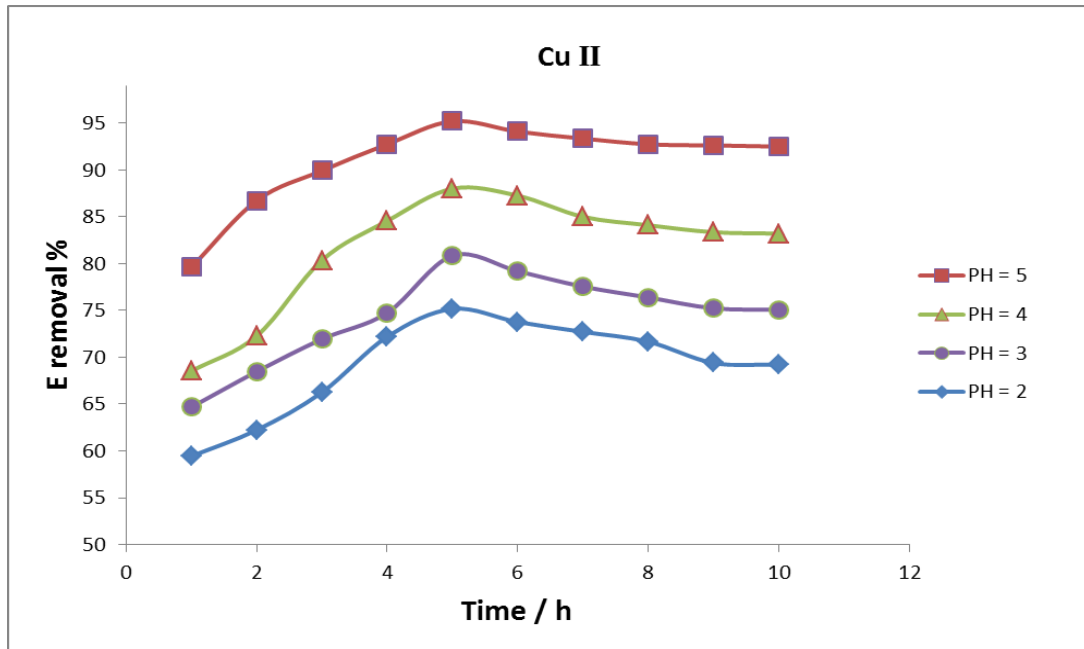
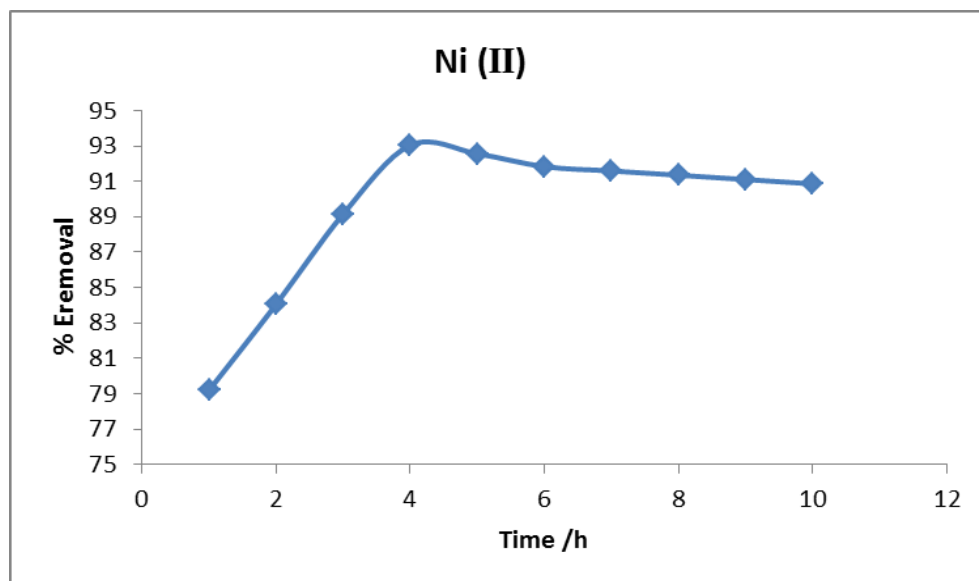
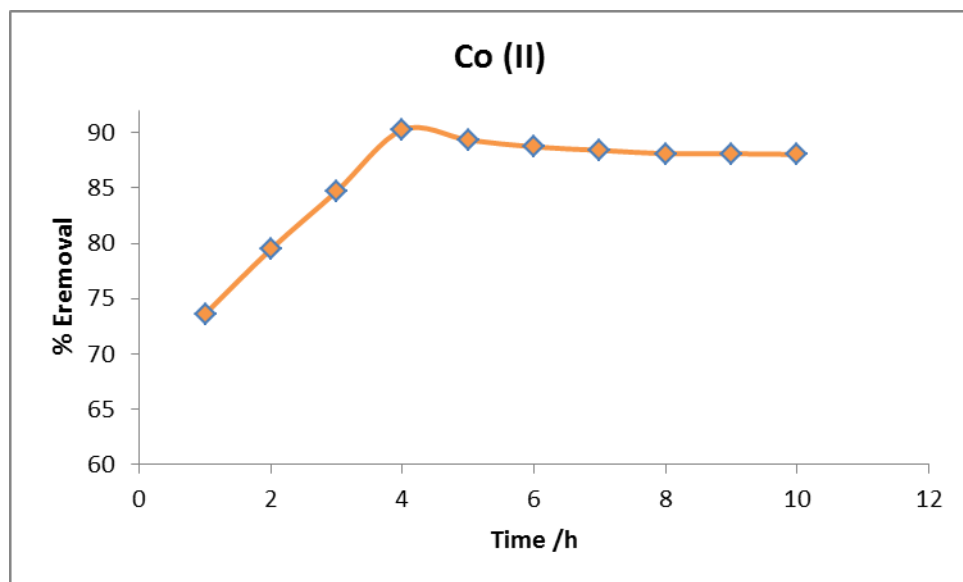


Figure 4-4 Effect of pH on the removal of metal ions (Co(II), Ni(II), and Cu(II) (concentration 10^{-4} M) by the RH-SiO₂PrADB(dose= 10^{-2} g)

4.4 Metal Uptake by Fe₃O₄ @ RH-SiO₂PrADB

4.4.1. Effect of vibration time on Removal of metal ions from aqueous solution by the ligand Fe₃O₄ @ RH-SiO₂PrADB

The effect of the reaction time of the ligand (Fe₃O₄ @ RH-SiO₂PrADB 10^{-2} g) with a solution of ions was studied in paragraph 4.3.1. It was noted through the results that the removal of all metal ions increases over time during the first four hours to reach a peak at the fourth hour, after which the concentration of ions reaches equilibrium. Where the removal percentage was (Co 90%, Ni 93%, and Cu 94%), which is shown in Figure (4-5). The reason for the increase in the removal of ions during a shorter period of time than the previous ligand (RH-SiO₂PrADB) is the presence of magnetic iron oxide, which gives the surface magnetic characteristics, which changes the surface charge and increases the withdrawal of positive ions [126][127].



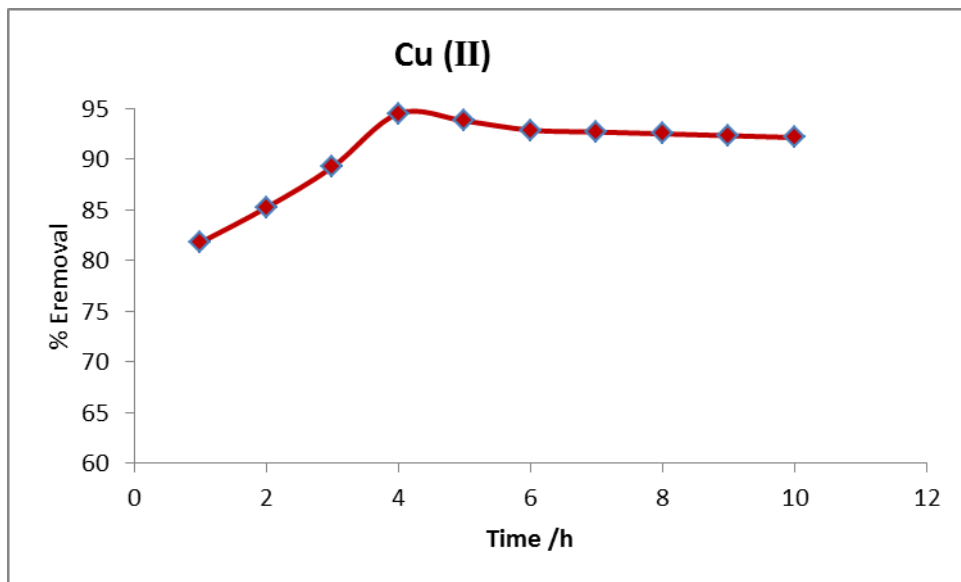
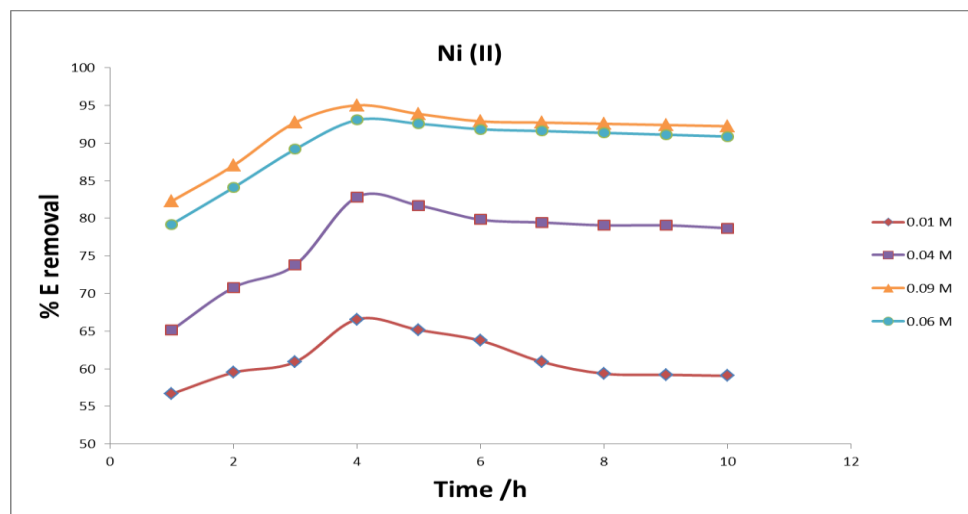
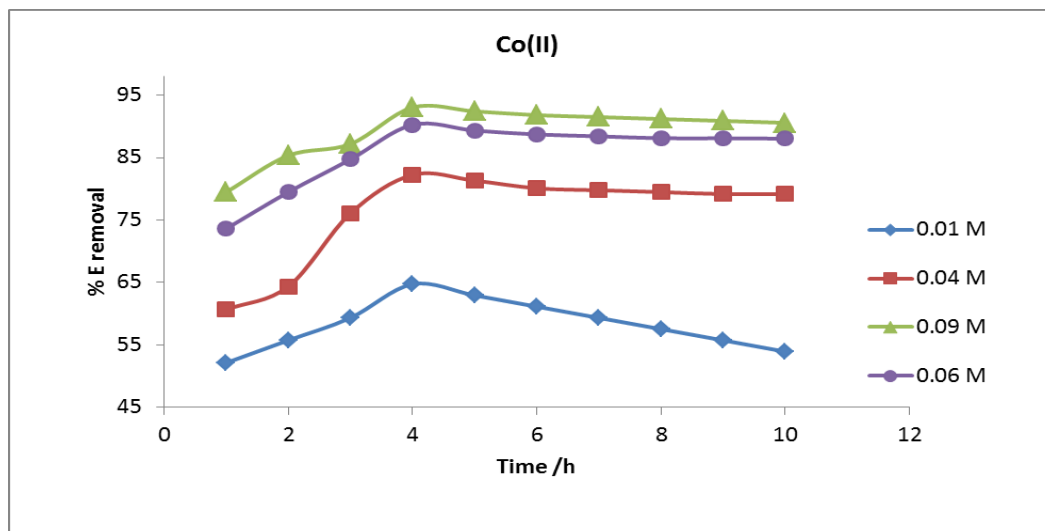


Figure 4-5 Effect of vibration time on removal of metal ions Co(II), Ni(II) and Cu(II)

4.4.10. Effects of concentration metal ions on the removal by the ligand $\text{Fe}_3\text{O}_4 @ \text{RH-SiO}_2/\text{PrADB}$

The effect of metal ion concentration was studied at different concentrations (0.01, 0.04, 0.06, 0.09 M) for each metal ion, which was removed by the $\text{Fe}_3\text{O}_4 @ \text{RH-SiO}_2/\text{PrADB}$ ligand (0.02 g). The results shown in Figure (4-6) show that the percentage of removal of ions increases with the increase of the concentration used, where the percentage of removal after four hours (Co 64%, Ni 66%, Cu 86%) when used 0.01 M, while it rises to (Co 93%, Ni 90%, Cu 97%) when 0.09 M is used after the same period of time has passed at the same time. This can be explained by the fact that as the concentration of ions increases, more adsorption sites are covered [128].



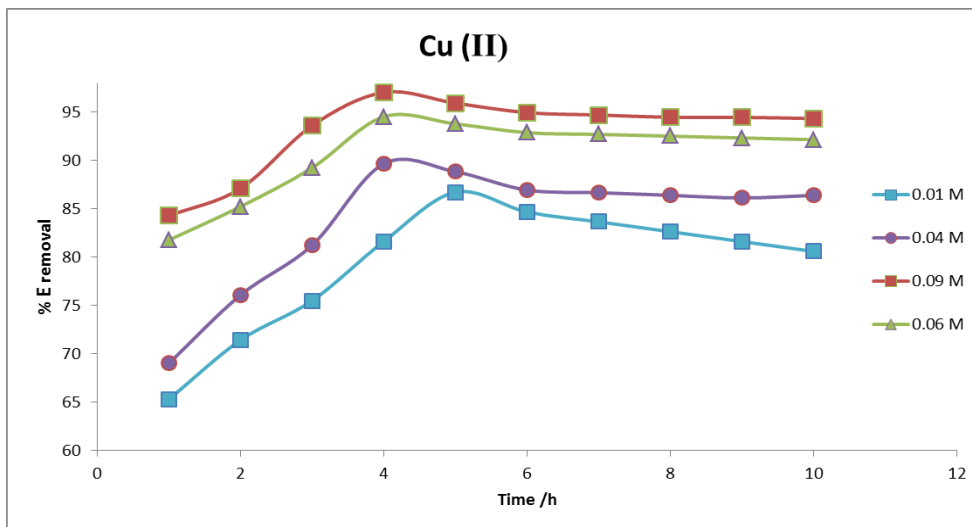
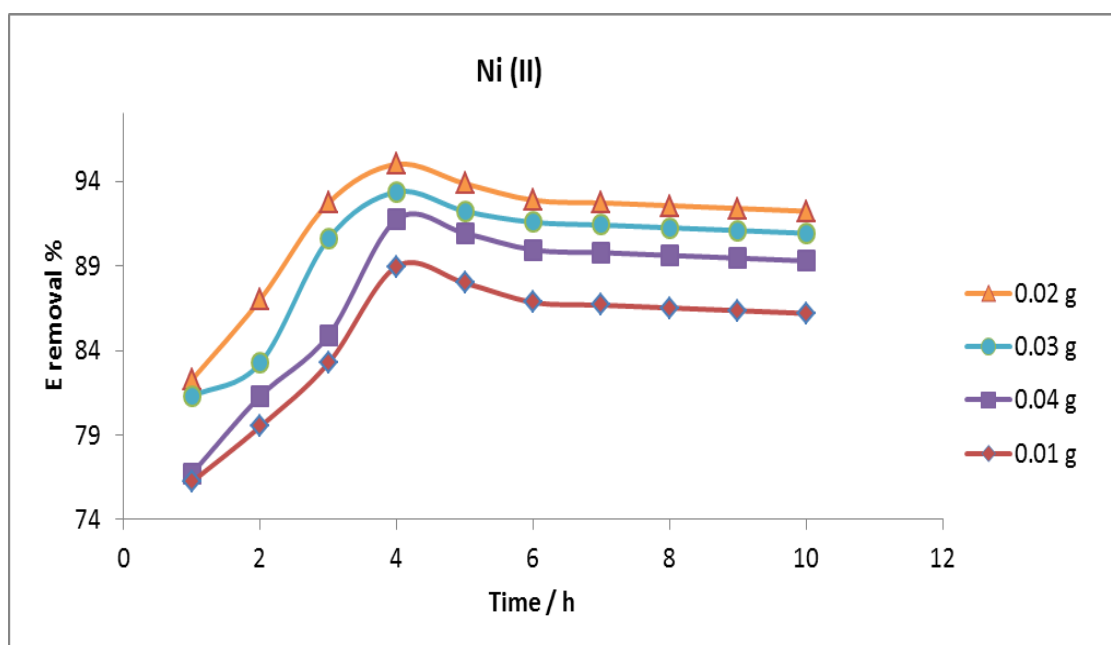
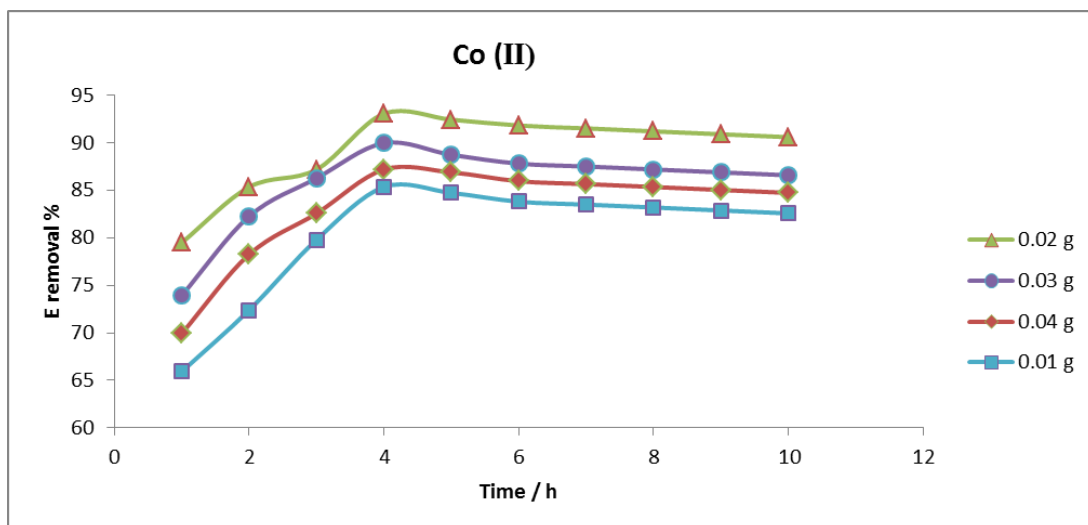


Figure 4-6 Effect of concentration of metal ions (Co(II), Ni II and Cu(II)) on the removal by the ligand Fe₃O₄@RH-SiO₂PrADB (dose= 0.1 g)

4.4.1.1. Effect of the weight of the Fe₃O₄@ RH-SiO₂PrADB

Different weights of the ligand were used, which are (0.1, 0.2, 0.3, 0.4 g) in a solution of metal ions at a concentration of 0.01 M. It was observed through the results as shown in Figure (4-7) that the removal rate of ions is as high as possible when using 0.2 g of the weight of the ligand Fe₃O₄@ RH-SiO₂PrADB, where the rates of removal of ions were (cobalt 93%, nickel 90%, and copper 97%), then the percentage decreased slightly when the weight of the ligand increased. This decrease in the removal value is explained by the agglomeration of the ligand at The use of weights higher than 0.2 g in the same volume used in the study, which causes agglomeration, closure of some active sites on the surface of the ligand, and this leads to a decrease in the surface area of the adsorbent surface[129].



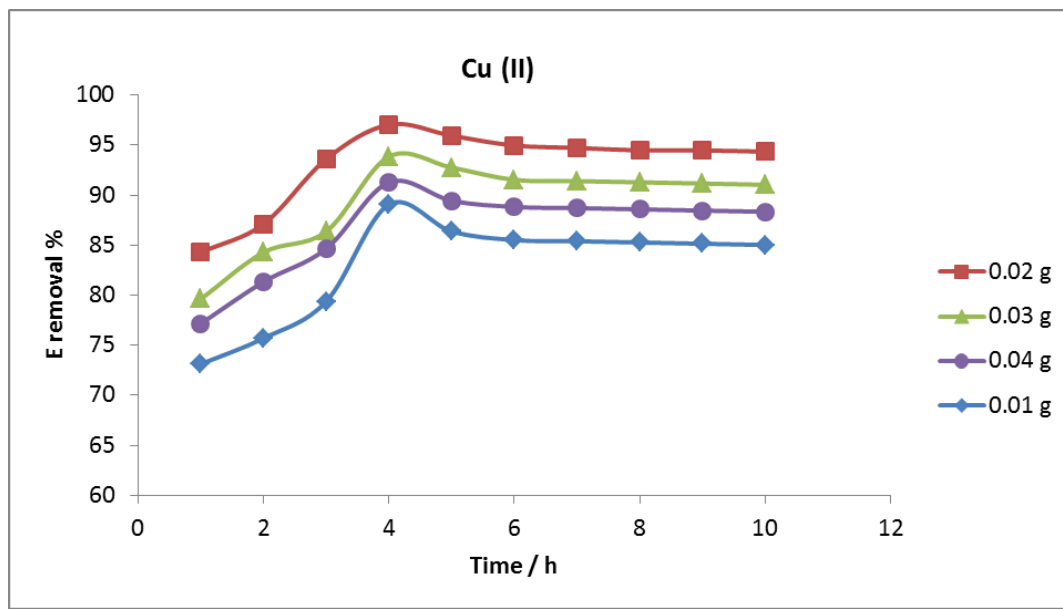


Figure 4-5 Effect of the weight of the Fe₃O₄@RH-SiO₂PrADB on the removal of metal ions (Co(II), Ni(II) and Cu(II) at a concentration 0.01 M

4.4.4. Effect of pH on E removal of metal ions

The effect of pH on the removal of metal ions from pH 6 to 9 was studied by the Fe₃O₄@RH-SiO₂PrADB ligand. The pH value of metal ions before the change (pH 6, 7, and 9 for Co²⁺, Ni²⁺ and Cu²⁺ respectively). The results showed as in Figure (4-6), that the percentage of metal ions removal decreased in acidic media when the pH is low, the concentration of H⁺ ions is very high in the solution, and therefore a competitive reaction will occur between them and the ions that carry a positive charge on the sites. In addition, the surface of the overlay contains hydroxyl groups in the silica, where the amount of H⁺ is low, and thus hydrogen bonding will occur between the chains on the surface. Thus, the surface is in a state of shrinking, which increases the difficulty of the diffusion of metal ions into the surface of the overlay. In addition, the Fe₃O₄ particles will react with the HCl which was used to adjust the pH and dissolve as FeCl₂ and FeCl₃ [129].

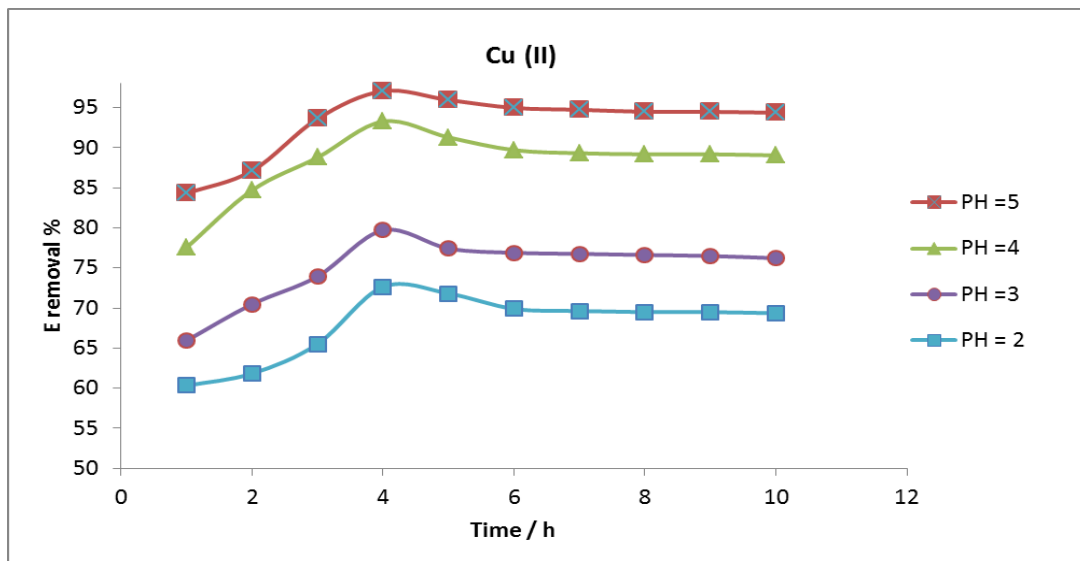
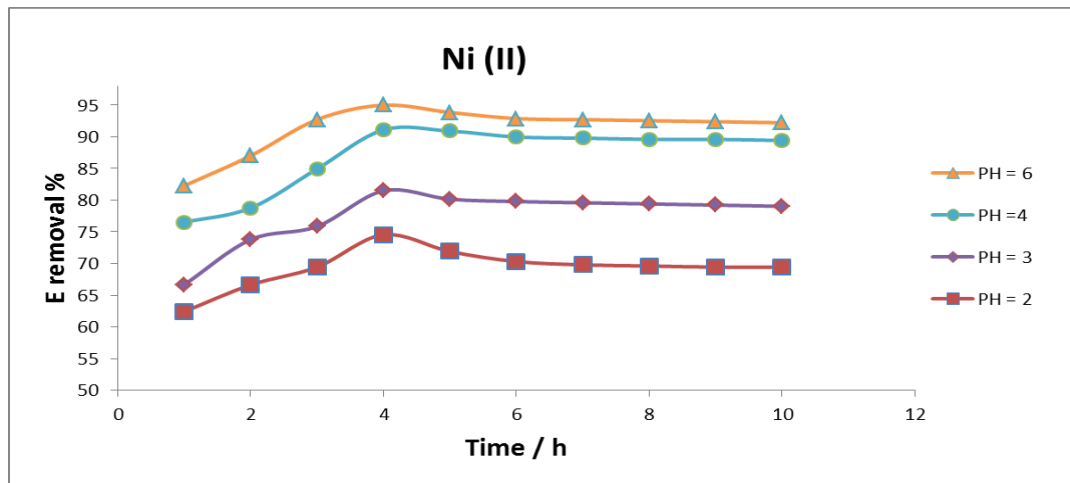
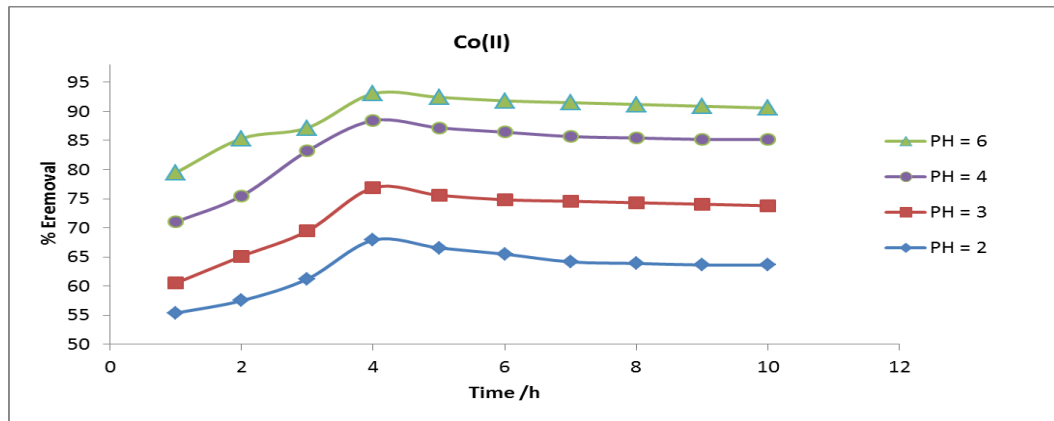


Figure 4-1 Effect of pH on the removal of metal ions (Co(II), Ni(II) at a concentration 10^{-4} M, and Cu(II) by the Fe_3O_4 @ RH-SiO₂-PrADB (0.1 g)

9. Conclusions

1- This study was based on the preparation of hybrid solid organosilicon ligand systems and was used in the uptake some of metal ions from an aqueous solution.

2- Extracted silica was prepared from Iraqi rice husks to be used to remove pollutants and get rid of pollution resulting from rice husks.

3 - The hybrid solid ligands (RH-SiO₂-PrADB & Fe³⁺O₂ @RH-SiO₂-PrADB) were applied in the removal of metal ions (Ni(II), Co(II), and Cu(II)) from aqueous solution. From this application can be concluded:

a- The removal of metal ions as a function of exposure time was shown to be enhanced in a nonlinear fashion and the increase in the removal of metal ions over time is due to diffusion factors.

b- That removal increases when the acidity of the solution increases

c- The ability to remove heavy metal has been increased with an increase in the concentration of metal ions, which may be due to the increased driving power of the concentration of metal ions.

d- The obtained results showed that the maximum removal increased as the mass of the ligand decreased for (Ni (II), Co (II), and Cu(II)) ions. This can be due to a block of donor sites of solid ligands by the ligand itself.

Future studies

To further pursue this area of study, the investigator would like to suggest the following as a future project:

١. It would be intriguing to take into account several sources for the synthesis of amorphous silica.
٢. It is of interest to study the functionalization of silica with various organic group types.
٣. creation of novel organosilica compounds appropriate for applications in the steel, cement, and insulation industries.
٤. Use additional parameters, like temperature, in uptake applications.
٥. Use other elements, in removal applications to help in little pollution.

REFERENCES



REFERENCES

٦. References

- [١] S. R. Kamath and A. Proctor, "Silica gel from rice hull ash: Preparation and characterization," *Cereal Chem.*, vol. ٧٥, no. ٤, pp. ٤٨٤–٤٨٧, ١٩٩٨, doi: ١٠.١٠٩٤/CCHEM.١٩٩٨.٧٥.٤.٤٨٤.
- [٢] T. Dawson *et al.*, *Physiological Plant Ecology: Ecophysiology and Stress Physiology of Functional Groups*. Walter Larcher , Joy Wieser , vol. ٧١, no. ٣. Springer Science & Business Media, ١٩٩٦. doi: ١٠.١٠٨٦/٤١٩٤٨٧.
- [٣] A. Kumar, B. Sengupta, D. Dasgupta, T. Mandal, and S. Datta, "Recovery of value added products from rice husk ash to explore an economic way for recycle and reuse of agricultural waste," *Rev. Environ. Sci. Biotechnol.*, vol. ١٥, no. ١, pp. ٤٧–٦٥, ٢٠١٦, doi: ١٠.١٠٠٧/s١١١٥٧-٠١٥-٩٣٨٨-٠.
- [٤] F. M. Muema, P. G. Home, and J. M. Raude, "Application of benchmarking and principal component analysis in measuring performance of public irrigation schemes in Kenya," *Agric.*, vol. ٨, no. ١٠, p. ١٦٢, ٢٠١٨, doi: ١٠.٣٣٩٠/agriculture٨١٠٠١٦٢.
- [٥] I. J. Fernandes *et al.*, "Characterization of rice husk ash produced using different biomass combustion techniques for energy," *Fuel*, vol. ١٦٥, pp. ٣٥١–٣٥٩, ٢٠١٦, doi: ١٠.١٠١٦/j.fuel.٢٠١٥.١٠.٠٨٦.
- [٦] K. M. Benson and W. N. Christine, "Adoption of climate change friendly New Rice for Africa (NERICA) varieties among farmers in Mwea West Sub-county, Kenya," *African J. Environ. Sci. Technol.*, vol.

REFERENCES

- ١٦, no. ٢, pp. ٧١–٧٨, ٢٠٢٢, doi: ١٠.٥٨٩٧/ajest٢٠٢١.٣٠٧٨.
- [٧] U. E. Simonis, *Decoupling natural resource use and environmental impacts from economic growth*, vol. ٤٠, no. ٤. UNEP/Earthprint, ٢٠١٣. doi: ١٠.١١٠٨/٠٣.٦٨٢٩١٣١١٣.٥٠٤٤.
- [٨] M. Gallery, “a Case O F Compromise : Working W I T H Guest Curators a Case O F Compromise :,” vol. ١٦, no. October ٢٠٠٣. Kenya, pp. ٢١–٣٠, ٢٠٠٦.
- [٩] K. Gautam *et al.*, “Production of biopolymers from food waste: Constrains and perspectives,” *Bioresour. Technol.*, vol. ٣٦١, p. ١٢٧٦٥٠, ٢٠٢٢, doi: ١٠.١٠١٦/j.biortech.٢٠٢٢.١٢٧٦٥٠.
- [١٠] S. M. Shaheen *et al.*, “Sustainable applications of rice feedstock in agro-environmental and construction sectors: A global perspective,” *Renew. Sustain. Energy Rev.*, vol. ١٥٣, p. ١١١٧٩١, ٢٠٢٢, doi: ١٠.١٠١٦/j.rser.٢٠٢١.١١١٧٩١.
- [١١] R. Siddique and M. Iqbal Khan, “Rice Husk Ash,” in *Engineering Materials*, Woodhead Publishing, ٢٠١١, pp. ٢٣١–٢٨١. doi: ١٠.١٠٠٧/٩٧٨-٣-٦٤٢-١٧٨٦٦-٥_٥.
- [١٢] D. P, *CRC Handbook of Chemistry and Physics*, W.M., vol. ٢٦٨, no. ١–٣. CRC press, ١٩٩٢. doi: ١٠.١٠١٦/٠٠٢٢-٢٨٦٠(٩٢)٨٥٠٨٣-s.
- [١٣] L. D. Fernández, E. Lara, and E. A. D. Mitchell, “Checklist, diversity and distribution of testate amoebae in Chile,” *Eur. J. Protistol.*, vol. ٥١, no. ٥, pp. ٤٠٩–٤٢٤, ٢٠١٥, doi: ١٠.١٠١٦/j.ejop.٢٠١٥.٠٧.٠٠١.
- [١٤] J. P. I. Burneau, A.; Gallas, “The surface Properties of silicas,” *Surf.*

REFERENCES

- Prop. silicas*, p. ٤٧٠, ١٩٩٨.
- [١٥] B. Jarrar, A. Al-Doaiss, A. Shati, M. Al-Kahtani, and Q. Jarrar, “Behavioural alterations induced by chronic exposure to ١٠ nm silicon dioxide nanoparticles,” *IET Nanobiotechnology*, vol. ١٥, no. ٢, pp. ٢٢١–٢٣٥, ٢٠٢١, doi: ١٠.١٠٤٩/nbt٢.١٢٠٤١.
- [١٦] P. A. Tsai, W. M. Chiu, C. E. Lin, and J. H. Wu, “Fabrication and Characterization of PLA/SiO₂/Al₂O₃ Composites Prepared by Sol-Gel Process,” *Polym. - Plast. Technol. Eng.*, vol. ٥٢, no. ١٤, pp. ١٤٨٨–١٤٩٥, ٢٠١٣, doi: ١٠.١٠٨٠/٠٣٦٠٢٥٥٩.٢٠١٣.٨٢٠٧٥١.
- [١٧] L. Wen, Xin Zhang, Kunyu Wang Yan Han, Lijing Han, Changyu Zhang, Huiliang Chen, Shan Dong, “Study of the thermal stabilization mechanism of biodegradable poly(L-lactide)/silica nanocomposites,” *Polym. Int.*, vol. ٦٠, no. ٢, pp. ٢٠٢–٢١٠, ٢٠١١, doi: ١٠.١٠٠٢/pi.٢٩٢٧.
- [١٨] F. Adam, H. Osman, and K. M. Hello, “The immobilization of ٣-(chloropropyl) triethoxysilane onto silica by a simple one-pot synthesis,” *J. Colloid Interface Sci.*, vol. ٣٣١, no. ١, pp. ١٤٣–١٤٧, ٢٠٠٩.
- [١٩] L. T. Zhuravlev, “Surface characterization of amorphous silica—a review of work from the former USSR,” *Colloids Surfaces A Physicochem. Eng. Asp.*, vol. ٧٤, no. ١, pp. ٧١–٩٠, ١٩٩٣.
- [٢٠] M. Wang, F. Duan, and X. Mu, “Effect of surface silanol groups on friction and wear between amorphous silica surfaces,” *Langmuir*, vol. ٣٥, no. ١٦, pp. ٥٤٦٣–٥٤٧٠, ٢٠١٩.
- [٢١] D. H. A. Al-Abbasy, “Synthesis and Characterization of Organosilicon Ligands and Used It in Removal of Some Divalent Metal Ions from

REFERENCES

- Their Aqueous Solutions,” *Univ. Kerbala*, no. April, ۲۰۱۹.
- [۲۲] M. Karnib, A. Kabbani, H. Holail, and Z. Olama, “Heavy metals removal using activated carbon, silica and silica activated carbon composite,” *Energy Procedia*, vol. ۵۰, pp. ۱۱۳–۱۲۰, ۲۰۱۴, doi: ۱۰.۱۰۱۶/j.egypro.۲۰۱۴.۰۶.۰۱۴.
- [۲۳] H. H. M. Al-Hmedawi, “Synthesis and Characterization of Heterogeneous Catalysts via Silica Obtained From Iraqi Rice Husks.” ۲۰۱۲.
- [۲۴] A. Zlatanic, D. Radojic, X. Wan, J. M. Messman, and P. R. Dvornic, “Monitoring of the Course of the Silanolate-Initiated Polymerization of Cyclic Siloxanes. A Mechanism for the Copolymerization of Dimethyl and Diphenyl Monomers,” *Macromolecules*, vol. ۵۱, no. ۳, pp. ۸۹۵–۹۰۵, ۲۰۱۸, doi: ۱۰.۱۰۲۱/acs.macromol.۷b۰۲۶۵۸.
- [۲۵] M. S. T. and T. Mondal, “Radiation curable polysiloxane: synthesis to applications,” *Soft Matter*, vol. ۱۷, no. ۲۶, pp. ۶۲۸۴–۶۲۹۷, ۲۰۲۱, doi: ۱۰.۱۰۳۹/d۱sm۰۰۲۶۹d.
- [۲۶] S. C. Shit and P. Shah, “A review on silicone rubber,” *Natl. Acad. Sci. Lett.*, vol. ۳۶, no. ۴, pp. ۳۵۵–۳۶۵, ۲۰۱۳, doi: ۱۰.۱۰۰۷/s۴۰۰۹-۰۱۳-۰۱۵۰-۲.
- [۲۷] K. M.- Pieńkowska, “Safety and Toxicity Aspects of Polysiloxanes (Silicones) Applications,” in *Concise Encyclopedia of High Performance Silicones*, ۲۰۱۴, pp. ۲۴۳–۲۵۱. doi: ۱۰.۱۰۰۲/۹۷۸۱۱۱۸۹۳۸۴۷۸.ch۱۶.
- [۲۸] N. V. Sastry, D. K. Singh, A. D. Thummar, G. Verma, and P. A. Hassan, “Effect of hydrocarbon surfactants on dexamethasone solubilization into

REFERENCES

- silicone surfactant micelles in aqueous media and its release from agar films as carriers,” *J. Mol. Liq.*, vol. 220, pp. 11–19, 2017, doi: 10.1016/j.molliq.2016.11.034.
- [29] K. Mojsiewicz-Pieńkowska, “Review of Current Pharmaceutical Applications of Polysiloxanes (Silicones),” in *Handbook of Polymers for Pharmaceutical Technologies*, V. Kumar Thakur and M. Kumari Thakur, Eds., Beverly, MA, USA: Scrivener Publishing LLC, 2010, pp. 363–381. doi: 10.1002/9781119041412.ch13.
- [30] N. M. El-Ashgar, I. M. El-Nahhal, M. M. Chehimi, F. Babonneau, and J. Livage, “Synthesis of polysiloxane-immobilized monoamine, diamine, and triamine ligand systems in the presence of CTAB and their applications,” *Phosphorus, Sulfur Silicon Relat. Elem.*, vol. 187, no. 3, pp. 392–402, 2012, doi: 10.1080/10426507.2011.610772.
- [31] F. Dong, X. Sun, and S. Feng, “Thermal degradation kinetics of functional polysiloxanes containing chloromethyl groups,” *Thermochim. Acta*, vol. 639, pp. 14–19, 2016, doi: 10.1016/j.tca.2016.07.007.
- [32] I. M. El-Nahhal, B. A. El-Shetary, K. A. R. Salib, N. M. El-Ashgar, and A. M. El-Hashash, “Polysiloxane-immobilized triamine ligand system, synthesis and applications,” *Phosphorus, Sulfur Silicon Relat. Elem.*, vol. 177, no. 3, pp. 741–753, 2002, doi: 10.1080/10426500210274.
- [33] N. M. El-Ashgar, I. M. El-Nahhal, M. M. Chehimi, F. Babonneau, and J. Livage, “A new route synthesis of immobilized-polysiloxane iminodiacetic acid ligand system, its characterization and applications,” *Mater. Lett.*, vol. 61, no. 23–24, pp. 4003–4008, 2007, doi: 10.1016/j.matlet.2007.02.050.

REFERENCES

- [٣٤] N. M. El-Ashgar, M. K. Silmi, I. M. El-Nahhal, M. M. Chehimi, and F. Babonneau, "Template Synthesis of Iminodiacetic Acid Polysiloxane Immobilized Ligand Systems and their Metal Uptake Capacity," *Silicon*, vol. ٩, no. ٤, pp. ٥٦٣–٥٧٥, Jul. ٢٠١٧, doi: ١٠.١٠٠٧/s1٢٦٣٣-٠١٥-٩٣٠٣-x.
- [٣٥] A. E. Danks, S. R. Hall, and Z. Schnepp, "The evolution of 'sol-gel' chemistry as a technique for materials synthesis," *Mater. Horizons*, vol. ٣, no. ٢, pp. ٩١–١١٢, ٢٠١٦, doi: ١٠.١٠٣٩/c〇mh٠٠٢٦٠e.
- [٣٦] L. P. Singh *et al.*, "Sol-Gel processing of silica nanoparticles and their applications," *Adv. Colloid Interface Sci.*, vol. ٢١٤, pp. ١٧–٣٧, ٢٠١٤, doi: ١٠.١٠١٦/j.cis.٢٠١٤.١٠.٠٠٧.
- [٣٧] M. Faustini, L. Nicole, E. Ruiz-Hitzky, and C. Sanchez, "History of organic–inorganic hybrid materials: prehistory, art, science, and advanced applications," *Adv. Funct. Mater.*, vol. ٢٨, no. ٢٧, p. ١٧٠٤١٥٨, ٢٠١٨.
- [٣٨] S. Ponyrko, L. Kobera, J. Brus, and L. Matějka, "Epoxy-silica hybrids by nonaqueous sol-gel process," *Polymer (Guildf)*, vol. ٥٤, no. ٢٣, pp. ٦٢٧١–٦٢٨٢, ٢٠١٣, doi: ١٠.١٠١٦/j.polymer.٢٠١٣.٠٩.٠٣٤.
- [٣٩] T. K. Tseng, Y. S. Lin, Y. J. Chen, and H. Chu, "A review of photocatalysts prepared by sol-gel method for VOCs removal," *Int. J. Mol. Sci.*, vol. ١١, no. ٦, pp. ٢٣٣٦–٢٣٦١, ٢٠١٠, doi: ١٠.٣٣٩٠/ijms١١٠٦٢٣٣٦.
- [٤٠] U. Schubert, "Chemistry and Fundamentals of the Sol-Gel Process," *Sol-Gel Handb.*, vol. ١–٣, pp. ١–٢٨, ٢٠١٥, doi: ١٠.١٠٠٢/٩٧٨٣٥٢٧٦٧٠٨١٩.ch٠١.
- [٤١] A. S. Dorcheh and M. H. Abbasi, "Silica aerogel; synthesis, properties

REFERENCES

- and characterization,” *J. Mater. Process. Technol.*, vol. 199, no. 1–3, pp. 10–26, 2008.
- [42] A. Du, B. Zhou, Z. Zhang, and J. Shen, “A special material or a new state of matter: A review and reconsideration of the aerogel,” *Materials (Basel)*, vol. 6, no. 3, pp. 941–968, 2013, doi: 10.3390/ma6030941.
- [43] S. C. Pillai and S. Hehir, *Sol-gel materials for energy, environment and electronic applications (advances in sol-gel derived materials and technologies)*, no. February. Springer, 2017. [Online]. Available: <http://link.springer.com/10.1007/978-3-319-00144-4>
- [44] J. P. Chen and W. S. Lin, “Sol-gel powders and supported sol-gel polymers for immobilization of lipase in ester synthesis,” *Enzyme Microb. Technol.*, vol. 32, no. 7, pp. 801–811, 2003, doi: 10.1016/S0141-0229(03)00020-8.
- [45] D. H. A. Al-Abbasy, “Synthesis and Characterization of Organosilicon Ligands and Used It in Removal of Some Divalent Metal Ions from Their Aqueous Solutions,” *Univ. Kerbala*, 2019.
- [46] V. De Zea Bermudez, L. D. Carlos, and L. Alcácer, “Sol-gel derived urea cross-linked organically modified silicates. 1. Room temperature mid-infrared spectra,” *Chem. Mater.*, vol. 11, no. 3, pp. 569–580, 1999, doi: 10.1021/cm980372v.
- [47] D. A. Stenger *et al.*, “Coplanar molecular assemblies of amino- and perfluorinated alkylsilanes: Characterization and geometric definition of mammalian cell adhesion and growth,” *J. Am. Chem. Soc.*, vol. 114, no. 22, pp. 8442–8448, 1992.

REFERENCES

- [48] V. A. Tertykh and L. A. Belyakova, "Solid-phase hydrosilylation reactions with participation of modified silica surface," in *Studies in Surface Science and Catalysis*, Elsevier, 1996, pp. 147–189. doi: 10.1016/S0167-2991(96)81020-7.
- [49] S. Dash, S. Mishra, S. Patel, and B. K. Mishra, "Organically modified silica: Synthesis and applications due to its surface interaction with organic molecules," *Adv. Colloid Interface Sci.*, vol. 140, no. 2, pp. 57–94, 2008, doi: 10.1016/j.cis.2007.12.006.
- [50] L. Peng, W. Qisui, L. Xi, and Z. Chaocan, "Investigation of the states of water and OH groups on the surface of silica," *Colloids Surfaces A Physicochem. Eng. Asp.*, vol. 334, no. 1–3, pp. 112–115, 2009, doi: 10.1016/j.colsurfa.2008.10.028.
- [51] A. R. Cestari, E. F. S. Vieira, R. E. Bruns, and C. Airoidi, "Some new data for metal desorption on inorganic-organic hybrid materials," *J. Colloid Interface Sci.*, vol. 227, no. 1, pp. 66–70, 2000, doi: 10.1006/jcis.2000.6841.
- [52] A. Ali *et al.*, "Synthesis, characterization, applications, and challenges of iron oxide nanoparticles," *Nanotechnol. Sci. Appl.*, vol. 9, pp. 49–67, 2016, doi: 10.2147/NSA.S99986.
- [53] L. MacHala, J. Tuček, and R. Zbořil, "Polymorphous transformations of nanometric iron(III) oxide: A review," *Chem. Mater.*, vol. 23, no. 14, pp. 3200–3272, 2011, doi: 10.1021/cm200397g.
- [54] A. V. Samrot, C. S. Sahithya, A. Jenifer Selvarani, S. Pachiyappan, and S. U. Suresh Kumar, "Surface-engineered super-paramagnetic iron

REFERENCES

- oxide nanoparticles for chromium removal,” *Int. J. Nanomedicine*, vol. 14, pp. 8105–8119, 2019, doi: 10.2147/IJN.S214236.
- [50] S. N. Sun, C. Wei, Z. Z. Zhu, Y. L. Hou, S. S. Venkatraman, and Z. C. Xu, “Magnetic iron oxide nanoparticles: Synthesis and surface coating techniques for biomedical applications,” *Chinese Phys. B*, vol. 23, no. 2, p. 37003, 2014, doi: 10.1088/1674-1056/23/2/037003.
- [51] P. Wu, J. Zhu, and Z. Xu, “Template-assisted synthesis of mesoporous magnetic nanocomposite particles,” *Adv. Funct. Mater.*, vol. 14, no. 4, pp. 340–351, 2004.
- [52] W. Zhao, J. Gu, L. Zhang, H. Chen, and J. Shi, “Fabrication of uniform magnetic nanocomposite spheres with a magnetic core/mesoporous silica shell structure,” *J. Am. Chem. Soc.*, vol. 127, no. 20, pp. 8916–8917, 2005.
- [53] D. A. Xavier and N. Srividhya, “Synthesis and Study of Schiff base Ligands,” *IOSR J. Appl. Chem.*, vol. 7, no. 11, pp. 06–10, 2014, doi: 10.9790/0736-071110610.
- [54] A. S. Munde, A. N. Jagdale, S. M. Jadhav, and T. K. Chondhekar, “Synthesis, characterization and thermal study of some transition metal complexes of an asymmetrical tetradentate Schiff base ligand,” *J. Serbian Chem. Soc.*, vol. 70, no. 3, pp. 349–359, 2010, doi: 10.2298/JSC09040809M.
- [55] K. Divya, G. M. Pinto, and A. F. Pinto, “Application of Metal Complexes of Schiff Bases As an Antimicrobial Drug: a Review of Recent Works,” *Int. J. Curr. Pharm. Res.*, vol. 9, no. 3, p. 27, 2017, doi:

REFERENCES

- 10.22109/ijcpr.2017.v9i3.19977.
- [61] A. B. MYSTAKIDES, "Dietary Department Grows With Hospital: New Equipment, Layout, and Services," *Hospitals (Lond.)*, vol. 37, pp. 100–102, 1963.
- [62] X. Yi, X. Fang, Y. Zhou, and W. Liu, "Synthesis and characterization of Schiff Base Aminodiphenylmethane condensation salicylaldehyde and its derivative," *Spec. Petrochemicals*, vol. 30, no. 1, pp. 28–31, 2013.
- [63] M. N. Uddin, "Metal Complexes of Schiff Bases Derived from 2-Thiophenecarboxaldehyde and Mono/Diamine as the Antibacterial Agents," *Mod. Chem.*, vol. 2, no. 2, p. 6, 2014, doi: 10.11648/j.mc.2014.2.2.11.
- [64] J. Cheng *et al.*, "Removal of Heavy Metal Ions from Aqueous Solution Using Biotransformed Lignite," *Molecules*, vol. 28, no. 13, pp. 90–102, 2023, doi: 10.3390/molecules28130090.
- [65] N. M. El-Ashgar, I. M. El-Nahhal, M. M. Chehimi, F. Babonneau, and J. Livage, "Extraction of Co, Ni, Cu, Zn and Cd ions using 2-aminophenylaminopropylpolysiloxane," *Environ. Chem. Lett.*, vol. 8, no. 4, pp. 311–316, 2010, doi: 10.1007/s10311-009-0223-0.
- [66] H. M. El-Kurd, I. M. El-Nahhal, and N. M. El-Ashgar, "Synthesis of new polysiloxane-immobilized ligand system di(amidomethyl)aminetetraacetic acid," *Phosphorus, Sulfur Silicon Relat. Elem.*, vol. 180, no. 7, pp. 1607–1611, 2005, doi: 10.1080/104265090880084.
- [67] F. Xie, X. Lin, X. Wu, and Z. Xie, "Solid phase extraction of lead (II),

REFERENCES

- copper (II), cadmium (II) and nickel (II) using gallic acid-modified silica gel prior to determination by flame atomic absorption spectrometry,” *Talanta*, vol. 74, no. 4, pp. 836–843, 2008, doi: 10.1016/j.talanta.2007.07.018.
- [78] N. M. El-Ashgar and I. M. El-Nahhal, “Preconcentration and separation of copper(II) by γ -aminopropylpolysiloxane immobilized ligand system,” *J. Sol-Gel Sci. Technol.*, vol. 34, no. 2, pp. 160–172, 2005, doi: 10.1007/s10971-005-1304-9.
- [79] I. M. El-Nahhal *et al.*, “Metal uptake by porous iminobis (N- γ -aminoethylacetamide)-modified polysiloxane ligand system,” *Microporous mesoporous Mater.*, vol. 70, no. 2–3, pp. 299–310, 2003.
- [80] F. R. Zaggout, I. M. El-Nahhal, and N. M. El-Ashgar, “Uptake of divalent metal ions (Cu^{2+} , Zn^{2+} , and Cd^{2+}) by polysiloxane immobilized diamine ligand system,” *Anal. Lett.*, vol. 34, no. 2, pp. 247–266, 2001, doi: 10.1081/AL-100001077.
- [81] D. H. Attol and H. H. Mihsen, “Synthesis of silica-salen derivative from rice husk ash and its use for extraction of divalent metal ions Co(II), Ni(II) and Cu(II),” *Indones. J. Chem.*, vol. 20, no. 1, pp. 16–28, 2020, doi: 10.221146/ijc.38008.
- [82] S. K. Abbas, Z. M. Hassan, H. H. Mihsen, M. T. Eesa, and D. H. Attol, “Uptake of Nickel(II) Ion by Silica-o-Phenylenediamine Derived from Rice Husk Ash,” *Silicon*, vol. 12, no. 5, 2020, doi: 10.1007/s12633-019-00207-4.
- [83] H. Ali and E. Khan, “What are heavy metals? Long-standing

REFERENCES

- controversy over the scientific use of the term ‘heavy metals’—proposal of a comprehensive definition,” *Toxicol. Environ. Chem.*, vol. 100, no. 1, pp. 7–19, 2018, doi: 10.1080/10772248.2017.1413602.
- [14] R. Dixit *et al.*, “Bioremediation of heavy metals from soil and aquatic environment: An overview of principles and criteria of fundamental processes,” *Sustain.*, vol. 7, no. 2, pp. 2189–2212, 2015, doi: 10.3390/su7022189.
- [15] L. Tahmasbi, T. Sedaghat, H. Motamedi, and M. Kooti, “Mesoporous silica nanoparticles supported copper(II) and nickel(II) Schiff base complexes: Synthesis, characterization, antibacterial activity and enzyme immobilization,” *J. Solid State Chem.*, vol. 258, pp. 517–525, 2018, doi: 10.1016/j.jssc.2017.11.015.
- [16] G. Anbarasu, M. Malathy, and R. Rajavel, “Synthesis and catalytic properties of copper(II) Schiff-base complex immobilized silica materials,” *J. Porous Mater.*, vol. 24, no. 5, pp. 1203–1211, 2017, doi: 10.1007/s10934-017-0366-5.
- [17] R. K. Sharma and D. Rawat, “Silica immobilized nickel complex: An efficient and reusable catalyst for microwave-assisted one-pot synthesis of dihydropyrimidinones,” *Inorg. Chem. Commun.*, vol. 17, pp. 58–63, 2012, doi: 10.1016/j.inoche.2011.12.014.
- [18] N. N. Greenwood, “Main group element chemistry at the millennium,” *J. Chem. Soc. Dalt. Trans.*, no. 14, pp. 2000–2066, 2001, doi: 10.1039/b103917m.
- [19] I. H. Cigerci, M. M. Ali, Ş. Y. Kaygisiz, and R. Liman, “Genotoxicity

REFERENCES

- assessment of cobalt chloride in *Eisenia hortensis* earthworms coelomocytes by comet assay and micronucleus test,” *Chemosphere*, vol. 144, pp. 704–707, 2016, doi: 10.1016/j.chemosphere.2015.09.053.
- [10] L. Chen, B. D. Li, Q. X. Xu, and D. Bin Liu, “A silica gel supported cobalt(II) Schiff base complex as efficient and recyclable heterogeneous catalyst for the selective aerobic oxidation of alkyl aromatics,” *Chinese Chem. Lett.*, vol. 24, no. 9, pp. 849–852, 2013, doi: 10.1016/j.cclet.2013.05.017.
- [11] M. D. Johnson and E. Larry, “Copper. Merck manual home health handbook. Merck Sharp and Dohme Corp., a subsidiary of Merck & Co,” *Inc. Retrieved*, vol. 7. Inc, 2008.
- [12] A. P. Ingle *et al.*, “Copper in medicine: Perspectives and toxicity,” *Biomed. Appl. Met.*, pp. 90–112, 2018, doi: 10.1007/978-3-319-74814-6_4.
- [13] W. J. Zhou, B. Albela, M. Y. He, and L. Bonneviot, “Design of a bio-inspired copper (II) Schiff base complex grafted in mesoporous silica for catalytic oxidation Dedicated to Georges Christou for his 70th birthday,” *Polyhedron*, vol. 64, pp. 371–376, 2013, doi: 10.1016/j.poly.2013.06.039.
- [14] G. Kheraldean Kara and M. Rabbani, “Experimental study of methylene blue adsorption from aqueous solutions onto Fe₃O₄/NiO nano mixed oxides prepared by ultrasonic assisted co-precipitation,” *J. Nanostructures*, vol. 9, no. 2, pp. 287–300, 2019.
- [15] T. T. Nguyen *et al.*, “Adsorptive removal of iron using SiO₂ nanoparticles extracted from rice husk ash,” *J. Anal. Methods Chem.*,

REFERENCES

- vol. 2019, 2019, doi: 10.1100/2019/6210240.
- [86] A. Y. Oyerinde and E. I. Bello, “Use of fourier transformation infrared (FTIR) spectroscopy for analysis of functional groups in peanut oil biodiesel and its blends,” *Br. J. Appl. Sci. Technol.*, vol. 13, pp. 1–14, 2016.
- [87] J. Nayak and J. Bera, “A simple method for production of humidity indicating silica gel from rice husk ash,” *J. Met. Mater. Miner.*, vol. 19, no. 2, pp. 10–19, 2017, [Online]. Available: <http://jmmm.material.chula.ac.th/index.php/jmmm/article/view/23>.
- [88] T. J. Al-hasani, H. H. Mihsen, and K. Mohammed, “Conversion of Rice Husk To A Nanoporous Material Via A Simple One - Pot Synthesis,” *Al- Mustansiriyah J. Sc*, vol. 23, no. 8, pp. 61–70, 2012.
- [89] T. J. Al-Hasani, H. H. Mihsen, K. M. Hello, and F. Adam, “Catalytic esterification via silica immobilized p-phenylenediamine and dithiooxamide solid catalysts,” *Arab. J. Chem.*, vol. 10, pp. S1492–S1500, 2017, doi: 10.1016/j.arabjc.2013.04.030.
- [90] H. H. Mihsen, “Synthesis, Characterization, and Biological Activitiy of Copper (II) Complexes Containing Bidentate Schiff Bases,” *Univ. Thi-Qar J. Sci.*, vol. 4, pp. 09–10, 2014, doi: 10.32792/utq/utjsci/vol4/2/8.
- [91] S. H. Chaki, T. J. Malek, M. D. Chaudhary, J. P. Tailor, and M. P. Deshpande, “Magnetite Fe₃O₄ nanoparticles synthesis by wet chemical reduction and their characterization,” *Adv. Nat. Sci. Nanosci. Nanotechnol.*, vol. 6, p. 3009, 2010.
- [92] J. Nayak and J. Bera, “A simple method for production of humidity

REFERENCES

- indicating silica gel from rice husk ash,” *J. Met. Mater. Miner.*, vol. 19, no. 2, pp. 10–19, 2009, [Online]. Available: <http://jmmm.material.chula.ac.th/index.php/jmmm/article/view/23>.
- [93] M. Thommes, “Physical adsorption characterization of nanoporous materials,” *Chemie Ing. Tech.*, vol. 82, no. 7, pp. 1099–1103, 2010.
- [94] A. Dias and V. S. T. Ciminelli, “Analysis of nitrogen adsorption-desorption isotherms for the estimation of pore-network dimensions and structure of ferroelectric powders,” *Ferroelectrics*, vol. 241, no. 1, pp. 9–16, 2000.
- [95] M. D. Donohue and G. L. Aranovich, “Classification of Gibbs adsorption isotherms,” *Adv. Colloid Interface Sci.*, vol. 76–77, pp. 137–152, 1998, doi: 10.1016/S001-8686(98)0044-X.
- [96] M. Ghadermazi, S. Moradi, and R. Mozafari, “Rice husk-SiO₂ supported bimetallic Fe-Ni nanoparticles: as a new, powerful magnetic nanocomposite for the aqueous reduction of nitro compounds to amines,” *RSC Adv.*, vol. 10, no. 55, pp. 33389–33400, 2020, doi: 10.1039/d0ra0381c.
- [97] J. Epp, “X-ray diffraction (XRD) techniques for materials characterization,” in *Materials characterization using nondestructive evaluation (NDE) methods (Elsevier, 2016*.
- [98] E. Lifshin, *X-ray Characterization of Materials*. John Wiley & Sons, 2008.
- [99] K. A. Nabieh, W. I. Mortada, T. E. Helmy, I. M. M. Kenawy, and Y. G. “Abou El-Reash 2021. ‘Chemically modified rice husk as an effective

REFERENCES

- adsorbent for removal of palladium ions,” *Heliyon*, vol. 7, p. 662, 2021.
- [100] A. D. Mohsin and H. H. Mihsen, “Uptake of Metal Ions (Co(II) and Ni(II)) by Silica-Salicylaldehyde Derived from Rice Husks,” *J. Inorg. Organomet. Polym. Mater.*, vol. 30, no. 6, pp. 2172–2181, 2020.
- [101] C.-D. Dong, C.-W. Chen, and C.-M. Hung, “Persulfate activation with rice husk-based magnetic biochar for degrading PAEs in marine sediments,” *Environ. Sci. Pollut. Res.*, vol. 26, pp. 33781–90, 2019.
- [102] M. Thompson, “Uncertainty functions, a compact way of summarising or specifying the behaviour of analytical systems,” *TrAC - Trends Anal. Chem.*, vol. 30, no. 7, pp. 1168–1170, 2011, doi: 10.1016/j.trac.2011.03.012.
- [103] H. H. Mihsen, T. J. Al-hasani, and K. Mohammed, “Synthesis and characterization of Nanoporous Material via Rice husk,” in *AIP Conference Proceedings*, 2017, pp. 147–156.
- [104] R. A. Fleck and B. M. Humbel, *Biological Field Emission Scanning Electron Microscopy: Volume I: Volume II*, vol. 1–2. John Wiley & Sons, 2019. doi: 10.1002/9781118763233.
- [105] S. A. Ajeel, K. A. Sukkar, and N. K. Zedin, “Extraction of high purity amorphous silica from rice husk by chemical process,” in *IOP Conference Series: Materials Science and Engineering*, IOP Publishing, 2020. doi: 10.1088/1757-899X/881/1/012096.
- [106] J. Hou *et al.*, “In-situ preparation of novel sedimentary rock-like Fe_3O_4 by rice-husk mesoporous silica as templates for effective remove As (III) from aqueous solutions,” *J. Environ. Chem. Eng.*, vol. 9, p. 105866, 2021.

REFERENCES

- [107] G. Kaykioglu and E. Gunes, “Comparison of acid red 114 dye adsorption by Fe_2O_3 and Fe_3O_4 impregnated rice husk ash,” *J. Nanomater.*, 2016.
- [108] M. Raposo, Q. Ferreira, and P. a Ribeiro, “A Guide for Atomic Force Microscopy Analysis of Soft- Condensed Matter,” *Mod. Res. Educ. Top. Microsc.*, vol. 1, pp. 708–769, 2007, doi: 10.1002/sia.2294.
- [109] A. Alhadhrami, G. G. Mohamed, A. H. Sadek, S. H. Ismail, A. A. Ebnalwaled, and A. S. A. Almalki, “Behavior of Silica Nanoparticles Synthesized from Rice Husk Ash by the Sol–Gel Method as a Photocatalytic and Antibacterial Agent,” *Materials (Basel)*, vol. 10, no. 22, p. 8211, 2022, doi: 10.3390/ma10228211.
- [110] Q. Liu, H. Wang, J. Liu, and H. Huang, “AFM image processing for estimating the number and volume of nanoparticles on a rough surface,” *Surf. Interface Anal.*, vol. 43, no. 10, pp. 1304–1309, 2011, doi: 10.1002/sia.3722.
- [111] M. Nasrollahzadeh, M. Atarod, S. M. S. Mohaddeseh Sajjadi, and Z. Issaabadi, “Chapter 6 - Plant-Mediated Green Synthesis of Nanostructures: Mechanisms, Characterization, and Applications.” 2019.
- [112] E. Huseynov, A. Garibov, and R. Mehdiyeva, “TEM and SEM study of nano SiO_2 particles exposed to influence of neutron flux,” *J. Mater. Res. Technol.*, vol. 9, no. 3, pp. 213–218, 2016, doi: 10.1016/j.jmrt.2016.11.001.
- [113] R. Vijayan, G. S. Kumar, N. S. Gopalu Karunakaran, S. Prabhu, and R. Ramesh, “Microwave combustion synthesis of tin oxide-decorated

REFERENCES

- silica nanostructure using rice husk template for supercapacitor applications,” *J. Mater. Sci. Mater. Electron.*, vol. 31, pp. 5738–40, 2020.
- [114] V. Paramarta, Y. Kristianto, A. Taufik, and R. Saleh, “Improve sonocatalytic performance using modified semiconductor catalyst SnO₂ and ZrO₂ by magnetite materials,” in *IOP Conference Series: Materials Science and Engineering*, 012042, IOP Publishing, 2017.
- [115] W. Guo, G. Li, Y. Zheng, and K. Li, “Nano-silica extracted from rice husk and its application in acetic acid steam reforming,” *RSC Adv.*, vol. 11, no. 50, pp. 34910–34922, 2021, doi: 10.1039/d1ra05200a.
- [116] S. Z. D. Cheng, C. Y. Li, B. H. Calhoun, L. Zhu, and W. W. Zhou, “Thermal analysis: the next two decades,” *Thermochim. Acta*, vol. 500, no. 1–2, pp. 59–78, 2000.
- [117] M. A. A. Akl, I. M. M. Kenawy, and R. R. Lasheen, “Organically modified silica gel and flame atomic absorption spectrometry: employment for separation and preconcentration of nine trace heavy metals for their determination in natural aqueous systems,” *Microchem. J.*, vol. 78, no. 2, pp. 143–156, 2004.
- [118] M. Kazemi Miraki, M. Arefi, A. Salamatmanesh, E. Yazdani, and A. Heydari, “Magnetic nanoparticle-supported Cu–NHC complex as an efficient and recoverable catalyst for nitrile hydration,” *Catal. Letters*, vol. 148, pp. 3378–3388, 2018.
- [119] A. D. Mohsin and H. H. Mihsen, “Preparation of novel absorbent derived from rice husk ash and its application for removing metal ions

REFERENCES

- (Co(II) and Ni(II)) from aqueous solutions,” in *AIP Conference Proceedings*, 2022, p. 030027. doi: 10.1063/50066820.
- [120] C. E. R. Barquilha, E. S. Cossich, C. R. G. Tavares, and E. A. Silva, “Biosorption of nickel (II) and copper (II) ions by *Sargassum* sp. in nature and alginate extraction products,” *Bioresour. Technol. Reports*, vol. 0, pp. 43–00, 2019.
- [121] S. S. Ahluwalia and D. Goyal, “Removal of heavy metals by waste tea leaves from aqueous solution,” *Eng. Life Sci.*, vol. 0, no. 2, pp. 108–112, 2000.
- [122] H. Liu, S. Feng, N. Zhang, X. Du, and Y. Liu, “Removal of Cu (II) ions from aqueous solution by activated carbon impregnated with humic acid,” *Front. Environ. Sci. Eng.*, vol. 8, pp. 329–336, 2014.
- [123] A. Abbas *et al.*, “Heavy metal removal from aqueous solution by advanced carbon nanotubes: critical review of adsorption applications,” *Sep. Purif. Technol.*, vol. 107, pp. 141–161, 2016.
- [124] D. F. Zhu, “Bridging the rice yield gap in China,” *Bridg. rice yield gap Asia-Pacific Reg.*, vol. 74, pp. 69–83, 2000, [Online]. Available: http://coin.fao.org/coin-static/cms/media/9/1317176.277.90/2000_16_high.pdf
- [125] N. D. Alkhatami, N. A. Alamrani, A. Hameed, S. D. Al-Qahtani, R. Shah, and N. M. El-Metwaly, “Adsorption of pharmaceutical ibuprofen over functionalized zirconium metal-organic frameworks; Batch experiment and mechanism of interaction,” *Polyhedron*, vol. 230, p. 116349, 2023, doi: 10.1016/j.poly.2023.116349.

REFERENCES

- [126] F. Ge, M. M. Li, H. Ye, and B. X. Zhao, "Effective removal of heavy metal ions Cd²⁺, Zn²⁺, Pb²⁺, Cu²⁺ from aqueous solution by polymer-modified magnetic nanoparticles," *J. Hazard. Mater.*, vol. 211–212, pp. 366–372, 2012, doi: 10.1016/j.jhazmat.2011.12.013.
- [127] Q. Wang, J. Li, C. Chen, X. Ren, J. Hu, and X. Wang, "Removal of cobalt from aqueous solution by magnetic multiwalled carbon nanotube/iron oxide composites," *Chem. Eng. J.*, vol. 174, no. 1, pp. 126–133, 2011, doi: 10.1016/j.cej.2011.08.059.
- [128] J. Wang, S. Zheng, Y. Shao, J. Liu, Z. Xu, and D. Zhu, "Amino-functionalized Fe₃O₄@SiO₂ core-shell magnetic nanomaterial as a novel adsorbent for aqueous heavy metals removal," *J. Colloid Interface Sci.*, vol. 349, no. 1, pp. 293–299, 2010, doi: 10.1016/j.jcis.2010.05.010.
- [129] M. Monier, D. M. Ayad, Y. Wei, and A. A. Sarhan, "Adsorption of Cu(II), Co(II), and Ni(II) ions by modified magnetic chitosan chelating resin," *J. Hazard. Mater.*, vol. 177, no. 1–3, pp. 962–970, 2010, doi: 10.1016/j.jhazmat.2010.01.012.

الملخص

يتجه العالم نحو استخدام أفضل الطرق العلمية للتخلص من التلوث البيئي. بعض العناصر المعدنية هي ملوثات طبيعية وصناعية مثل الكوبالت والنحاس والنيكل. كما تعتبر قشور الأرز من الملوثات التي تنتج يومياً في جميع أنحاء العالم. ولذلك تم استخدام قشور الأرز لإنتاج مركبات للتخلص من بعض العناصر الملوثة، وبالتالي القضاء على نوعين من الملوثات في نفس الوقت. تم تحضير سيليكات الصوديوم من قشور الأرز، ثم تفاعل مع ٣-أمينوبروبيل ثلاثي إيثوكسي سيلان لإنتاج $\text{RH-SiO}_2\text{PrNH}_2$ عبر طريقة sol-gel التي تم تشخيصها باستخدام FTIR وأظهرت أن الاهتزازات NH و NH_2 تم امتصاصها عند ٣٢٨٣ و ٣١١٣ سم^{-١} على التوالي. ثم تفاعل $\text{RH-SiO}_2\text{PrNH}_2$ مع ٢-amino-٣,٥-dibromobenzaldehyde لينتج $\text{RH-SiO}_2\text{PrADB}$ والذي تم تمييزه باستخدام عدة تقنيات (FTIR, XRD, N_2 Adsorption-Desorption Analysis) : FESEM-EDX, CHN, AFM, TEM, TGA/DTA

يعرض طيف FT-IR مجموعة الأزوميثين (C=N) ممثلة بالذروة عند ١٦٤٢ سم^{-١}. أظهر أطياف XRD الطبيعة غير المتبلورة للمركب المحضر. يشير التحليل العنصري لمركب $\text{RH-SiO}_2\text{PrADB}$ إلى أن نسبة الكربون والنيتروجين هي ١٦.٦٣% و ٦.٤%. تظهر صور FESEM زيادة في خشونة السطح الخارجي للعينة مع زيادة في معدل تراكم الجسيمات النانوية نتيجة ترابط $\text{RH-SiO}_2\text{PrNH}_2$ مع مركب ٢-amino-٣,٥-Dibromobenzaldehyde. كما أكدت صور FAM زيادة واضحة في معدل الخشونة لتصل إلى ١٦.٢٤ نانومتر. يشير هذا الارتباط الناجح لـ $\text{RH-SiO}_2\text{PrNH}_2$ مع مركب ٢-amino-٣,٥-Dibromobenzaldehyde. بينما أظهرت صور TEM، وجود مجموعات كروية مرتبطة ببعضها البعض. وقد وجد أن متوسط حجم الجسيمات هو ٣٥ نانومتر، وهذه القيمة تتفق مع نتائج تحليل FESEM و XRD. وبين تحليل TGA أن نسبة الفقد وصلت إلى (٥٣.٤٨%) بسبب تبخر جزيئات الماء الممتزة وتفكك مركب ٢-أمينو-٣,٥-ثنائي بروموبنزالدهيد، وبالتالي كسر روابط السيلانول ونجاح عملية التخليق. وإنتاج مركب ذو ثباتية عالية. كانت المساحة المحددة وقطر المسام لـ $\text{RH-SiO}_2\text{PrADB}$ تستخدم تحليل BET، وتم تحديدها لتكون مساوية لـ ٣.٨١٨ م^٢/جم، و ١.٢١ نانومتر، على التوالي.

بالإضافة إلى ذلك، تمت معالجة سيليكات الصوديوم بإضافة Fe_2O_3 لإنتاج سلكيات نانوية مغناطيسية. باتباع نفس الطريقة السابقة، تم إنتاج $Fe_2O_3@RH-SiO_2PrADB$ ويتميز بعدة تقنيات (TGA/DTA ، TEM ، AFM ، CHN ، FESEM-EDX ، XRD ، FTIR)

أظهر طيف FT-IR نطاق امتصاص عند 636.5 و 570.9 cm^{-1} بسبب رابطة Fe-O بالإضافة إلى نطاقات نفس الامتصاص للمركب RH-SiO₂PrADB. أظهر مركب طيف XRD إزاحة واضحة في الذروة العريضة عند ($2\theta = 22.5^\circ - 28.8^\circ$) بسبب مركب RH-SiO₂PrADB والقمم الحادة عند ($2\theta = 29.2^\circ, 35.4^\circ, 39.1^\circ, 42.4^\circ, 47.9^\circ, 57.0^\circ, 62.8^\circ, 67.0^\circ$) بسبب التركيب المكعب لـ Fe_2O_3 وقد لوحظ أن المركب المحضر غير متبلور.

تم تحضير ليكاندات صلبة هجينة لامتناس أيونات المعدن من محلولها المائي باستخدام ظروف مختلفة مثل:- زمن التعرض، الرقم الهيدروجيني، تركيز أيون المعدن، وكتلة الليكاند.



جامعة كربلاء

كلية العلوم

قسم الكيمياء

إزالة بعض الأيونات الفلزية بواسطة ليكاند متعدد المنح مثبت على البولي سيلوكسان

رسالة

مقدمة لكلية العلوم / جامعة كربلاء وهي جزء من متطلبات نيل درجة الماجستير في علوم الكيمياء

كتب بواسطة

أيام طارق عبد الكاظم

بكالوريوس. كيمياء (٢٠١٣) / جامعة واسط

يشرف عليها

الأستاذ الدكتور. حيدر حميد محسن

و

الاستاذ المساعد. شيماء ابراهيم سعيد

٢٠٢٤ ميلادي

١٤٤٥ هجري